Adsorption of EOR polymers and surfactants on Carbonate Minerals

by

Mohamad Shoaib

A thesis

presented to the University of Waterloo

in fulfillment of the

thesis requirement for the degree of

Master of Applied Science

in

Chemical Engineering

Waterloo, Ontario, Canada, 2014

AUTHOR'S DECLARATION

I hereby declare that I am the sole author of this thesis. This is a true copy of the thesis, including any required final revisions, as accepted by my examiners.

I understand that my thesis may be made electronically available to the public.

Abstract

Polymer and Surfactants are widely used to improve the oil recovery from a reservoir. One of the main issues with injection of these chemicals is their adsorption over reservoir rock surfaces. The first part of this study focuses on understanding the adsorption characteristics of a newly proposed polymer "Schizophyllan" for application in high temperature (120°C) and high salinity (250 g/l) carbonate reservoirs which are typical in Middle East. In the static adsorption experiments, the effect of parameters like mineral type, salinity, background ions, and temperature on adsorption was investigated. We find that adsorption density over minerals decreases with salinity and temperature. The adsorption of the polymer is higher on carbonate rocks compared to silica and kaolin. Dynamic adsorption using the core flow experiments is also studied. The adsorption in the presence of oil is low compared to the adsorption when there was no oil in the core. The change in viscosity of polymer as a result of flowing through the core has also been reported.

In the second part we study the adsorption of a switchable surfactant (Neutral to Cationic) which is a promising candidate for CO_2 foam for mobility control. The adsorption shows a significant reduction with an increase in salinity and temperature. This is a promising result for further selection of this surfactant for the field applications.

Acknowledgements

I would like to express my deepest gratitude to my supervisors Dr. Ali Elkamel and Dr. Ahmed Abdala (The Petroleum Institute-Abu Dhabi) firstly for providing me an opportunity to work with them and secondly for their valuable and unconditional support during the duration of this thesis. Their wisdom has changed the way I see academics and research.

I would also like to thank Dr. Yuri Leonanko and Dr. Aiping Yu for taking out precious time out of their busy schedule to serve on my thesis committee.

At The Petroleum Institute, I thank Dr. Ali Sumaiti for supervising and discussing the core flow experiment and results.

Dr. Rehan ,Mrs. Sabna, Mrs. Haya, Mr. Vinu, Mr. Vishnu, Mr. Priyadarshan and Syed M.Raza Quadri for helping me with countless things during the entire thesis.

At University of Waterloo, I thank Mrs. Judy Caron and my friends Aashish Gaurav and M. Altamash Jauhar for their support during the entire thesis.

I acknowledge the financial support from the Abu Dhabi National Oil Company under the OSC project grants.

Dedication

This thesis is dedicated to my friends

Table of Contents

List of Figures

List of Tables

Chapter 1: Introduction

1.1 Introduction

Enhanced Oil Recovery (EOR) is a well-established & proven technology to increase the recovery factor of depleting oil reservoirs. During its lifetime a reservoir passes through primary, secondary and tertiary stages of production. It is primarily during the tertiary stage that external materials are injected into the reservoir to enhance the production. The injection techniques used during this stage are known as EOR techniques. One such technique is the mixing of water soluble polymers with the injection brine to increase its viscosity which results in enhanced oil production. The increment in oil production happens as a result of reduced mobility of water because of its higher viscosity than before which is attributed to the polymers. Polymers are mixed with the injection brine for the purpose of enhanced viscosity which results in mobility control of water. However, as the polymer slug propagates in the reservoir it interacts with the porous media. Such interaction results in the loss or retention of polymer which makes the propagating polymer slug lean. Retention of polymer will lead to loss of polymer which will increase the total amount of polymer which has to be injected to achieve the recovery goal. This will increase the overall cost of the project. Apart from the direct economic consequences it may also decrease the reservoir permeability. Of course, some projects have experienced severe problems because of the higher adsorption [1] .It will also result in advancement of water bank ahead of polymer solution which will greatly reduce the

affectivity of the process. In some cases a desired value of adsorption is required to obtain the expected residual resistance factor. In a very heterogeneous reservoir, the injected fluids follow the high permeability path which leads in shutting these zones thus making a positive impact. This will lead to more of the fluid going to the low permeability zones which will result in better vertical sweep efficiency. The polymer flooding project in Minnelusa in Wyoming utilized this mechanism to improve the oil recovery [2-4].The adsorption estimated in the lab greatly varies from the adsorption experienced in the field. Thus to optimize a polymer slug it is important to know and manage the maximum amount of polymer adsorption[5].

Another method which has gained lot of attention nowadays is the use of CO_2 in EOR.

CO_2 EOR has exhibited strong growth in the past 30 years and has expanded despite fluctuations in oil price. However, there are several issues challenging the oil recovery, economic efficiency and applicability of the process. The oil recovery efficiency is low and the CO2 utilization rate, the amount of CO2 injected to recover an incremental barrel of oil, is high. This is due to the low viscosity of CO2 compared to oil and water and the resulting unfavorable mobility ratio. This, combined with reservoir heterogeneities, leads to poor sweep efficiency and bypass of un-contacted oil. This issue can be prevented by injected surfactant with CO_2. The role of the surfactant is to generate in situ a CO_2 in water emulsion/foam with reduced mobility as to improve sweep efficiency beyond that possible with the WAG process. This process is also known as CO_2 foam mobility

control. The surfactant chosen for this process should also exhibit low adsorption on the reservoir rocks.

1.2 Objectives

The main objective of this research is to study the adsorption behavior of Schizophyllan and Ethomeen-C12 over carbonate minerals. The effect of different parameters on adsorption density will be investigated. The over plan is:

Adsorption of Schizophyllan:

- **a.** Concentration measurement of Schizophyllan
- **b.** Adsorption kinetics at different temperature
- **c.** Adsorption on different minerals (Natural, Reservoir)
- **d.** Effect of Salinity level on adsorption
- **e.** Effect of background ions on adsorption
- **f.** Effect of conditioning on adsorption
- **g.** Effect of temperature on adsorption
- **h.** Effect of adsorption on MWD of polymer
- **i.** Microcalorimetry of adsorption
- **j.** Adsorption in core flow experiments
- **k.** Mechanical degradation of polymer in core flow experiments

Adsorption of Ethomeen-C12:

- **a.** Concentration measurement of Ethomeen-C12

b. MWD of Ethomeen C-12

c. Solubility of Ethomeen in DI water and brine

d. Adsorption on different minerals (Natural, Reservoir)

e. Effect of temperature on adsorption

1.3 Thesis Structure

Chapter 2 describes the technical background which is followed by the literature review of retention of polymers in porous media.

Chapter 3 focuses on the static adsorption of Schizophyllan. The effects of parameters like mineral type, salinity, background ions and temperature have been studied.

Chapter 4 presents the dynamic adsorption of Schizophyllan which is measured using core flow experiments. The viscosity of the core flooding effluents has also been presented.

Chapter 5 presents the adsorption of Ethomeen C-12 on carbonate minerals. Solubility, MWD of C-12 has also been studied.

Chapter 6 summarizes the thesis and provides some future recommendations.

Chapter 2: Technical Background and Literature Review

2.1 The significance of EOR

Global energy demand will increase by 52% over the period 2010-2035 with fossil fuels accounting for the 84% of this surge. Out of this increment, oil will retain the largest share. Given this fact in place ,oil demand will increase from 81.2 to 100.2 mboe/d from 2010 to 2035 [6]. This demand will be fulfilled by available and the newly to be discovered oil fields. According to the current trends the rate of replacement of depleting fields by newly discovered fields is declining at a fast rate [7]. According to the analysis of 1600 fields by IEA, the production from a field declines at an average rate of 6% once it has surpassed the peak production. [8].Therefore keeping in mind the prospective shortage in oil resources with difficult findings of new oil fields, the only available option to avoid this crisis is taking the most oil out of the reserves in place by utilizing the enhanced recovery methods. A 1% increase in the total global recovery factor has the potential to deliver three years of oil consumption at today's level which would be around 88 billion barrels[9].Given the fact that middle east has majority of the oil reserves in the world , the EOR potential is also likewise.

2.2 Enhanced Oil Recovery Overview

2.2.1 Three stages of oil field development

After the completion of oil wells the field becomes ready/online for production. At this stage oil recovery which is the extraction of oil from subsurface to the surface starts. During its life a field will pass through three phases of production. The first phase of its life is known as primary recovery phase which means production using the natural energy or pressure within the reservoir. This energy is derived from one or a combination of six driving mechanisms which are: Rock & liquid expansion, depletion drive, gas cap drive, water drive and gravity drainage drive[10].As the time passes these drives start weakening resulting in pressure reduction. During the primary recovery stage only a small percentage (around 10%) of total oil in place is recovered. At a certain point of time when because of the low reservoir pressure the production becomes diminutive enough resulting in uneconomical operation of the field, production team starts assessing the pressure maintenance strategies. This is done by water/gas injection and this process or phase is known as secondary recovery method or phase. The aim of the secondary recovery process is to push hydrocarbons towards the well bore while maintaining the pressure. The secondary stage is called off when the water cut reaches an uneconomical level. This production problem is also known as excessive water production[11].Incorporated, primary and secondary phases result in around 15% to 40% of original oil in place[12]. After these two phases are over there is still lot of oil left in the reservoir which can't be recovered and this oil is known as residual oil. This oil is still

in place because it was not contacted and swept or it is trapped by capillary forces. This residual oil is recovered during the third phase known as tertiary recovery or enhanced oil recovery. Injecting external materials which were not initially present in the reservoir to recover residual oil is known as enhanced oil recovery (EOR) [13].Depending upon the basic recovering mechanism, EOR is classified into

- Chemical methods which works on alteration of capillary and viscous forces
- Miscible gas injection which extracts oil with a solvent and
- Thermal methods which rely upon reduction of residual oil viscosity.

Figure 2-1 shows the overall recovery stages and Table 2-1 presents the classification of EOR processes whereas Table 2-2 presents the preferred EOR methodology according to the properties of the field.

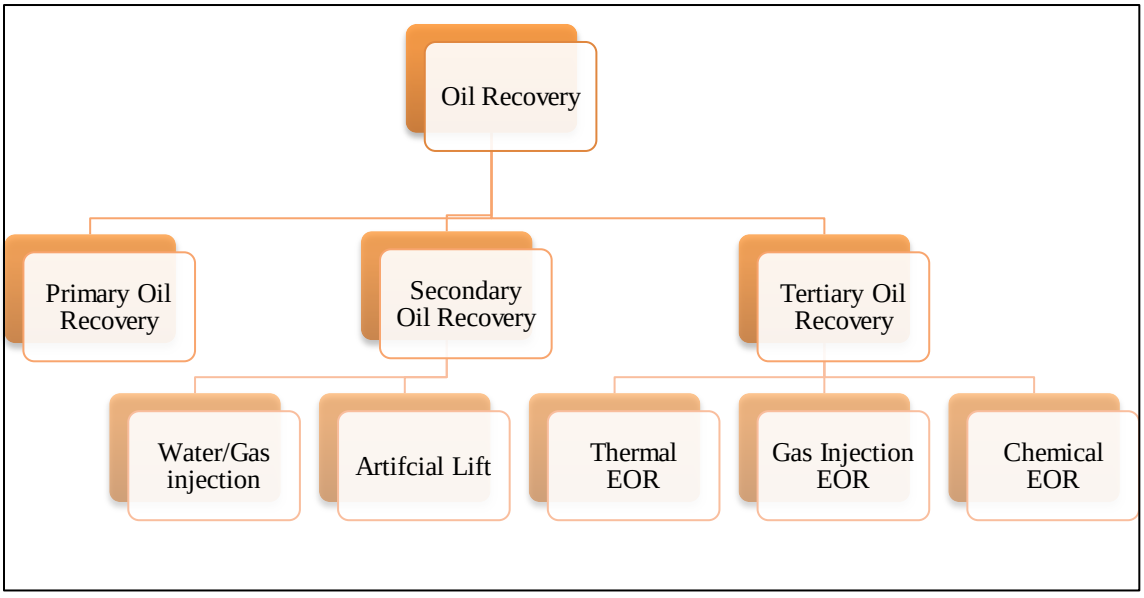

Figure 2-1: 3 Stages of Recovery

Table 2-1: Current and Past EOR methods [14]

Chemical EOR
- Alcohol-miscible solvent flooding - ASP Flooding - Gels for water shutoff - Low IFT waterflooding - Microbial injection - Micellar/polymer(surfactant) flooding - Polymer Flooding
Gas Injection EOR
- CO_2 Flooding - Flue gas injection - Inert gas injection - Nitrogen injection
Hydrocarbon injection
- Enriched gas drive - High pressure gas drive - Miscible solvent flooding
Thermal Methods
- Hot water flooding - In-Situ combustion - Reverse combustion - Standard forward combustion - Steam flooding - Steam and hot water injection - Steam stimulation - Surface mining and extraction

Table 2-2: Screening Criterion for EOR Methods

EOR Method	Formation type	Viscosity (cp)	Gravity (°API)	Oil Sat. (%PV)	Avg. Perm. (md)	Depth (ft)
Chemical EOR						
Micellar/ Polymer, ASP and Alkaline Flooding	Sandstone preferred	<35	>20	>35	>10	<9000
Polymer Flooding	Sandstone preferred can work in carbonates	<150,>10	>15	>50	>10	<9000
Gas Injection EOR						
CO_2	Sandstone or carbonate	<10	>22	>20	Not Critical	>2500
Hydrocarbon	Sandstone or carbonate	<3	>23	>30	Not Critical	>4000
Nitrogen and flue gas	Sandstone or carbonate	<0.4	>35	>40	Not critical	>6000
Immiscible gases	Sandstone or carbonate	<600	>12	>35	Not Critical	>1800
Thermal EOR						
Combustion	High porosity sandstone	<5000	>10	>35	>50	<11,500
Steam	High porosity sandstone	<100,000	8-25	>40	>200	<5000

2.2.2 EOR by Formation Type (Lithology)

Reservoir formation type(carbonate or sandstone) is one of the main considerations for EOR methods, often restricting the applicability of specific EOR methods [14, 15]. Most of the EOR projects as shown in Figure2-2 have been implemented in sandstone reservoirs, as derived from the data gathered by Vladimir and Manrique [7] from some 1,507 international EOR projects**.** It is also very clear that thermal and chemical EOR projects are the preferred and most suitable methods in sandstone as well as carbonate reservoirs with carbonate formations suiting for chemical EOR.

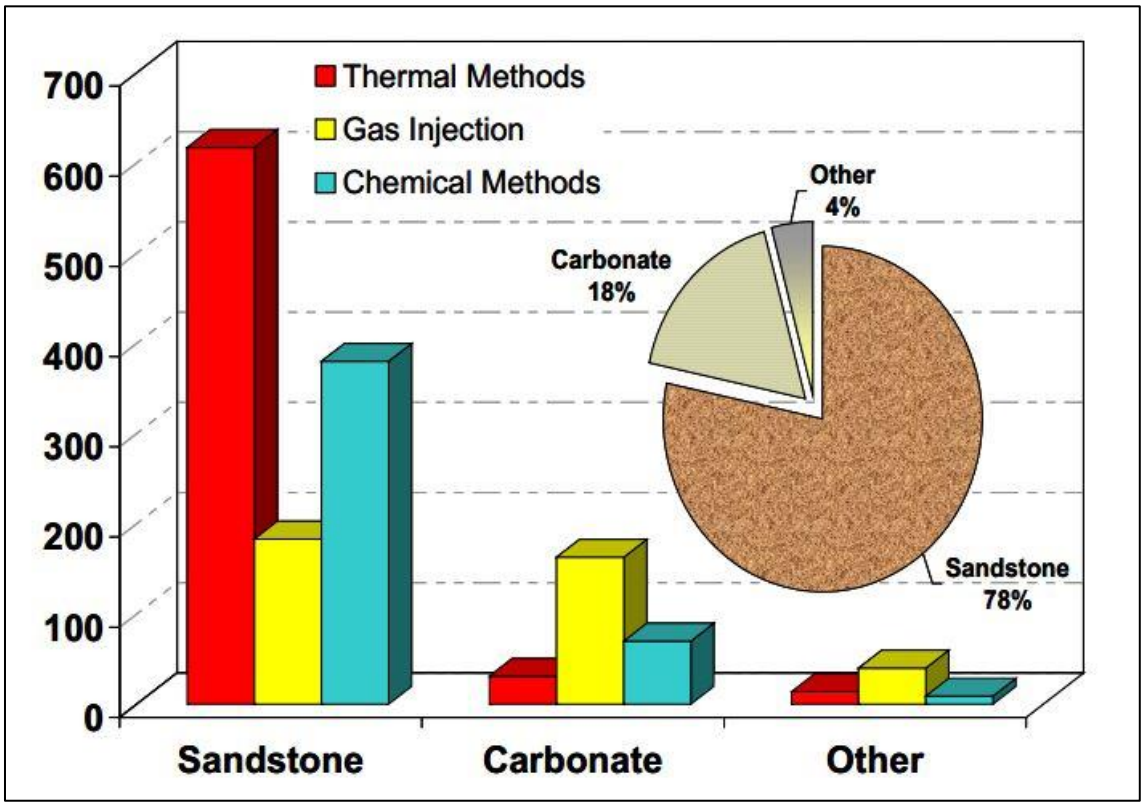

Figure 2-2: EOR Methods in different lithology

It is well known that majority of the world's hydrocarbon reserves are in carbonate reservoirs with 60% of world's oil and 40% gas[16]. Compared to sandstone reservoirs, which normally are homogenous or single-porosity formations, carbonate reservoirs are multiple-porosity exhibiting petrophysical heterogeneities[17]. Carbonate reservoirs usually have low porosity and can be fractured easily. These two characteristics with the oil-to-mixed wet rock characteristics of carbonate reservoirs lead to the low recovery factor from these reservoirs. As a consequence of heterogeneity the injected EOR fluids flow through the fracture network and ultimately bypassing the oil in the rock matrix which contributes nothing to the recovery factor. The high permeability in the fractured or heterogeneous zones with low equivalent porous fraction results in an early breakthrough of the injected fluids. A number of EOR field projects have been implemented and referenced in carbonate reservoirs in the literature [18-21]. Most of these fields have been implemented with gas injection EOR methods with CO_2 remaining the top utilized method. Polymer flooding assisted with surfactants has been the only famous and most utilized chemical EOR methods in carbonate formations. There are a number of increasing polymer projects in Canada, U.S and Middle East. Polymer flooding is also gaining interest in heavy crude oil recovery in Canada[22].

2.2.3 Introduction to Chemical EOR

Based on the material balance the overall recovery efficiency from a reservoir is defined as:

$$RF = \frac{Np}{N} = \frac{Total\ Oil\ Produced}{Amount\ of\ oil\ originally\ in\ place} \quad \textbf{Equation 2-1}$$

In a simple manner, recovery factor can also be mathematically written as[23]

$$RF = Sweep\ Efficiency * Displacement\ Efficiency \quad \textbf{Equation 2-2}$$

To improve total oil recovery both the weep and displacement are evaluated for an improvement[10]

Sweep efficiency is also known as macroscopic displacement efficiency. It is the efficiency of displacing fluid to sweep in horizontal and vertical direction with effectively moving the displaced oil towards the production well. So that the overall sweep efficiency is the product of horizontal and vertical sweep efficiency.

$$Sweep\ Efficiency = (E_{Vertical} * E_{Arial}) \quad \textbf{Equation 2-3}$$

It depends on the thickness of the reservoir, heterogeneities present, fractures, gas-oil and oil-water contacts position, flow rate, pattern of injection, density difference between the displacing and displaced fluid etc. [24]. The sweep efficiency is improved by injecting fluids which are more viscous compared to connate fluids. This is done by adding small concentrations of polymer in injecting water which can impart it high viscosities. This will provide a better mobility and viscous fingering control which will help in overcoming the reservoir heterogeneities[25]. The mobility of a fluid is defined as:

$$\boldsymbol{Mobility = \lambda = \frac{\mu}{k}} \qquad \textbf{Equation 2-4}$$

Where, μ and k are fluid viscosity and permeability of reservoir to the fluid respectively. The mobility ratio is the ratio between water mobility and oil mobility.

$$\boldsymbol{Mobility\ Ratio = \frac{\lambda_o}{\lambda_w} \ll 1\ (desired\ value)} \qquad \textbf{Equation 2-5}$$

The desired value of this ratio to get a plug like flow for the displacement of oil by water is less than 1. Given this value less than 1, the fingering of water in oil zones is depressed as a result a greater volume of reservoir will be contacted and swept by water. The effect of polymer on mobility control is shown in Figure 2-3[26] .Polymer flooding does not improve the local displacement efficiency [27].

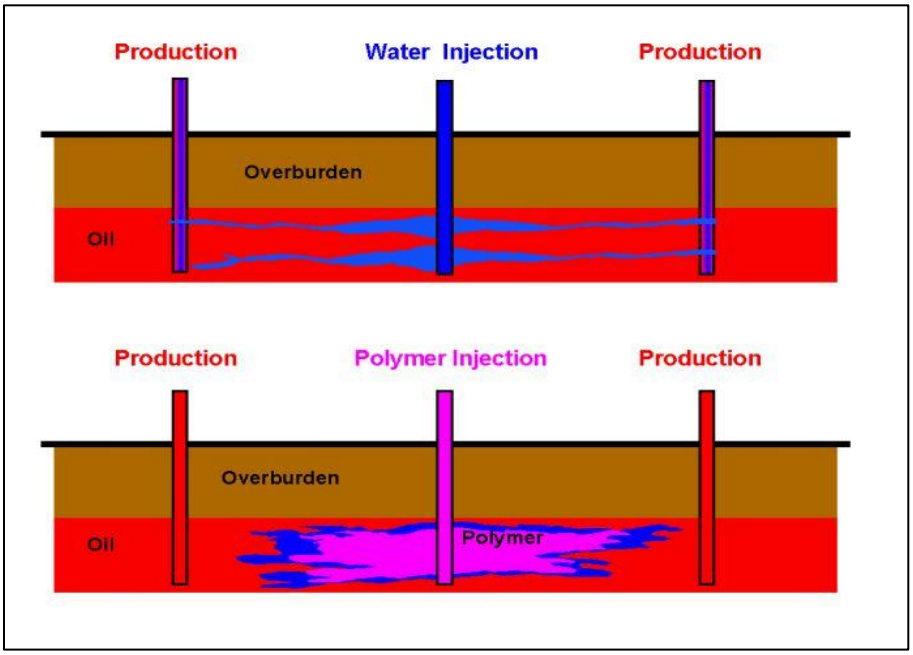

Figure 2-3: Mobility Control by Polymer Flooding

The **displacement efficiency** is the efficiency of displacing fluid to displace and mobilize the oil while contacting at pore scale. It can be written as ratio of amount of oil recovered to the amount initially present in swept volume.

$$\boldsymbol{Displacement\ Efficiency} = \frac{(\boldsymbol{S_{oi}} - \boldsymbol{S_{or}})}{\boldsymbol{S_{oi}}} \qquad \textbf{Equation 2-6}$$

Where, S_{oi} = initial oil saturation, and S_{or} = residual oil saturation.

The displacement efficiency is also known as microscopic displacement efficiency. During waterflooding even if all the oil is contacted, there is still small bob of oil which is trapped within pores as shown in Figure 2-4[26] . This is because the viscous or gravity drive forces are not able to overcome the capillary forces. The oil droplets are trapped by capillary forces due to the high interfacial forces between oil and water. The dimensionless capillary number which is the ratio of viscous to capillary forces determines the extent to which oil is trapped by the pores.

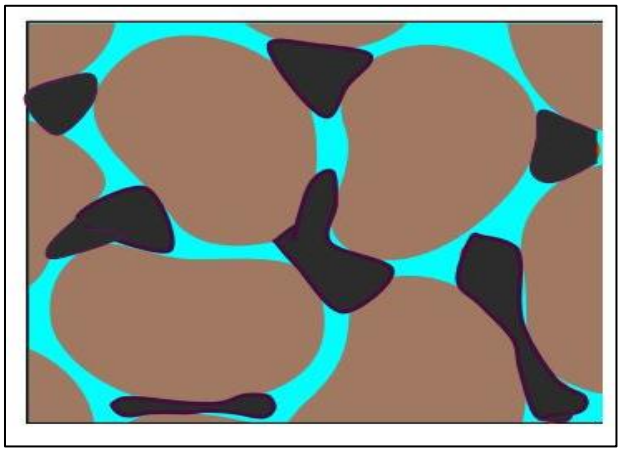

Figure 2-4: Trapped Oil inside Pores

It can be written as:

$$N_c = \frac{v * \mu}{\sigma} \qquad \textbf{Equation 2-7}$$

Where v is the velocity μ is the viscosity and σ is the interfacial tension.

As per the definition of capillary number the higher its value the more oil can be mobilized. This number should be of the order of 10^{-3} to reduce the residual oil saturation to near zero. The effect of capillary number on residual oil saturation is shown in Figure 2-5 [26] Now mathematically, to increase this number either the fluid velocity should be increased or the interfacial tension should be brought down. The velocity increment by several magnitudes to achieve the desired capillary number is difficult compared to reduction of interfacial tension (IFT). So, the most logical step to increase the microscopic efficiency is by the reduction of IFT which is achieved by the use of surfactants[24].This increment in capillary number is not achieved by polymer[28].Table 2-3 presents some commercially successful polymer flooding projects. Table 2-4 presents the type of EOR methods with their recovery mechanisms.

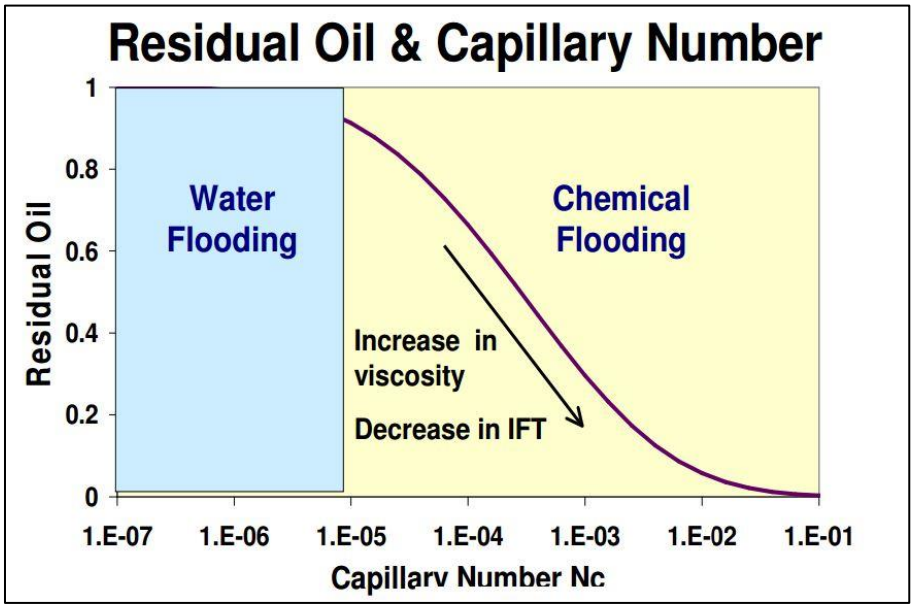

Figure 2-5: Residual Oil as a function of Capillary Number

Table 2-3: Polymer Flood Field Project

Property	Median (171 projects)	Marmul	Oerrel	Courtenay	Daqing
Permeability (md)	75	15,000	2,000	2,000	870
%OOIP at startup	76	92	81.5	78	71
HPAM Conc.(ppm)	460	1000	1500	900	1000
WOR at startup	3	1	4	8	10
Reservoir temperature (°F)	120	115	136	86	113
Projected IOR,%OOIP	4.9	25*	13	30	11
Projected bbl oil/lbm polymer	27	461	230	499	155

Table 2-4: Mechanism of EOR Methods

EOR Method		Pressure Support	Sweep Improvement	IFT Reduction	Wettability Alteration	Viscosity Reduction	Oil Swelling	Incremental Recovery Factor
Chemical	Polymer	✓	✓					Low
	Surfactant	✓		✓	✓			Moderate
	ASP	✓	✓	✓	✓			High
Water Flood	Water Flood	✓						Base Case
Gasflood immiscible	Hydrocarbon						✓	Moderate
	CO2					✓	✓	High
	Nitrogen	✓						Moderate
Gasflood miscible	Hydrocarbon		✓			✓	✓	High
	CO2		✓			✓	✓	High
	CO2 WAG	✓	✓			✓	✓	Highest
Thermal	Steam					✓		High
	High P Air					✓	✓	High

2.3 Polymer Flooding

Polymer flooding is a mature method for the recovery improvement of a depleting oil reservoir. The largest implemented polymer flooding project is in the Daqing field in China which as of 2005 has experienced about 220,000 barrels per day incremental oil production with a 12% OOIP incremental oil recovery. Some of the best polymer field projects have given an increment of 1STB per $2 of polymer injected[29]. Over the past 40 years a large number of polymer flooding projects have been implemented in reservoirs at different conditions. The reservoir temperatures have been from 10 to 110℃, brine salinities from 0.3 to 21.3%, permeabilites from 0.6 to 15000 md and the percentage of OOIP from 36 to 97.1%[20]. Compared to carbonates, most of these projects have been implemented in sandstone reservoirs[30]. So conceptually, polymer flooding has the potential to improve the oil recovery from a reservoir. However, there are number of factors which have restricted the use of this EOR method. Those factors are discussed one by one.

2.3.1 Cost Effectiveness

The mobility reduction per unit cost of polymer or viscosity provided per unit cost under the reservoir conditions is one of the most important criterions whiles selecting a polymer. Low cost of the polymer would mean higher concentrations and larger polymer slug sizes will be economical which will lead to greater oil recovery, more profits and potential applications of the polymers. Compared to 1970s, the oil price which was

around USD 3/bbl has gone up to more than USD 100 while the cost of the most widely used EOR polymers, Polyacrylamide copolymers or hydrolyzed polyacrylamide (HPAM) has stayed the same at USD 1.50/lb. The quality of commercial HPAM polymer and the molecular weight has also improved dramatically. This is the reason behind an impulsive increment in the number of polymer flooding projects. Earlier projects were done at a relatively small amounts of polymer (i.e., low polymer concentration sand small pore volumes of polymer solution), but now we know the more we inject the better the polymer flood will be, which is easier at today's polymer price. So, we can say that this factor has been in control and would not be a worrying criterion for the successfulness of the project[31].

2.3.2 Thermal and Chemical Degradation

While in the reservoir, the injected polymer should remain intact for a long time in order to get a technically and economically successful polymer flood project. The traditional polymers HPAM and Xanthan which have been utilized in some of the biggest and successful polymer projects degrade or precipitate in very high-temperature, high-salinity reservoirs[32]. This is the biggest issue with the traditional EOR polymers which is responsible for limiting the use of polymer EOR only in low temperature and low salinity reservoirs compared to harsh environments [33]. In fact, some study shows that due to the unavailability of a suitable polymer candidate the selection of another EOR method over polymer flooding was preferred for some reservoirs which were most suited for polymer EOR[34, 35]. Most of the HPAM field applications have been in fields with low

temperature (<70℃) and low salinity. Higher temperature promotes the rate of hydrolysis of HPAM which increases the amount of polyacrylic acid in the backbone which is very sensitive to hardness, as a result of increasing salinity the polymer precipitates[36]. Also, the coil conformation of HPAM molecules makes them very sensitive to ionic environments[37, 38]. So this poor temperature and salinity tolerance make them unsuitable in such fields.

Xanthan, a biopolymer which is a polysaccharide is another very famous polymer which has got ample attention for EOR. It has a very similar backbone to glucose which is neutral while having the charged side chains. The side chains are the acetate and pyruvate groups which makes it a polyelectrolyte polymer. Besides its ionic nature, viscosity is not affected much by salinity which is attributed to its high molecular weight and rigidity of chains [39, 40].Relative to HPAM it has better high temperature response. Its viscosity remains unaffected or it does not degrade thermally till 80°C after which it gets destroyed at above 100°C[41, 42]. Thus, it can be concluded that much of these problems which arises because of the thermal degradation, salinity intolerance will be sorted out if a new candidate polymer capable of handling these is available in market. Figure 2-6 shows the current salinity and temperature envelope with in which today's chemical EOR can be implemented as compared to some famous chemical EOR projects[43]. Thus there is a great need to identify a polymer which can exceed these limits. In our case this-limit has been defined according to the Abu Dhabi reservoirs. The overall criterion provided for the selection of a polymer is:

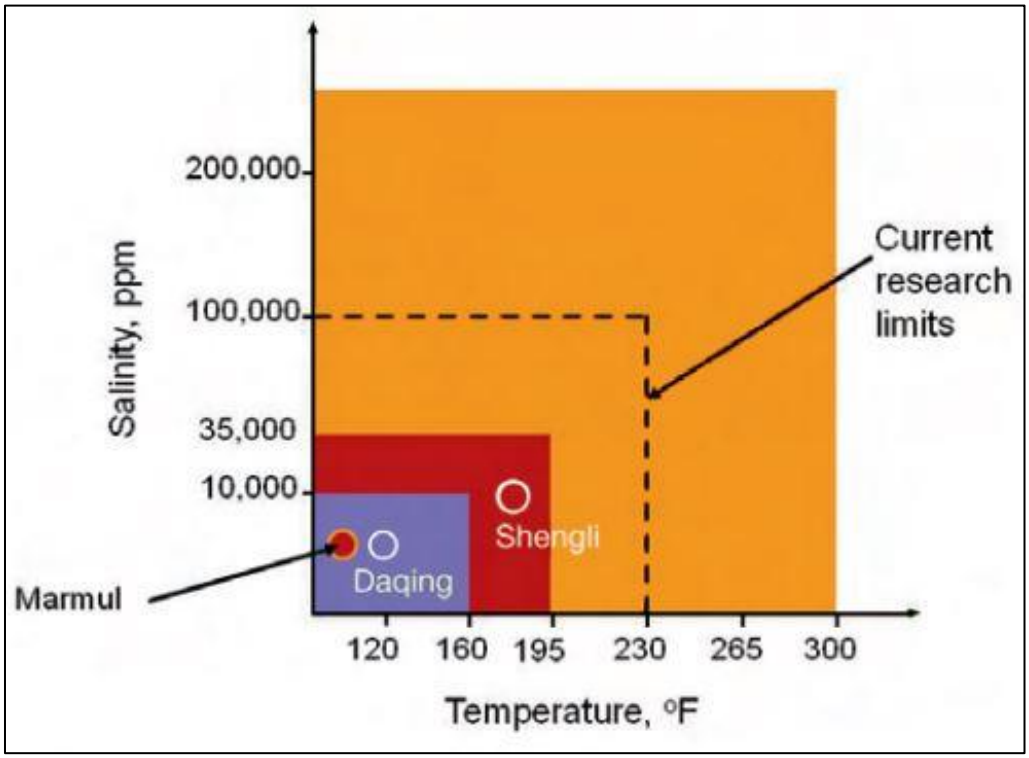

Figure 2-6: Limitations of Chemical EOR

- **Rheological behavior**: Polymer which has a high thickening ability at a low concentration is required so that it is economical. It should exhibit shear thinning behavior so that the cost of injection is also low and it does not have any problem in flowing through the low permeability portions of the reservoir.
- **Thermal stability**: It should have great resistance to thermal degradation so that the viscosity of the polymer solution is maintained at the high reservoir temperature for periods of months or years.
- **High salinity tolerance**: The selected polymer should have excellent tolerance to very high salinity levels (up to 250000 ppm)) in order to maintain appreciable viscosity level.

- **Manageable Adsorption**: Low adsorption level is required in order to minimize losses which otherwise will result in higher costs and other technical problems.

After screening a number of polymers supplied by different chemical suppliers, our group at The Petroleum Institute -Abu Dhabi was able to select a polymer which is showing excellent character and has passed all the first three preliminary selection criterions. This polymer *'Schizophyllan'*(SPG) which is a β-1,3:β-1,6 glucan polysaccharide was first evaluated by Udo Rau et al.[44] in 1992 for its potential in high temperature and high salinity reservoirs. However, due to the low oil price during that time the work did not go through. Later on in 2011, Leonhardt et al. [45] from *Wintershall-Germany* presented their work on this polymer for use in EOR. This polymer is showing exceptional salinity and temperature resistance. Another work done on this polymer during 1985 talks about its remarkable thermal properties, the stable structure of this polymer till 135 °C has been reported[46].Long term thermal studies done in our lab has shown very little loss in viscosity due to thermal degradation in high salinity brine (250 g/l). The thermal stability of this polymer is attributed to its triple helical structure which is stable till 140°C because of the intramolecular hydrogen bonding [47, 48]. It transforms to a single chain above this temperature. Figure 2-7[45] shows the viscosity vs temperature of Schizophyllan compared to xanthan and sulfonated PAAM. It clearly shows no change in viscosity but after 140°C. Its non-ionic nature also makes it tolerant to very high salinity.

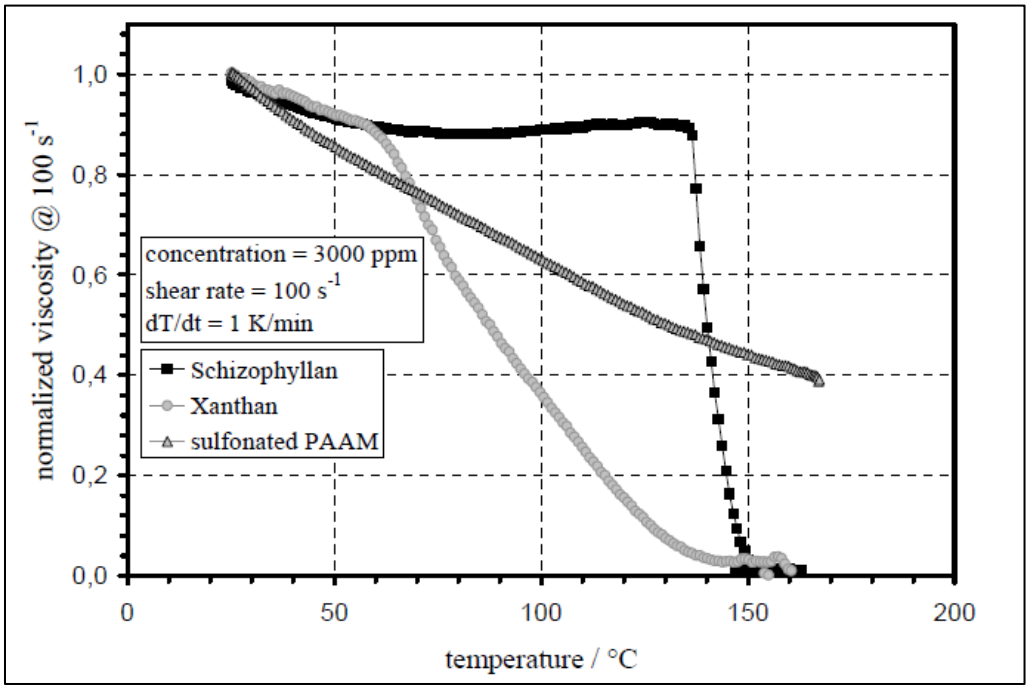

Figure 2-7: Viscosity of SPG vs Temperature

2.3.3 Adsorption/Retention

After the first three preliminary screening criterions listed earlier have been passed, the next screening criterion is adsorption characteristics of this polymer over carbonate minerals, which is also the focus of this thesis. The adsorption of EOR polymers is of great importance and can be a big problem in low permeability polymer flooding projects [49, 50].

2.4 EOR Chemical's Retention

2.4.1 Polymer Retention in porous media

There are three main mechanisms by which polymer retention occurs in a porous media. Depending upon the nature of the field combination of these may prevail in a polymer flood. These are:

- Hydrodynamic Retention
- Mechanical Entrapment
- Polymer Adsorption

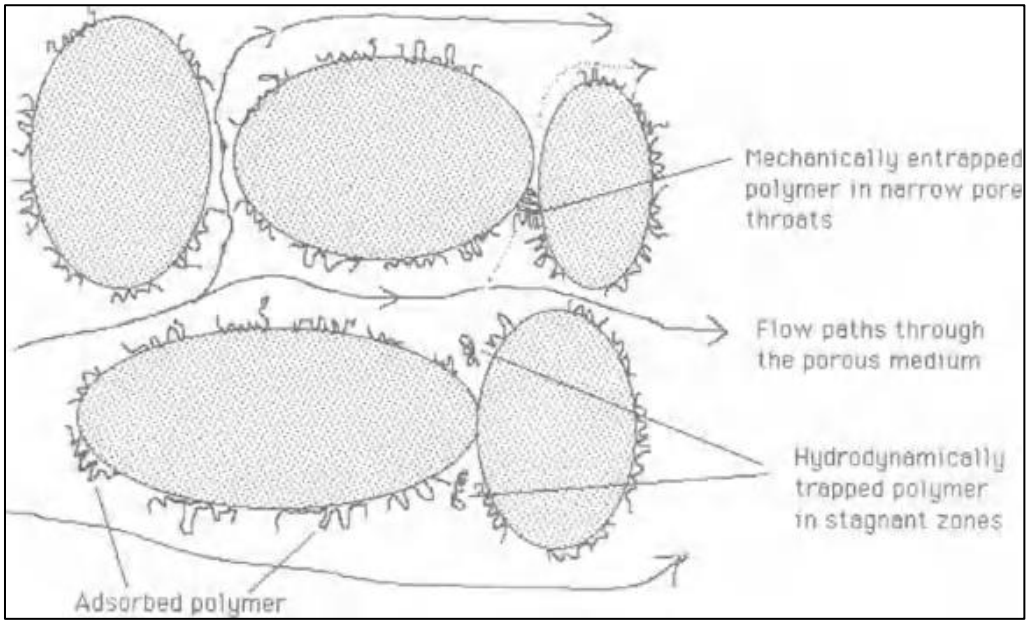

Figure 2-8: Polymer retention mechanisms

2.4.2 Hydrodynamic Retention

Hydrodynamic retention is one of the most complicated and least understood mechanisms of retention. It was first noticed by changing the flow rate in experiments which already attained the steady state or the dependence of retention on flow rate in experiments [51-53]. It is characterized by abnormal production of polymer when flow rate is reduced suddenly[54].Because of this it is possible to produce the effluents of high concentration than the injected sample. This type of retention seems to be reversible as the amount of polymer retained during the increase in flow rate is produced as the flow rate is reduced[51].Another way to demonstrate it is by stopping the flow and then restarting. This will also result in an increment in the concentration of effluent. This was studied by Zaitoun and Kohler [55] in xanthan adsorption experiment in sand and kaolinite packs. Another study by Sorbie et al[56] on HPAM also showed the same thing. Chauveteau and Lecourtier [57] explained the criterion for the hydrodynamic entrapment to occur. They concluded that the radius of gyration of molecule should be more than half the dimension of restriction in pore structure. The Peclet number for the polymer flow should be high enough to avoid the diffusion of molecules towards the region of large restriction and hydrodynamic barriers are small enough not being able to force the molecules through restrictions. The high Peclet number requirement is the reason why hydrodynamic entrapment is observed when the flow rate is increased. The first condition of radius of gyration is met in flow through low permeability and small particle size. They also concluded that hydrodynamic entrapment of semi-rigid polymers such as xanthan is less

likely to occur as its structure makes it possible for hydrodynamic orientation to be parallel with the opening axes. Overall, it can be summarized that the hydrodynamic retention is a rate-dependent mechanism which is less understood and can be avoided. Also, the contribution of this retention mechanism is not very large to the overall levels of polymer retention hence it is not a very important effect in field-scale polymer floods. However, it should be understood carefully to draw proper conclusion and adsorption results from the core flooding experiments.

2.4.3 Mechanical Entrapment

Mechanical retention of polymer molecules is similar to a filtration process where large molecules are retained by small pores or lodged in narrow flow channels. This type of retention may lead to blocking of the reservoir if the entrapment is acting upon the average size of distribution. Polymer showing such type of behavior will not be selected for polymer flooding. This type of entrapment mechanism dominates in the porous media where pore radius (r_p) < 3* radius of gyration(R_G), which happens in low permeability media [58]. This is one big reason that the polymer flood is used in high permeability formations [59-61]. Gogarty [62] estimated the molecular size of HPAM molecules in the porous media and compared it with the pore size, concluding a significant retention as it flows through the Berea sample. In one of his experiments it took 10 pore volumes of the polymer injection to reach the input level concentration confirming significant mechanical retention. This can be visualized by assuming the pore structure as a large interconnected network with a huge number of alternative 'routes' connecting the inlet

and the outlet of a core. Some of these network paths would consist of narrow pore throats. Thus, as the polymer solution pass through these narrow paths, the molecules would be trapped. This will block these pores and there may even more upstream of the blockage. If this representation of mechanical entrapment is correct then the concentration in effluent would reach the injected concentration after many pore volumes have been injected. Mechanical entrapment is confirmed when the static adsorption is less or negligible compared to dynamic adsorption because the extra amount accumulated in flow experiment is attributed to mechanical entrapment. This was studied by Szabo[63, 64] .He injected HPAM in Berea cores and sandpack and compared the static adsorption results which were of the level of 3-4 μg/g and independent of the polymer concentration used to the retention levels observed in the dynamic flow tests which were up to five times larger than these figures, indicating the leading role of mechanical entrapment. He injected two concentrations 600ppm and 1200ppm and found the retention to be 15 μg/g and 50 μg/g respectively. The dependence of retention on concentration also provides an evidence of the presence of mechanical entrapment. Another study done by Dominguez and Willhite [52] on HPAM also showed the same effect of concentration. Vela et al. [65] studied the effect of permeability and concentration on the retention of polyacrylamide. They concluded the retention to be concentration and permeability dependent. Figure 2.9 shows the retention level as a function of permeability.

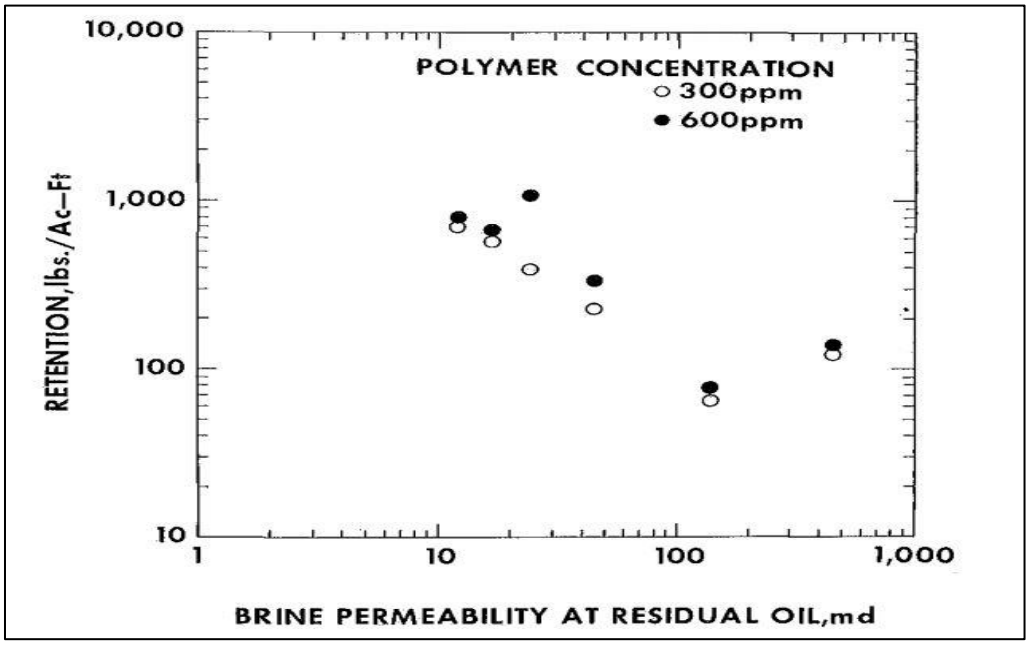

Figure 2-9: Polymer retention as a function of permeability

As discussed above the process of mechanical entrapment is very similar to filtration. This filterability of high molecular weight hydrolyzed polyacrylamide was investigated by Gogarty and Smith independently[62, 66]. Gogarty passed a 400ppm of polymer solution through different sizes nuclepore filters. The effective size determined by him is from 0.5 to about 2.0 microns in a solution free from electrolyte while it is from 0.4 to about 1.5 microns in a 600 ppm NaCl solution. This also shows the effect of salts on the hydrodynamic molecular size of ionic polymers. Smith predicted the size of the same polymer in 0.5% NaCl solution which came in the range of 0.3 to about 1 micron. Figure 2-10 shows the results from Gogarty.

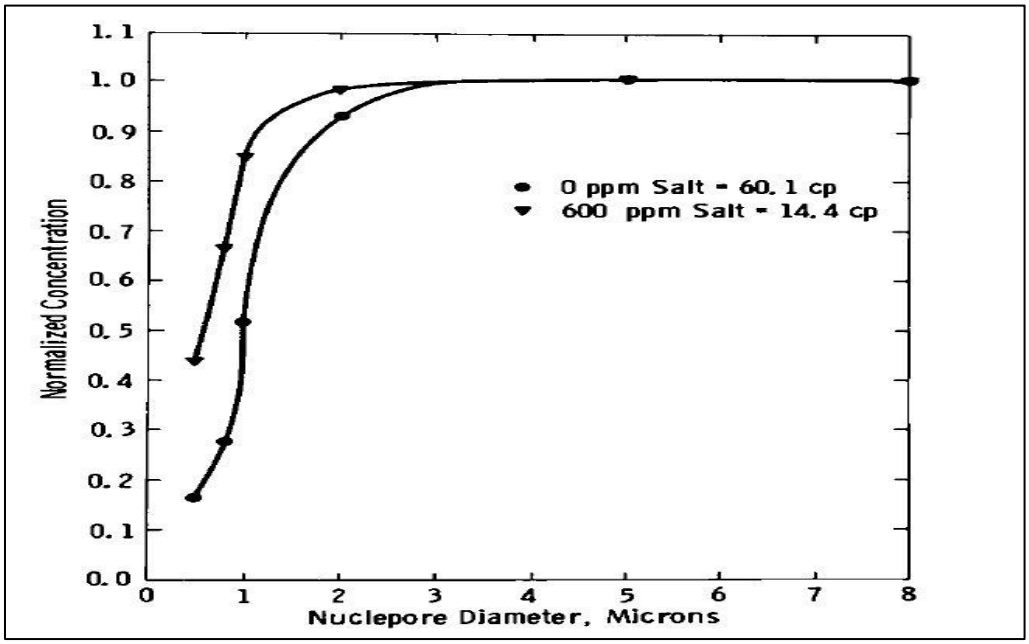

Figure 2-10: Filtration of HPAM with Different Size Nuclepore Filters

Possible sites of polymer retention by mechanical retention are shown in Figure 2.11. The first site i.e. the surface sites are occupied during the adsorption which will be discussed later in other section. The remaining retention sites illustrates how because of mechanical forces, the size of the constriction or the size of the polymer coil the polymer molecules could become entrapped.[67, 68]. Crevice sites are the sites which capture the polymer coils by wedging it in the contact areas near two grains or the convex surfaces of two grains. Constriction sites on the other hand are those sites which seize the molecules because they have pores which are too small for the polymer coil to penetrate. Cavern sites can be visualized as those sites which capture the molecules because of a decrease in

velocity caused by a tortuosity in flow path or a reduction in permeability in the direction of flow[69].

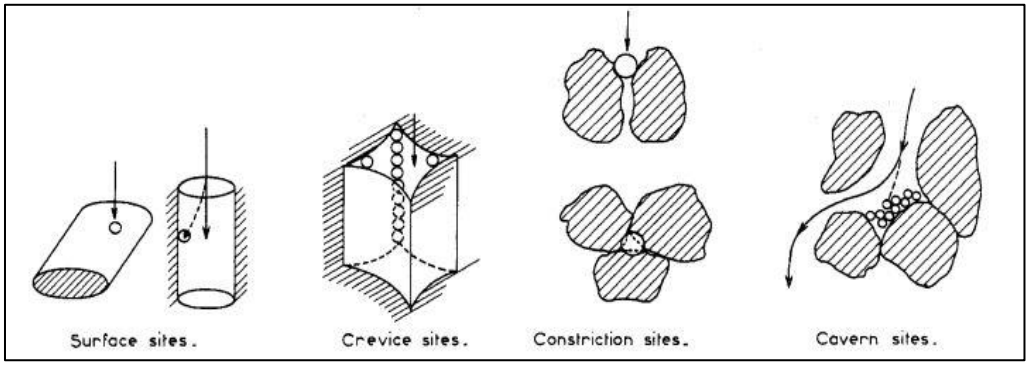

Figure 2-11: Polymer retention sites in porous media

A widely used and important term in polymer flooding is *inaccessible pore volume* which is closely related to the mechanical entrapment mechanism. This effect was first reported in 1972 by Dawson and Lantz[70]. They observed that when there is no adsorption or the adsorption level in porous media has reached the saturation the polymer molecules run faster than the tracer.

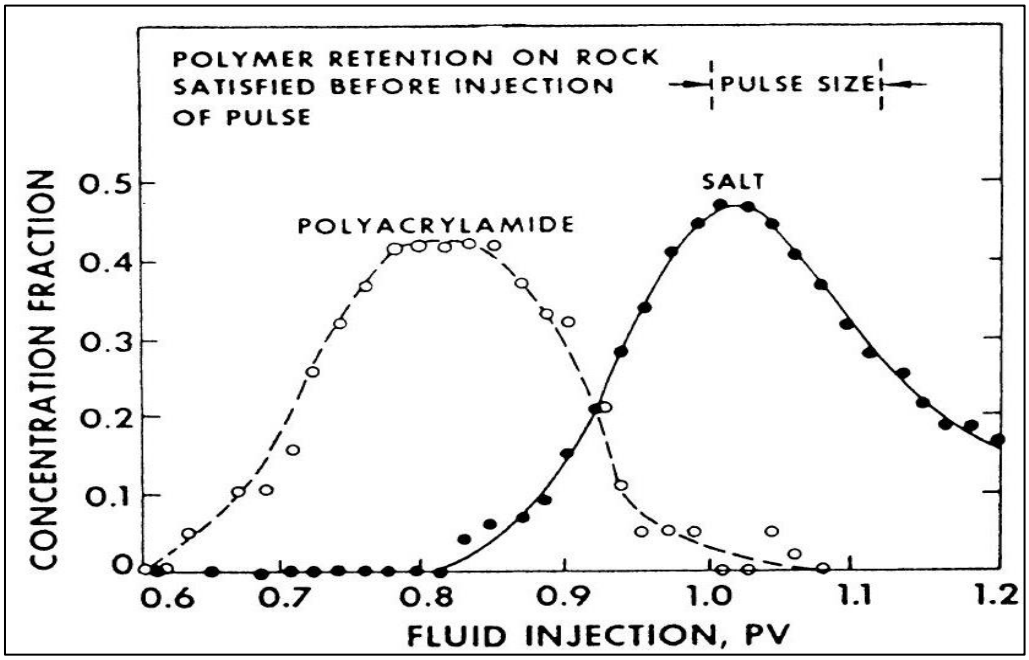

Figure 2-12: Early breakthrough of polymer due to IPV

This was because the polymer molecules flow only through the pores which are larger in size leaving behind a considerable amount of pores which can't be accessed by the molecules. They termed it '*inaccessible pore volume'* IPV. The same effect is shown in figure 2.12. IPV has been experienced with all the polymers (synthetic, biopolymers) flowing in different types of porous media. The IPV could range from 1to 30% or more depending upon the type of porous media[71]. IPV becomes more pronounced as the ratio of permeability to porosity decreases[13].

2.4.4 Polymer Adsorption

Adsorption is a more fundamental property of polymer-rock system and can't not be avoided or reduced to the level to which the other two retention mechanisms can be prevented. It is reported as mass of polymer/ mass of rock or by mass of polymer/unit area of rock. Polymer adsorption is generally classified based upon the type of interaction between the surface and polymer. If the energy change during the process is more than twice of k_BT the adsorption is termed as chemisorption and considered irreversible due to the presence of high desorption energy. Chemisorption involves the formation of a covalent bond between the polymer and surface which hold it firmly. If the attraction is weak and is of the order of k_BT , it is termed as physisorption[72].Physisorption proceeds through Van der Waal forces , electrostatic interactions or hydrogen bonding[73]. Figure 1.4 shows the two cases. For large polymer molecules the sum of the adsorption energies of monomers will lead to a high energy change which makes physisorption irreversible. This leads to isotherms which have a high-affinity nature, i.e. at low concentrations, the adsorption density rises sharply, while at higher concentrations it reaches a pseudo-plateau [72]. Adsorption of polymer over surface only proceeds if the attractive interaction exceeds the entropy lost associated with adsorption[74]. The adsorption of a polymer molecule from bulk solution to being fully attached on to the surface can be seen as a mechanism involving number of stages as a function of time. Initially, the molecule diffuses nearby the surface and makes a stagnant layer. Then the molecule approaches near the surface so as to be attracted by the surface resulting in adsorption which is faster

than the bulk diffusion. After it the polymer molecule collapses and spread onto the surface[75].On a whole, the polymer molecules set their conformations which correspond to minimum free energy[76]. It is thought that the polymer adsorbs as a series of trains, loops and trails over the solid surface as shown in Figure 2-14[11, 76].

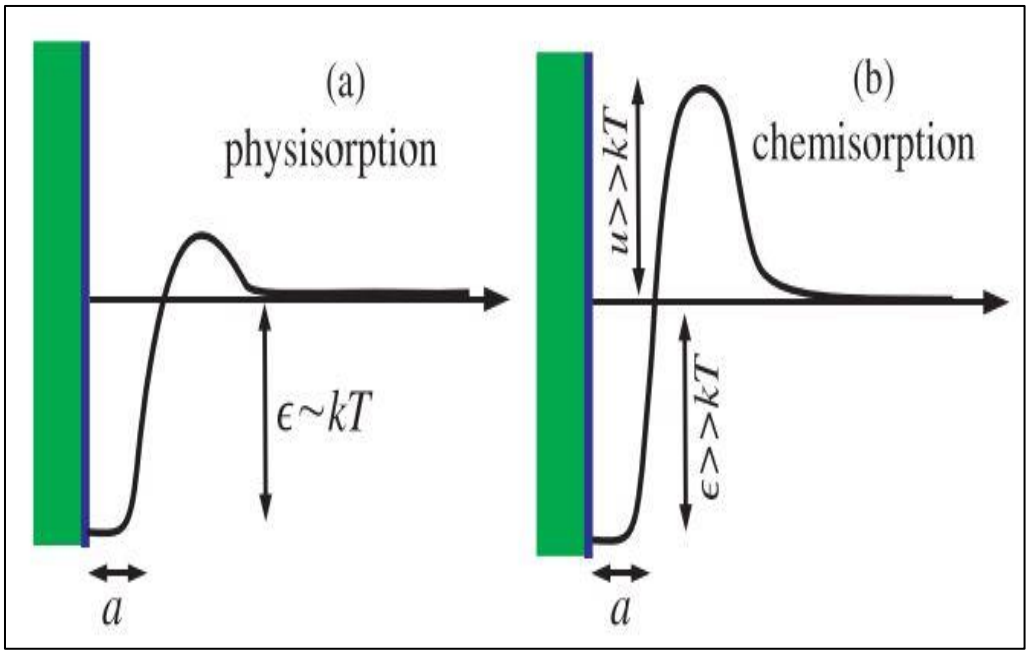

Figure 2-13: Types of Adsorption (a) Physisorption (b) Chemisorption

Trains are the segments of the polymer molecule which are attached to the surface and are the bound section of the molecule acting as the anchors of molecule. The extended parts at both the ends of the molecule are referred as tails. In between the trains are the loops which extend into the solution. Trains are the longest portion of the molecule and have a dominating role in effective hydrodynamic thickness of the adsorbed layer[77]. The polymer segment density as a function of distance from the interface can be viewed as shown in Figure 2-15[25].During the adsorption of the molecule a number of

thermodynamic interactions take place. These are between the segment-surface, segment-solvent and segment-segment. These interactions have an enthalpy associated to them. The conformational entropy term which is a measure of the number of chain configurations available to the adsorbed molecule to the number available for a free molecule in solution also governs the process. The entropy change by the displacement of solvent molecules from the surface by the polymer molecules is also responsible for the thermodynamics of the process. It is also important that the adsorbed polymer does not have a fixed configuration; rather different segments of the polymer chain are in constant motion changing from attached train segments to unattached loop or tail segments[11].

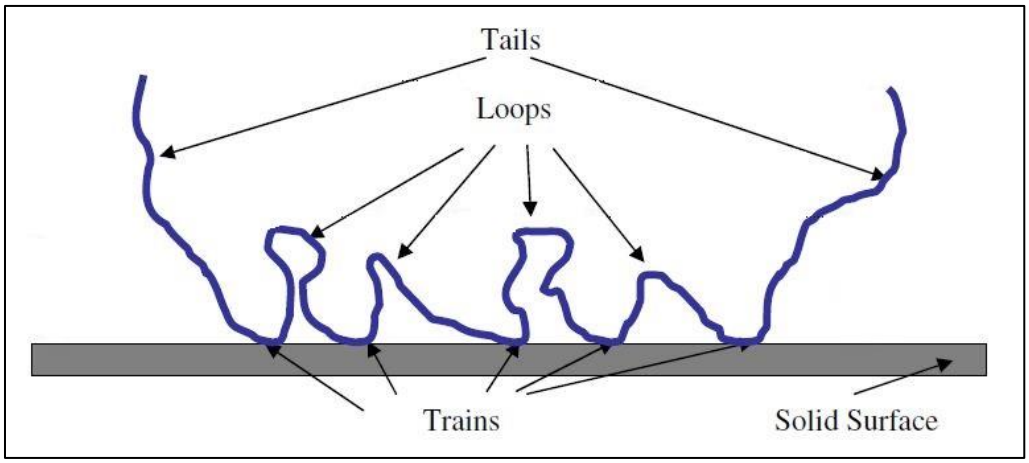

Figure 2-14: Conformation of adsorbed molecule over the surface

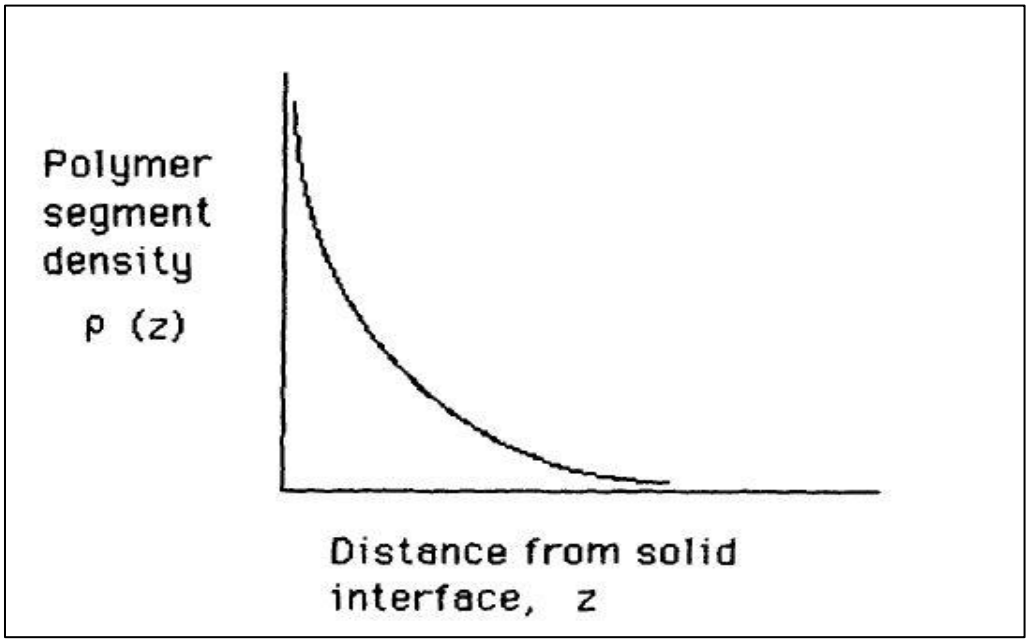

Figure 2-15: Segment distribution function

The plateau Γ_p adsorption density strongly depends on polymer flexibility. For polymer like xanthan which is rigid and is flattened on the surface, Γ_p is independent of molecular weight and is governed by polymer-polymer electrostatic interactions so that the adsorption value increases from100 µg/m² to 600-800 µg/m² as the electrostatic repulsion decreases. For polymers which are flexible such as polyacrylamides, adsorption density goes up with molecular weight primarily at high adsorption energy such as in the case of anionic HPAM adsorbing on a negative surface like sand and above critical salinity , the adsorption value may vary intensely from low values of 80 µg/m² which corresponds to 0.3 monolayer when adsorption energy is nearly zero, to very high values (8000 µg/m² or 30 monolayers) when adsorption occurs on a positively charged surface at low

salinity[78-80].There is another view on dependence of adsorption capacity on molecular weight which says the adsorption density will decrease with increasing molecular weight because the adsorption sites are more accessible to low molecular weight molecules than the higher ones[81].

One other important factor in adsorption studies is the time required to attain the equilibrium. Most of the time the equilibration time is dependent upon the time of access to the surface. As discussed previously as the macromolecules reach the surface a number of changes are expected to occur. These changes are:

- Conformation change from bulk to adsorbed state
- Adjustment in conformation due to the arrival of new molecules
- Exchange of molecules due to the preferential adsorption of high molecular weight fractions
- Change in charge density near the surface which results in retrogradation of polymer and surface ionization. [25, 82]

During the early stages of adsorption, each macromolecule will have the same conformation as in solution. As the thermodynamic equilibrium is approached molecular conformation is expected to be modified with an increasing number of segments which will be in contact with the solid surface for both flexible and rigid polymers. For polyelectrolytes the adsorbed train will align in an increasing number. This reorganization inside the adsorbed layer occurs irrespective of the presence of free molecules on top of the adsorbed layer. However, the presence of free molecules on the

top will decrease the reorganization time t_R. This reorganization i.e. desorption and re-adsorption of these trains in other sites and the desorption step which is assumed to be the slower step is accelerated if free molecules start competing to decrease the probability of re-adsorption at the same location. This is the reason for an increment in exchange rate with an increment in polymer concentration [83]. Since the reorganization time tR is assumed to be a function of time of desorption of trains and loop reorganization, it is (t_R) is expected to increase both with segmental adsorption energy and the average number of segments in a train[57]. The exchange of macromolecules between solution and adsorbed layer occurs even with a strictly monodisperse polymer. This exchange requires penetration of free molecules through adsorbed layer overcoming osmotic pressure due to higher polymer concentration inside adsorbed layer. Although penetration implies a reputation process expected to be slow, this time is thought to be negligible compared to train desorption time. However, the rate of exchange is molecular weight dependent and is higher when high molecular weight molecules replace lower molecular weight ones in the adsorbed layer, leading to a preferential adsorption of high molecular weight molecules. In other words, the proportion of high molecular weight molecules is expected to be higher in adsorbed layer than in free polymer solution at thermodynamic equilibrium [57, 84]. Thus, the adsorption of polymers over rock surface depends on a number of factors like type and size of polymer molecules, concentration of the polymer, and type of rock, salinity and temperature. It may take several days to reach the adsorption equilibrium in laboratory

2.4.4.1 Effect of Concentration on Adsorption Level

The effect of concentration on adsorption of polymers onto rock surface has been a topic of immense interest and controversy. There is an ample amount of literature present to address this issue with some researchers favoring the Langmuir type adsorption isotherm of polymers [85-90]. Langmuir isotherm assumes the adsorption to be reversible and concentration dependent is used in simulators to represent the polymer retention (adsorption) in porous media [91-93]. On the other hand, researchers also concluded the adsorption of macromolecules on surfaces to be an irreversible process [54, 94, 95]. Guoyin et al.[96] investigated the effect of concentration of hydrolyzed polyacrylamide retention in porous media. They break the adsorption curve in three regimes depending upon the concentration. The first regime is the diluted regime and the adsorption in this regime is independent of concentration, similar to this is the third regime i.e. the concentrated regime which is also concentration independent. The middle portion in the curve is semi-dilute regime which is concentration depended and the adsorption increases with an increase in concentration. In the dilute region, polymer molecules are as a free coil in solution and take a flat orientation on the rock surface during adsorption. Most of the polymer is in contact with the surface and it is given a term 2D by Peterson and Kwei [97] . Polymer adsorption is continued until the maximum surface coverage is reached. This region can be utilized to reduce the polymer retention by injecting a low concentration of sacrificial polymer. The semi dilute regime is termed as 3D adsorption regime. In this regime, some polymer molecules will be adsorbed with all their segments

in contact with the surface and some partially. So, an increase in concentration will increase the total adsorption. In the third regime one end of the polymer is attached to the rock surface while majority of molecule's portion is in free solution. Increasing the concentration will not affect the adsorption as all the adsorption sites have been filled or occupied, so the adsorption is concentration independent. This whole mechanism is shown in Figure 2-16.

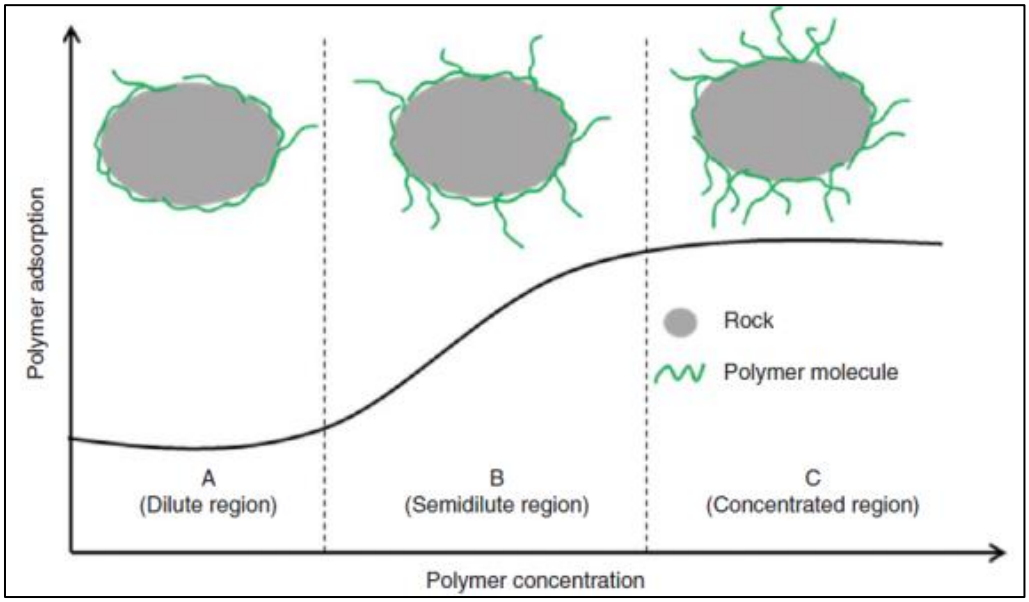

Figure 2-16: Proposed polymer adsorption mechanism by Seright

2.4.4.2 Reported Adsorption Plateau Levels for EOR Polymers [54]

Table 2-5: Adsorption of HPAM

Polymer	Conc. (ppm)	TDS (ppm)	Porous Media (ppm)	Permeability (md)	Retention µg/g
HPAM	500	Brine	Miocene Sand	53	120
HPAM	500	0	Ottawa Sand	-	160
Pusher 700	500	Surfactant	Reservoir Core	80	13
HPAM	300	13,340	Reservoir Core	17	100
Pusher 500	750	20,000	Berea Sandstone	550	26
Pusher 700	750	20,000	Berea Sandstone	550	23
Pusher 1000	750	20,000	Berea Sandstone	550	28
HPAM	750	1,000	Reservoir Rock	200	7
HPAM	750	70,000	Reservoir Rock	300	72
HPAM	750	1,270	Reservoir Rock	1500	27

Table 2-6: Adsorption of Xanthan

Polymer	Conc. (ppm)	TDS (ppm)	Porous Media (ppm)	Permeability (md)	Retention µg/g
Kelzan M	750	Brine	Nevada Sand	6000	9
Xanflood	750	20,000	Berea Sandstone	550	14
Xanthan Broth	750	Surfactant	Reservoir Core	80	13
Biopoly mer	750	Brine	Berea Sandstone	550	13.5
Xanthan	1,350	-	-	-	151
Xanthan	2,450	-	-	-	114
Scleroglu can	560	-	Sand	-	58
Scleroglu can	850	-	Sand	-	117
Scleroglu can	1,450	-	Sand	-	149
Xanthan	500	-	Reservoir Rock	1500	76

2.5 Chemistry of Schizophyllan

Schizophyllan is a non-ionic, homoglucan polysaccharide which is an extracellular product of *Schizophyllum Commune*. It has backbone of β glucopyranose (Figure 2-17) residue units linked at 1→3 position with a single β glucopyranose linked via 1→6 linkage to every third unit of the backbone (Figure 2-18).In aqueous solutions it adopts a triple helical structure which is the ground behind its well-known viscosifying properties and thermal stability up to 120°C[98].It dissociates into a single chain dimethyl sulfoxide(DMSO) and regains the triple helical structure if DMSO is exchanged with water[99]. The triple helix has a pitch (per residue) of 0.30± 0.02nm and diameter of 2.6±0.4nm.The triple helix structure is stabilized by interchain hydrogen bonds[100]. It forms physical gels with borate ions $B(OH)_4$ as a result of chelation of borate ions through the hydroxyl groups[98]. It has a molecular weight

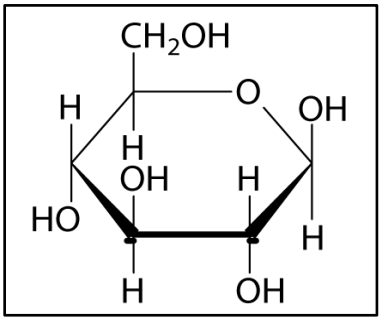

Figure 2-17: Structure of β-D-Glucose

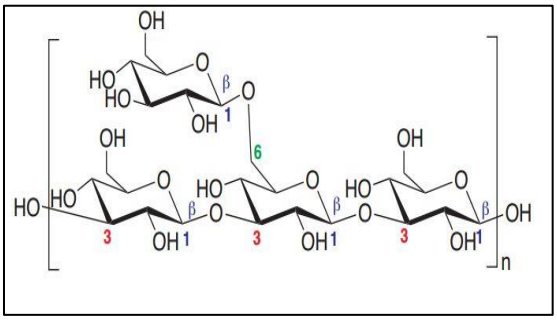

Figure 2-18: Structure of Schizophyllan

2.6 Mechanism of Adsorption

Starch which is a polysaccharide is used in mineral floatation since it was patented by Lange as a selective adsorbate for the removal or depression of phosphate from quartz [101].Carboxymethyl cellulose and guar gum are used to depress hydrophobic gangue minerals such as talc and graphite. Guar gum is also used in potash floatation process to adsorbed preferentially over slimes such as clays, carbonates and quartz so that these particles do not adsorb a cationic amine collector which is meant for the floatation of potash [102].Despite the extensive use of polysaccharides in adsorption applications, the adsorption mechanism of polysaccharides over mineral surface is not completely understood. Several mechanisms have been proposed over time which will be discussed one by one.

2.6.1 Hydrogen Bonding

Despite the low strength of hydrogen bond which is of the order of 2×104 joule/mole the cumulative energy of adsorption becomes significant for polysaccharides with high molecular weight[103].Hydrogen bonding occurs between the hydrogen atom of polysaccharide and oxygen atoms present on mineral surface. If the polysaccharide is able to form hydrogen bonds with mineral surface oxygen atoms, then before adsorption each of the species should be involved in hydrogen bonding either with water or internally so that the formation of a polysaccharide-mineral hydrogen bond is a result of two hydrogen bonds split-up. Because the energetics of such a process is not easily justified this mechanism can only be applied if there are factors available which will

contribute to the polysaccharide-mineral hydrogen bond stability[104].Some results have also been published including one which uses urea a hydrogen bonding breaker to examine the role of hydrogen bonding. The results show a decrease in adsorption value of polysaccharide in the presence of urea giving this mechanism a ray of hope and can not to be ruled out completely[105, 106].

2.6.2 Electrostatic Interactions &Salt linkage

Electrostatic interactions are important while dealing with ionic polymers. In our case the polymer is a polysaccharide which is a non-ionic polymer. This leaves a very narrow space for these types of attractive or repulsive interactions. However as discussed previously, Schizophyllan forms a physical gel with borate ions which raises the probability of cations present in the brine acting as a bridge for the adsorption and hence the possibility of adsorption proceeding through this type of mechanism.

2.6.3 Acid-Base Interaction

The hydroxyl groups (-OH) present in polysaccharide and over the mineral surface have been proposes to play an important role in adsorption mechanism. The hydroxyl groups on mineral surface depending upon the metal ion to which it is attached can act as a Bronsted acid (proton donor) or Bronsted base (proton gainer).It has been proposed that mineral surface will donate an –OH group with two protons coming from the polysaccharide hydroxyl groups to form a five membered polysaccharide-metal ring complex. According to this mechanism, during the interaction with polysaccharide

mineral surface metal-hydroxylated species act as a Bronsted base so that stronger basicity of the mineral surface will lead to stronger adsorption. Also, the natural polysaccharides such as dextrin, guar gum and starch adsorb strongly over metal oxides/hydroxides of Pb, Ni, Ca, and Mg compared to Si. This is because the former are more basic as compared to later which is acidic[107]. This has been supported by the fact that glucose adsorbed in a considerably large amount on alumina surface than on acidic alumina surface[108].It is known that the isoelectric point(iep) of solid oxides is an indication of Bronsted character with higher iep representing a basic surface compared to lower iep value which depicts an acidic surface. Now, the ieps of calcite, lead, nickel and magnesium are between 9 -12, compared to quartz which has an iep 2[109-112]. This indicates stronger adsorption over basic surface compared to acidic. This iep concept is also supported from the use of starch in separation of oxide minerals from quartz. Quartz which has an iep around 2 deprives itself from polysaccharide adsorption while iron oxide minerals which have ipes around 6-7 preferentially allows polysaccharide to get adsorbed over its surface and is depressed[107].Apart from the basicity of the surface, the density of surface metal hydroxyl groups also affects the adsorption with higher densities resulting in stronger adsorption. This was confirmed by the fact that the adsorption of Baker dextrin on Pb-coated quartz was much lesser than on the galena surface because of the lower density of hydroxylated groups on the Pb-coated quartz surface [113, 114].However, the adsorption of guar gum over oxide minerals have been reported to be

pH independent indicating no role of acid-base interactions rather than supporting the proposed hydrogen bonding theory[115].

Chapter 3: Static Adsorption of Schizophyllan

3.1 Materials and Methods for Static Adsorption of Schizophyllan

Minerals: Four minerals calcite, dolomite, kaolin and silica as shown in Table 3-1 are used in static adsorption experiments. These are the same minerals which were used by Kun Ma[116] at Rice University, a collaborator university of The Petroleum Institute. The same minerals were used by Leyu Cui in his experiments[117] .The BET surface area of these minerals was measured using a Quantachrome Autosorb-3b BET Surface Analyzer which uses multipoint BET to fit the adsorption of the Nitrogen gas. Minerals from the same stock were shipped from Rice University for the adsorption experiments. BET Surface area, particle size and the zeta potential at the adjusted pH is listed in Table 3-1. This zeta potential was measured in 0.01 mol/L NaCl solution with a suspension of 1.0 wt% absorbent material. Further analysis of these rocks will be presented in the following chapter.

Table 3-1: Characterization of minerals used

Mineral	BET Surface Area (m^2/g)	Size(μm)	Resource	ζ potential (mV)
Calcite	1.67	5	Alfa Aesar	4.2 ± 7.2 (pH 9.8)
Dolomite	0.97	≤74	Car Pool Co.	8.0 ± 3.5 (pH 10)
Kaolin	26.60	0.1 – 4	Sigma Aldrich	-38.0 ± 7.6 (pH 4.8)
Silica	1.16	≤10	US Silica Co.	-47.3 ± 2.5 (pH 6.0)

Reservoir Minerals: The other set of minerals used were supplied by ADNOC from their fields. The minerals were crushed in a basic analytic mill from IKA (Cat #: IKA2900000) to make them homogenize and be able to use it for adsorption experiments.

Table 3-2: Reservoir Rocks Used for Adsorption

Mineral	Resource
R-5	ADNOC
R-9	ADNOC
R-11	ADNOC
R-138	ADNOC

The BET surface area of these reservoir minerals was measured according to the method explained later on in this chapter.

3.1.1 Chemicals &Salts

Schizophyllan

Schizophyllan was supplied by Wintershall-Germany as a broth. Solutions of different concentration in brine were prepared by diluting the stock solution. A lyophilized powder form was also received from Invivogen-France. MW as specified by the supplier is 3-4 M- Dalton.

Salts

$CaCl_2.2H_2O$, KCl, $MgCl_2.6H_2O$, $NaHCO_3$, NaCl, Urea were obtained from Merck – Germany.

3.1.2 Characterization of carbonate minerals

X-ray diffraction (XRD): The crystallographic structure of the carbonaceous materials to know the physic-chemical makeup was studied using an X-ray Diffractometer (PANalytical, X'pert Pro MPD), with a Cu-Kα radiation (Figure 3-1, [118]).

Figure 3-1: PANalytical X'Pert Pro MPD X-ray Diffractometer

Scanning Electron Microscope (SEM): An SEM was used to study the morphology and mineral identification of the samples. Approximately 20 μg of the samples were set on standard aluminium SEM sample holders (stabs) using conductive super glue and an FEI Quanta 250 FEG SEM (Figure 3-2, [119]) was used for analysis. Imaging studies were performed at 20kV.

Figure 3-2: Quanta SEM

Fourier Transform Infrared Spectroscopy (FTIR): FTIR spectra of Schizophyllan and all the minerals used was done using Fischer Scientific FTIR instrument. For all samples the number of scans was set at 64 with a resolution of 4 cm^{-1} .

N2 Adsorption: Nitrogen isotherm at 77K was used to determine the surface area of the samples by means of a surface area and pore size analyzer (Quantachrome, Autosorb 6iSA). Degassing of samples was done for 8 hours at 423K prior to N2 adsorption, in order to remove any residual water and/or organic vapors. The Barrett-Joyner-Halenda method (BJH) was used to determine the pore size distribution (PSD).

Figure 3-3: Quantachrome surface area and pore size analyzer

3.2 Schizophyllan Concentration Determination

Concentration determination is a critical step in studying the adsorption behavior of polymers, especially for polysaccharides. A number of methods like size exclusion chromatography, radioactive labelling, organic carbon content, metachromatic method, precipitation, viscosity measurement, refractive index etc. have been reported [120]. Each of the method has some technical inefficiency because of which a different method is used. This method is known as Phenol-Sulphuric Acid method. It was first introduced by Dubois in 1956 [121].The method developed is one of the most widely utilized method to determine the total sugar content in samples and the work has been cited more than 30,000 times since it was reported. This method works on the breakdown of polysaccharide into monosaccharides which are then dehydrated in the presence of Sulphuric acid to give hydroxymethylfurfuraldehydes, which reacts with phenol to form a golden color complex proportional to the polymer concentration(at a fixed phenol amount) with a peak at around 480-195 nm. The whole reaction scheme is shown in Figure 3-4:

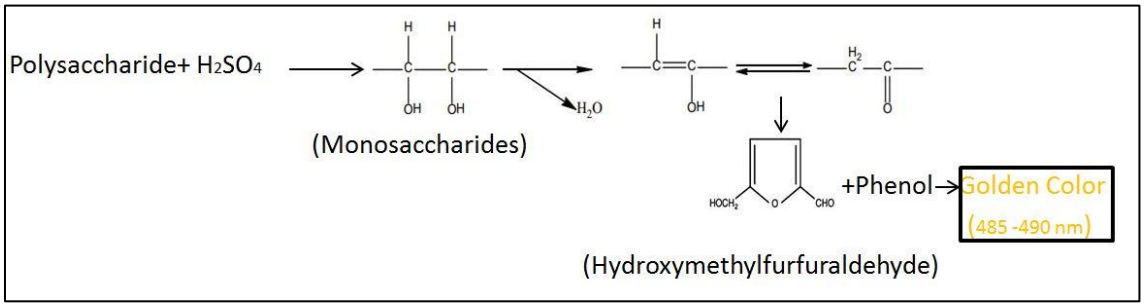

Figure 3-4: Phenol Sulphuric Acid Method Reaction Pathway

Calibration line: Calibration line is generated by measuring the absorbance of known concentration samples. This line is used to estimate the concentration of supernatant sample after adsorption. The first experiment to validate the authenticity of the method was run for polymer solutions in reservoir brine obtained from ADNOC. The entire procedure is as follows:

Step1: Prepare multiple samples of known concentration, 5,10,15,20 and 25 ppm. To check the error in the method seven different samples of each concentration was made.

Step2: Take 200 μl of solution from the sample prepared and pour into the 15ml tube which already has 2800 μl water. To this total solution of 3000 μl add 50 μl of phenol (80% by weight in water). Repeat the same procedure for all the concentrations and their replicates.

Step3: To each of these tubes, add 5ml of conc. (95%) H_2SO_4. This would result in an exothermic reaction which will give a golden color complex.

Step4: Wait for the reaction to complete the tube is back to normal temperature which will take around 2 hours.

Step5: Measure the absorbance of each tube to get an absorbance vs concentration curve. Table 3-3 shows the absorbance value of each concentration with all their replicates along with the average of the seven values with standard deviation. Figure 3-5 shows the calibration line with the error bars. As clear from the standard deviation, the method is reproducible with minor error of less than 3%.

Table 3-3: Absorbance vs Concentration off all replicates

Conc. (ppm)	Replicate Number								St.dev.
	1	2	3	4	5	6	7	Avg.	
5	0.234	0.210	0.218	0.212	0.185	0.204	0.201	0.209	0.015
10	0.363	0.353	0.362	0.357	0.33	0.362	0.389	0.359	0.017
15	0.452	0.440	0.460	0.436	0.464	0.445	0.444	0.449	0.010
20	0.558	0.547	0.605	0.551	0.566	0.547	0.545	0.560	0.021
25	0.700	0.657	0.702	0.683	0.687	0.694	0.690	0.687	0.015

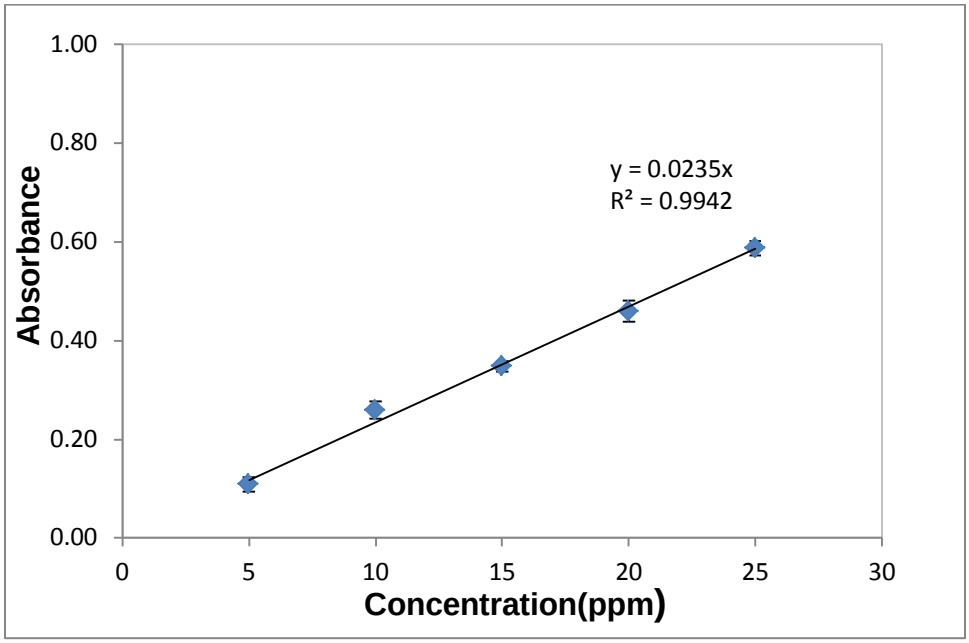

Figure 3-5: Absorbance Vs Concentration

3.3 Adsorption Experiment (Static)

(a) Firstly, a stock solution of required salinity and biopolymer was made by diluting the stock solution received from Wintershall. For some experiments reservoir brine obtained from ADNOC is also used.

(b)A known amount of rock samples/crushed rock was added to the known volume of polymer solution in a 50 ml corning centrifuge tube (Corning Product #430290).

(c)The tube was flushed repeatedly with nitrogen gas and then sealed. Nitrogen blanket was used in all the experiments to prevent biodegradation.

(d)The tube was placed over a reciprocating water bath shaker at 200 rpm for time required to attain the equilibrium. The temperature of the shaker can be maintained from room to 99℃ by placing a top lid to prevent the evaporation of water.

(e)After that, the tube was kept static over night before it was centrifuged for 30 minutes to settle down all the rocks.

(f)The above process was replicated in parallel for another tube without any addition of rock. This tube served the purpose of calibration standard. This will be called **reference sample** in this thesis.

(g)After the centrifugation, supernatant samples were used for titration. From each tube three samples were drawn to act as replicates.

(h) The adsorbed amount was calculated by getting the final concentration from calibration curve.

3.4 Experiment Scheme

Effect of several parameters on adsorption capacity to understand the adsorption mechanism is studied. The experiment plan is presented in Table 3-4.

Experiment Condition	Mineral Type	Temp.(°C)	Salinity	Background Ions
Levels	4Natural,4 Reservoir	Different	Different	Different

More details of the entire experiment with experiment condition will be included in results section.

3.5 GPC of Supernatant after Adsorption:

GPC of the supernatant after adsorption experiment was done in order to characterize the type of chains which are adsorbing over the calcite surface. If the higher molecular weight molecules are adsorbing in greater extent we will see a diminishing peak corresponding to the molecular weight. The GPC was done using Agilent 1260 HPLC System with a RI Detector. The column used is PL aquagel-OH MIXED-M 8 μm column .The schematic of the system is shown in Figure 3-6[122]. A flow rate of 0.5 ml/minute and 2 injections were used for the experiment. The system was stabilized for 24 hours before use and the single experiment time was 30 minutes.

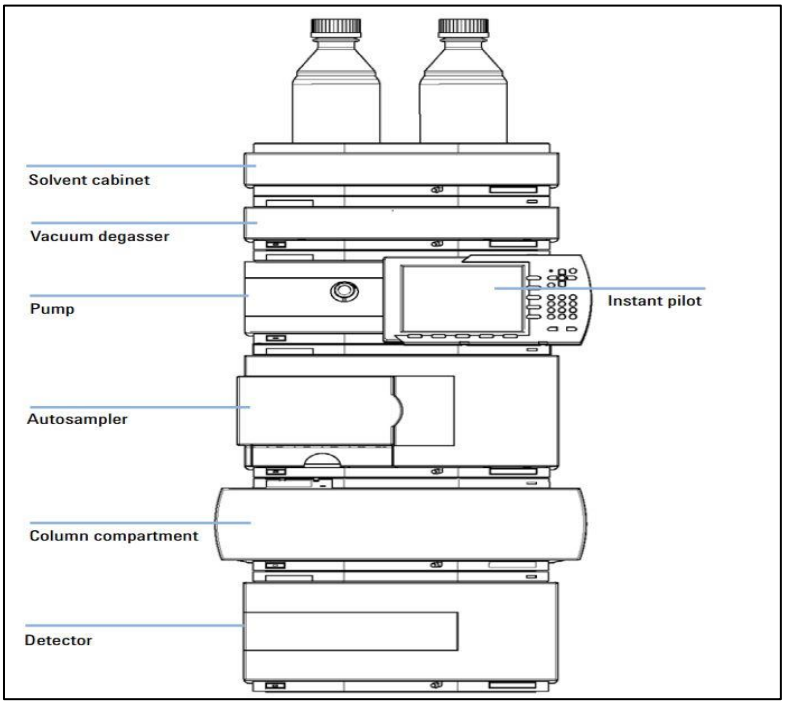

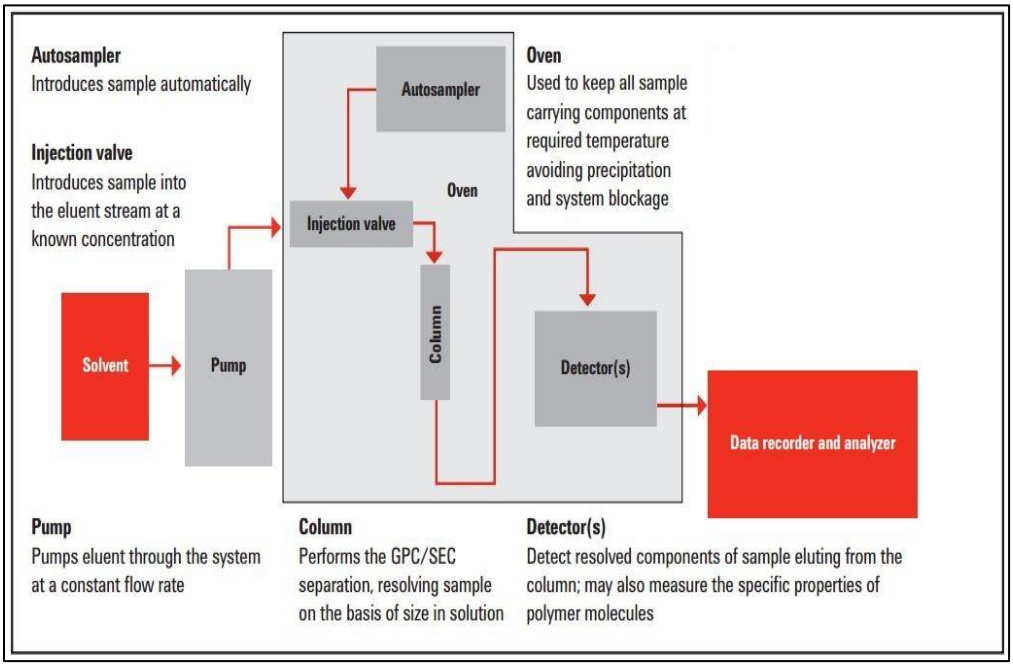

Figure 3-6: Schematic of GPC

3.6 Microcalorimetry of Static Adsorption

The enthalpy of adsorption as determined by the famous Clausius-Clapeyron equation can lead to erroneous and completely misrepresented results. There have been cases when the enthalpy evaluated by this equation is positive while the actual enthalpy is negative[123]. To avoid this, the enthalpy of adsorption is calculated by using Precision Solution Calorimetry using the TAM III instrument from TA Instrument[124]. TAM III employs the thermostat technology to precisely control the liquid bath temperature to within 0.0001 ℃, and can be operated in isothermal, step-isothermal or temperature-scanning mode. It has a baseline drift of 1-4 mJ with an accuracy of less than 0.1%. The polymer solution is filled in the vessel and the powder mineral is filled in SolCal Ampoules which is mounted on the mixer. The whole setup is lowered into the TAM III and once the system stabilizes the ampoule is crushed which is the start of the adsorption process. The system keeps a track of temperature which can be converted to Heat Flow. Figure 3-7 shows the SolCal setup which is lowered into the TAM III.

Figure 3-7: SolCal Setup

3.7 Static Adsorption: Results and Discussion

3.7.1 Characterization of material used

a. Schizophyllan:

Figure 3-10 shows the FTIR spectra of Schizophyllan. The peak around 3300-3450 cm^{-1} corresponds to stretching vibrations of OH groups[125].Another peak around 2930 cm^{-1} is assigned to C-H stretching vibrations. The band near 1640 cm-1 is due to the associated water. Absorption in this range is common for polysaccharides. The band 890cm^{-1} is attributed to C-H variable angle vibration of β-pyranoside. This confirms the β-glycosidic band and pyranose ring in Schizophyllan. The absorption at 1034 cm^{-1} could be assigned to C-O stretching of polysaccharide [126]

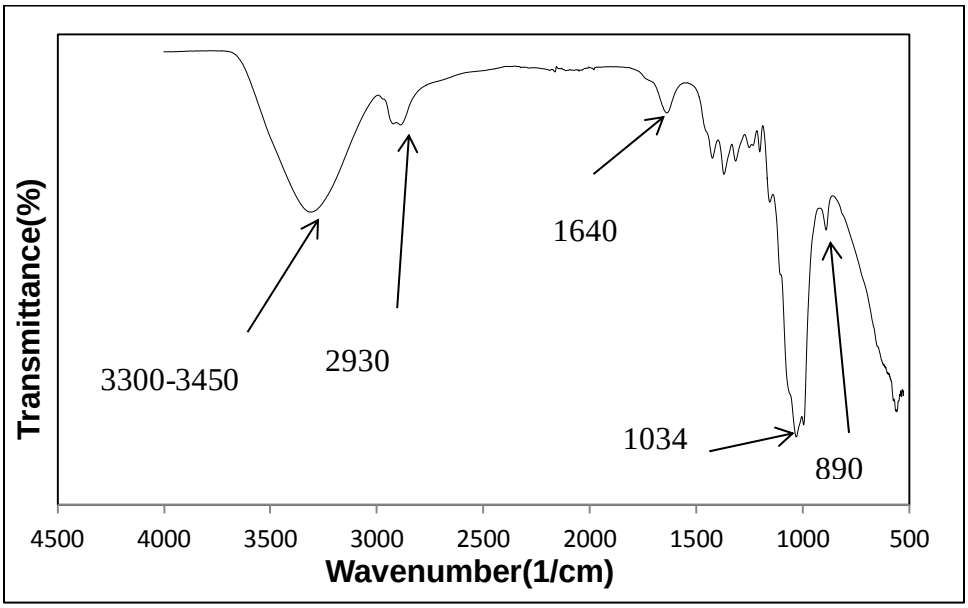

Figure 3-8: FTIR Spectra of Schizophyllan

b. Minerals

FTIR:

Calcite: The presence of peaks at 876 and 712cm^{-1} confirms the calcite nature of rock

Dolomite: The presence of a peak at 730 cm^{-1} which is the in plane bending mode of $CO3^{-2}$confirms the mineral to be Dolomite[127].

Kaolin: The presence of 3685, 3620 cm^{-1} doublet which is the characteristic for the kaolin group confirms the rock to be Kaolin[128]

Silica: The bands at 780 & 1080 cm-1 corresponds to Si-O symmetrical & asymmetrical stretching vibrations respectively. While the band at 685 cm-1 corresponds to Si-O symmetrical bending vibration[129]. This confirms the Silicate nature of the rock.

R-5, R-9, R-11: All the three rocks have a characteristic peaks (876&712) of a calcite rock which confirms their nature to be Calcite.

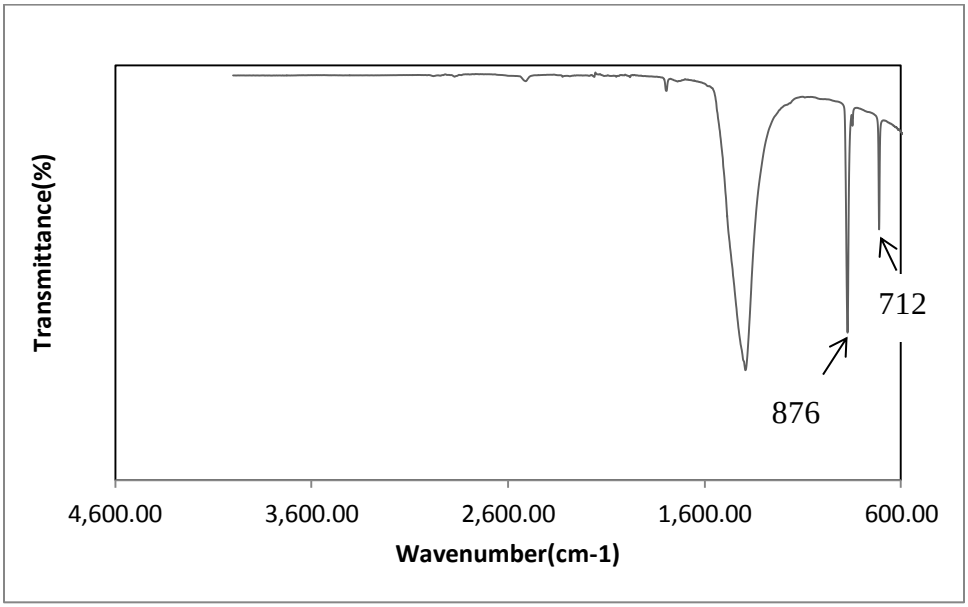

Figure 3-9: FTIR Spectra of pure Calcite

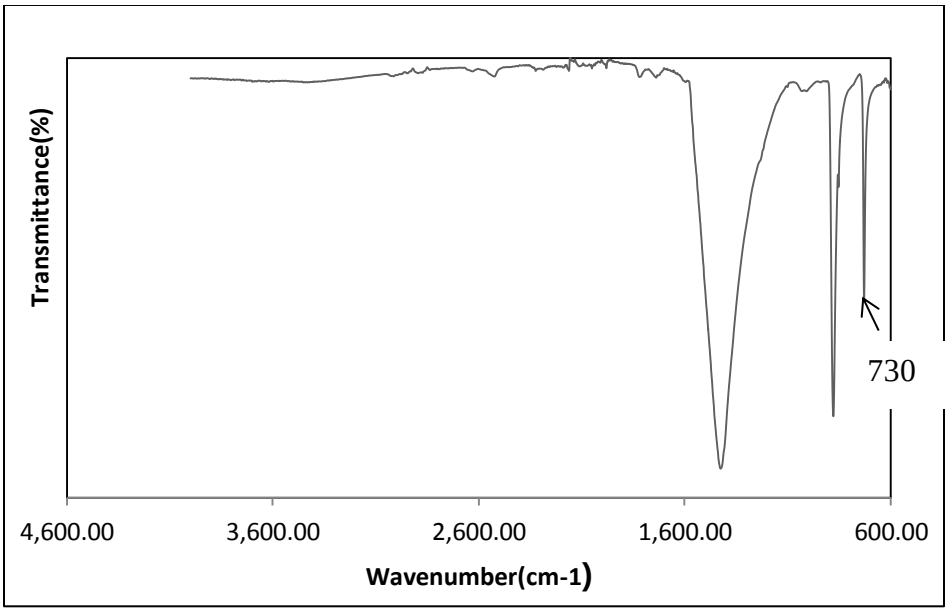

Figure 3-10: FTIR Spectra of pure Dolomite

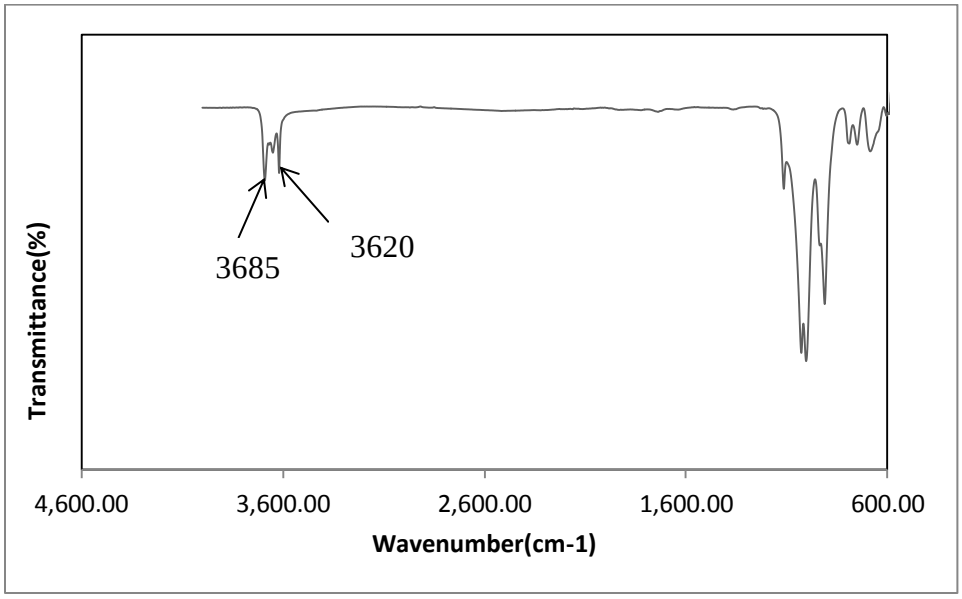

Figure 3-11: FTIR Spectra of pure Kaolin

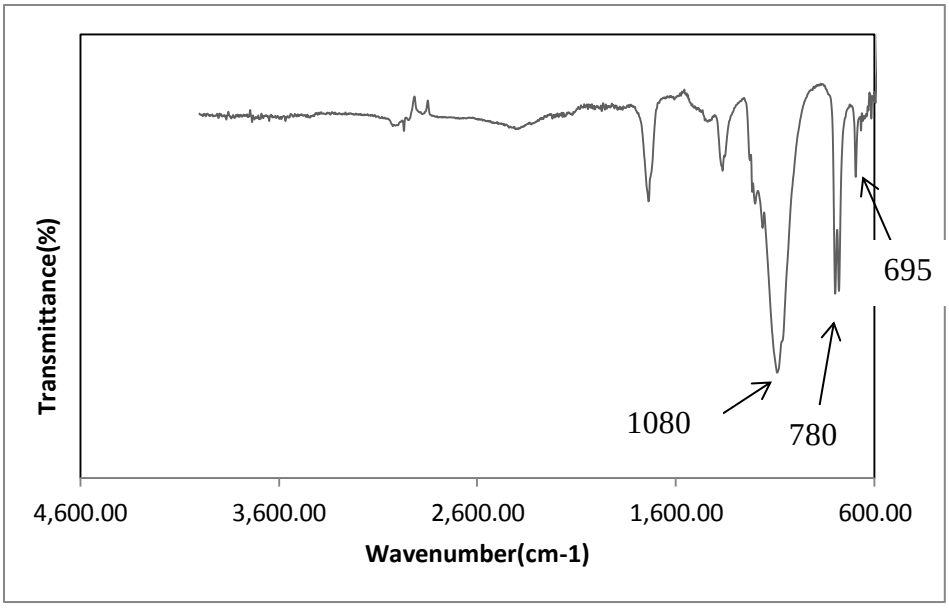

Figure 3-12: FTIR Spectra of pure Silica

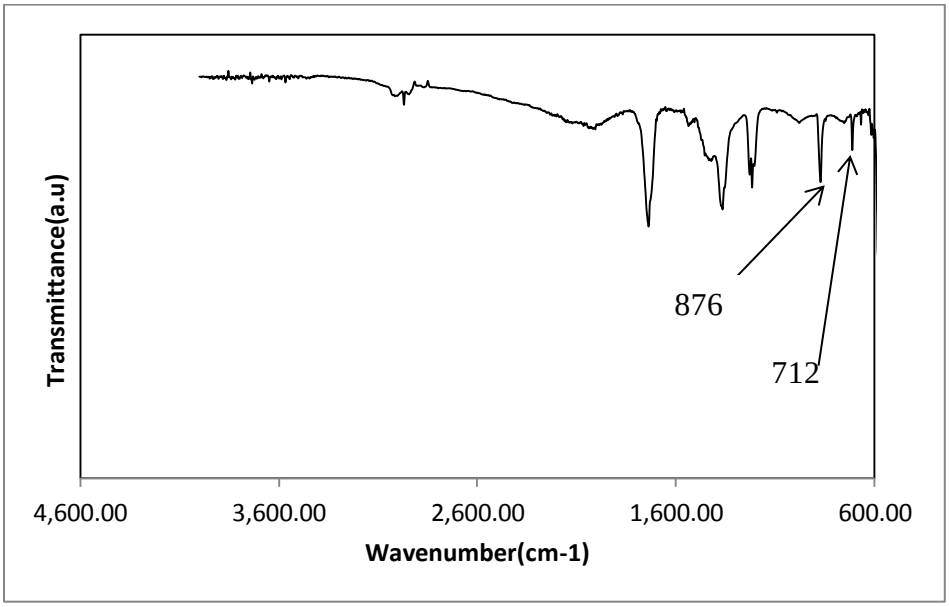

Figure 3-13: FTIR Spectra of R-5

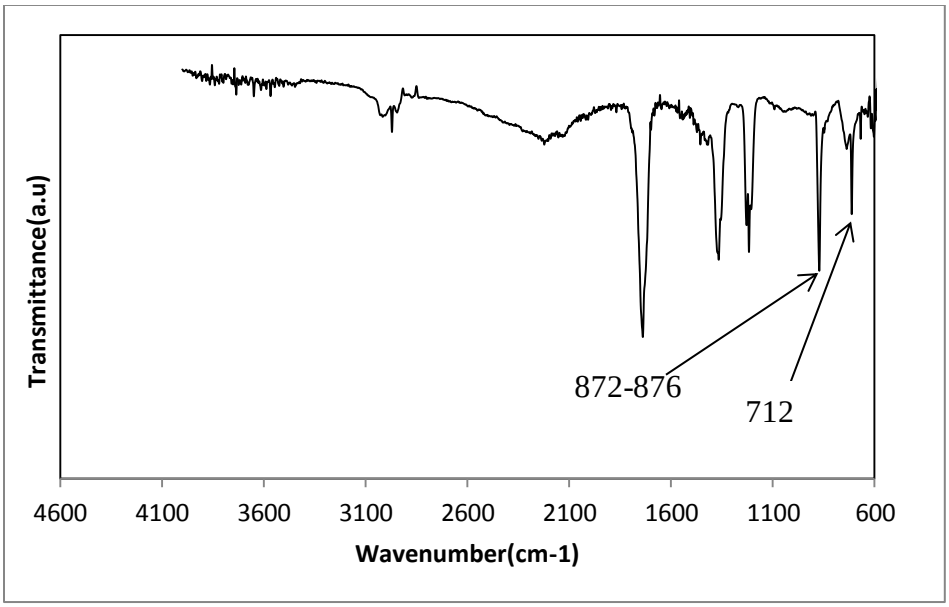

Figure 3-14: FTIR Spectra of R-9

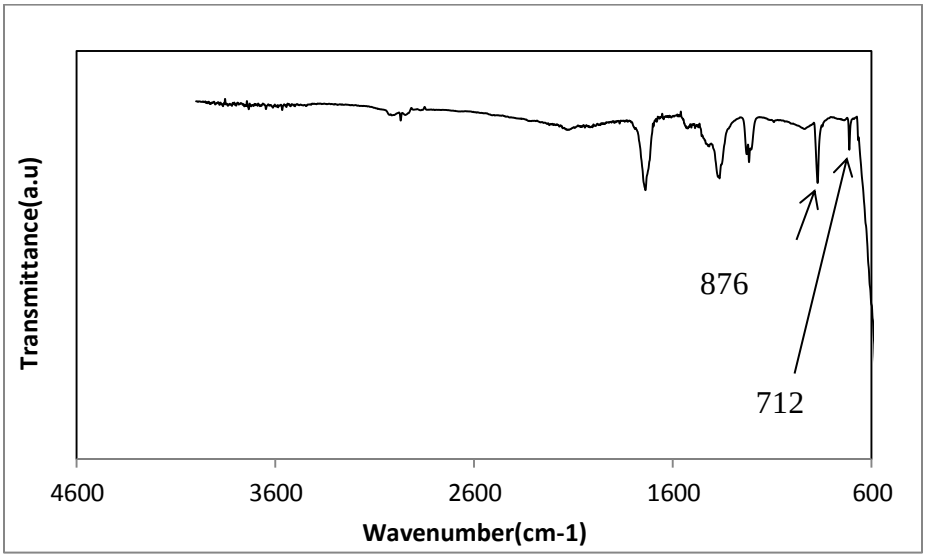

Figure 3-15: FTIR Spectra of R-11

X-Ray Diffraction: The X-RD spectrograph of all the minerals used is presented in Appendix A. Table 3-4 presents the mineralogical composition of each mineral used.

Table 3-4: X-RD Analysis of Minerals Used

Mineral	% Calcite	%Dolomite	%Quartz	Kaolinite
Calcite	96.95	3.05	0	0
Dolomite	0.024	99.97	0	0
Kaolin	0	0	0	100
Silica	0	0	100	0
R-5	83	17	0	0
R-9	92.85	7.15	0	0
R-11	96.09	3.90	0	0

The natural minerals are necessarily in their purest form. While the Quantitative phase analysis of X-RD reveals that the Reservoir rocks are mostly calcite and dolomite with traces of silica.

SEM of Reservoir Rock:

R-5: Figure 3-18 shows the SEM image of rock R-5. The Energy-dispersive X-ray spectroscopy (EDX) of this rock gives the following elemental composition (Table3-6). The analysis shows that it is purely carbonate in nature. The particle size is less than 10 μm.

Table 3-5: EDX of R-5

Element	Wt. %	At %
C	37.60	51.94
O	35.68	37.00
Ca	26.72	11.06

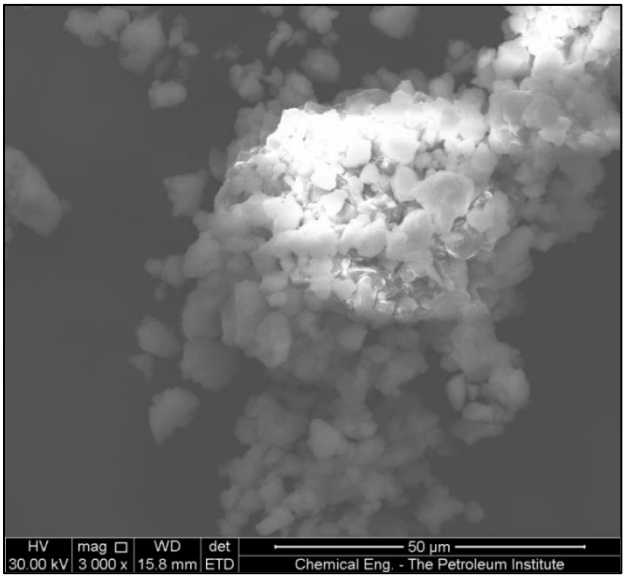

Figure 3-16: SEM of R-5

R-9: Table 3-7 presents the elemental makeup of rock R-9. It seems to have some traces of Aluminium. Figure 3-19 shows its image. The average particle size is around 8μm.

Table 3-6: EDX of R-9

Element	Wt. %	At %
C	36.50	52.52
O	30.45	32.89
Al	01.61	01.03
Ca	31.44	13.56

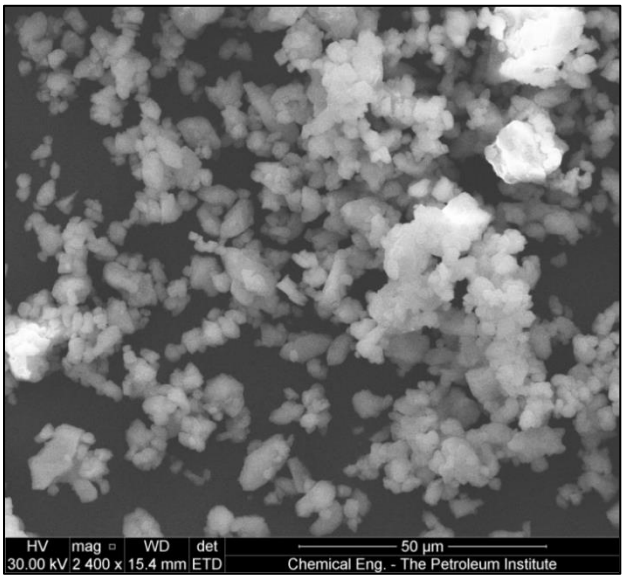

Figure 3-17: SEM image of R-9

R-11: Table 3-8 presents the elemental makeup of rock R-11. It seems to have some traces of Aluminium. Figure 3-19 shows its image. The average particle size in this case is also close to 8μm.

Table 3-7: EDX of R-11

Element	Wt. %	At %
C	19.38	31.13
O	41.48	50.02
Ca	39.14	18.84

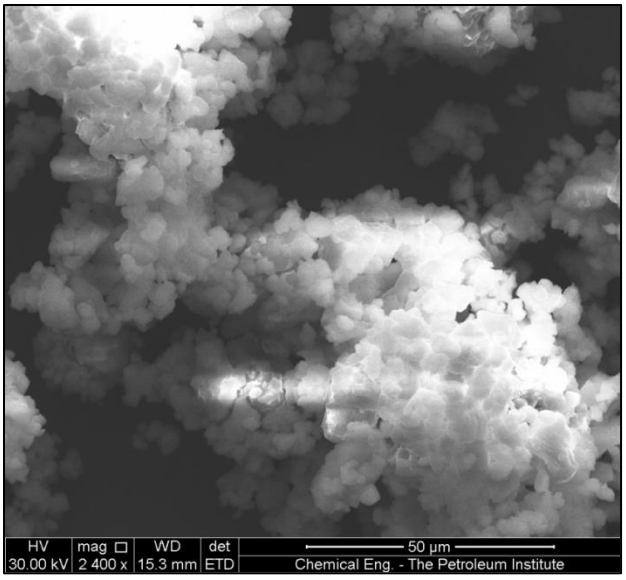

Figure 3-18: SEM image of R-11

3.7.2 Adsorption Kinetics

a. Room Temperature (25°C):

Rock	Salinity/Brine	Polymer to Rock (mg/g)	Temp(°C)	$C_{initial}$ (ppm)
Calcite	Reservoir Brine	20	25	200
Dolomite	Reservoir Brine	20	25	200
Kaolin	Reservoir Brine	20	25	200
Silica	Reservoir Brine	20	25	200

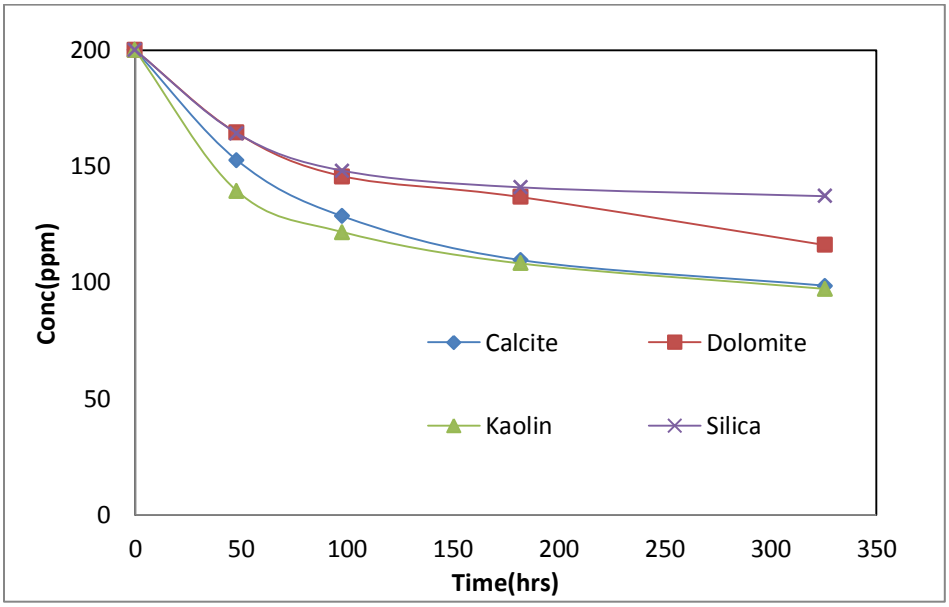

Figure 3-19: Time required in reaching equilibrium at 25°C

b. Temperature=75°C

Rock	Salinity/Brine	Polymer to Rock	Temp(°C)	$C_{initial}$ (ppm)
Calcite	Reservoir Brine	20	75	200
Dolomite	Reservoir Brine	20	75	200
Kaolin	Reservoir Brine	20	75	200
Silica	Reservoir Brine	20	75	200

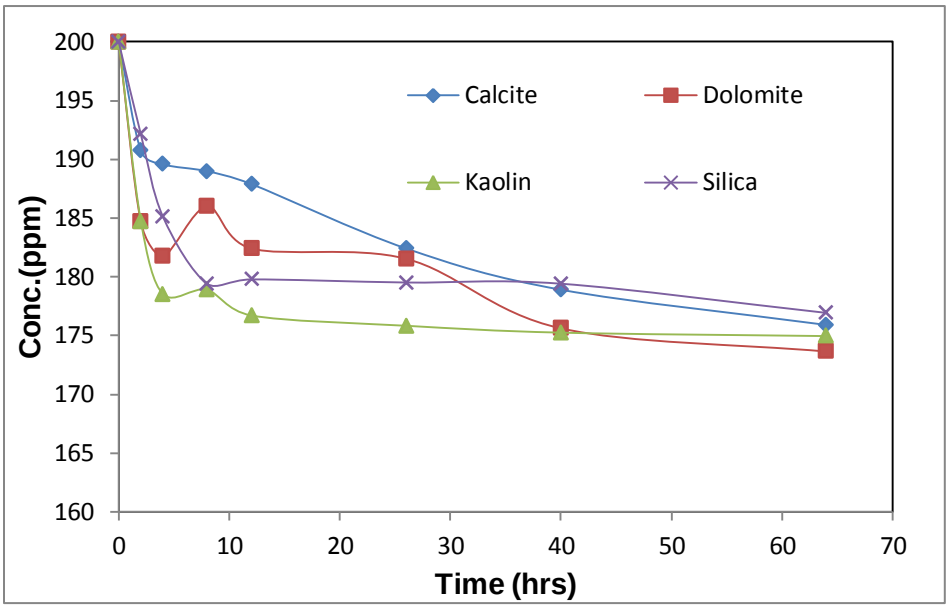

Figure 3-20: Time required in reaching equilibrium at 75°C

3.7.3 Adsorption on different minerals

Rock	Salinity/Brine	Polymer to Rock	Temp(°C)	C initial (ppm)
Calcite	Reservoir Brine	2,4,10,16,20	70	200
Dolomite	Reservoir Brine	2,4,10,16,20	70	200
Kaolin	Reservoir Brine	2,4,10,16,20	70	200
Silica	Reservoir Brine	2,4,10,16,20	70	200

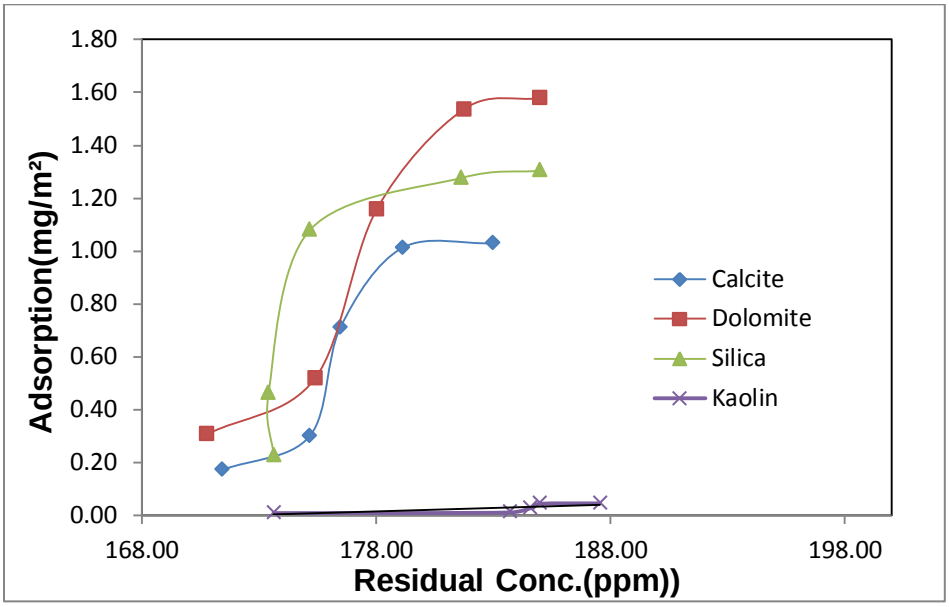

Figure 3-21: Adsorption over different minerals

Rock	Salinity/Brine	Polymer to Rock (mg/g)	Temp(°C)	$C_{initial}$ (ppm)
Calcite	Reservoir Brine	10,15,30,40,50	25	200
R-138	Reservoir Brine	10,15,30,40,50	25	200

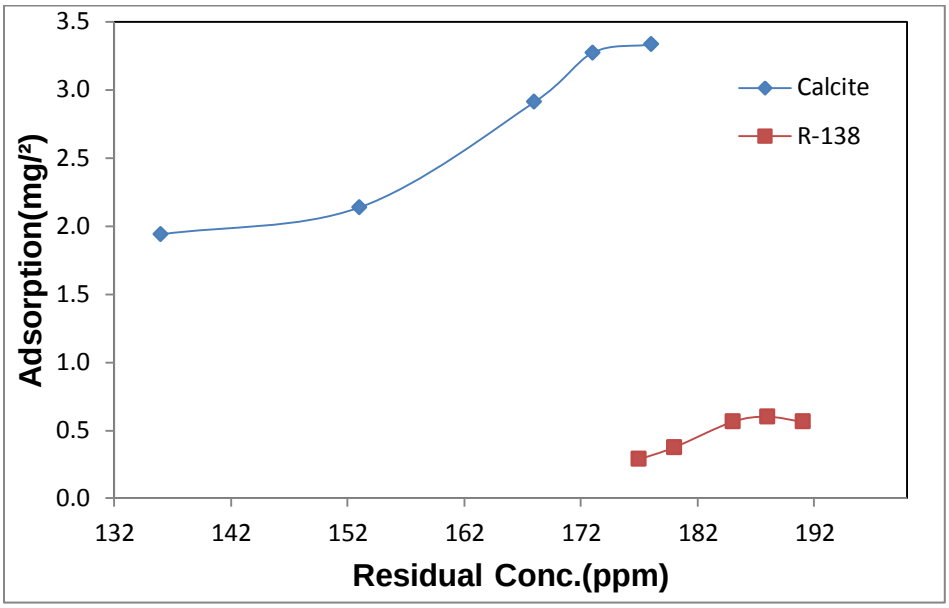

Figure 3-22: Adsorption over Formation mineral compared to Calcite

3.7.4 Effect of Salinity on Adsorption

Rock	Salinity/Brine	Polymer to Rock (mg/g)	Temp(°C)	C initial (ppm)
Calcite	100%,50%,0%	10,15,30,40,50	25	200

Where 100% Salinity corresponds to:

TDS	100%
NaCl, g/L	181.8
$CaCl_2$, g/L	58.2
$MgCl_2$, g/L	12.0

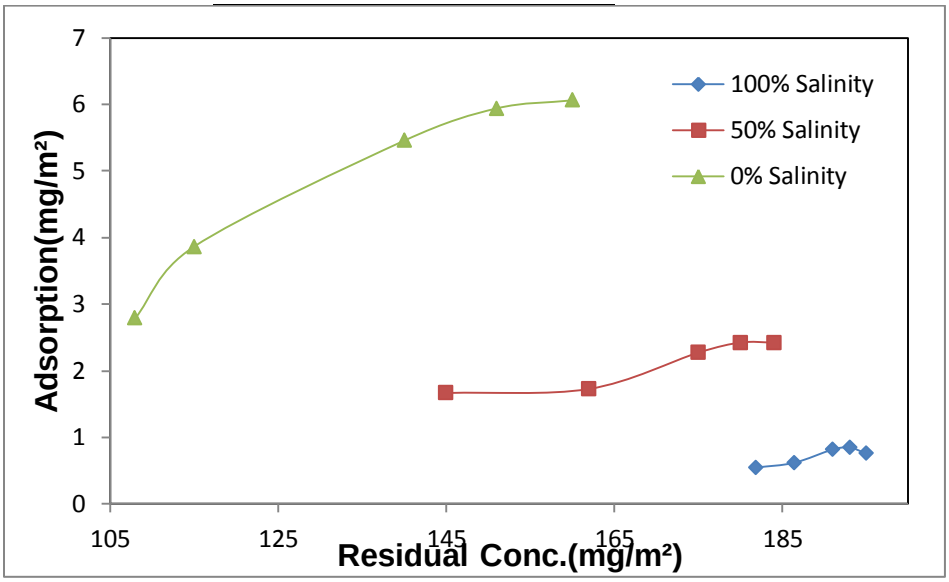

Figure 3-23: Effect of Salinity on adsorption over Calcite with Ci=200ppm

Rock	Salinity/Brine	Polymer to Rock (mg/g)	Temp(°C)	C initial (ppm)
Calcite	100%,50%,0%	25,37.5,75,100,125	25	500

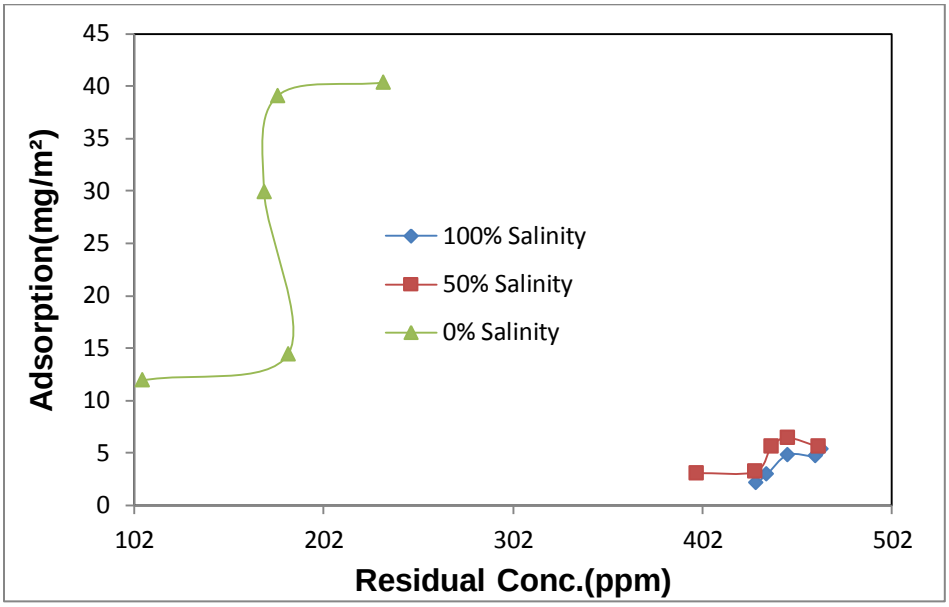

Figure 3-24: Effect of Salinity on adsorption over Calcite with Ci=500ppm

Rock	Salinity/Brine	Polymer to Rock	Temp(°C)	C initial (ppm)
Calcite,Dolomite,Kaolin,Silica	100%,50%,0%	30	25	200

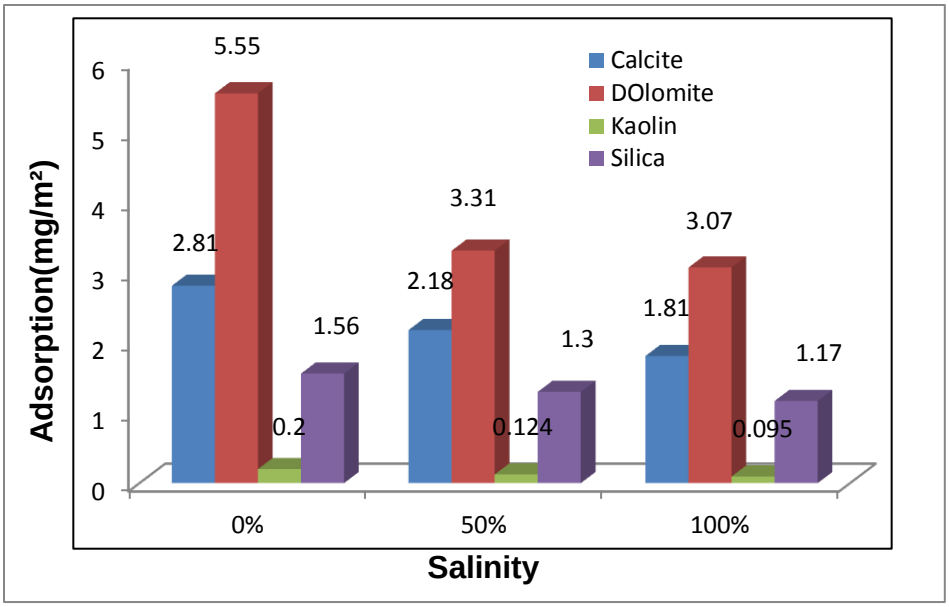

Figure 3-25: Effect of Salinity on Adsorption over four minerals

Rock	Salinity/Brine	Polymer to Rock	Temp(°C)	$C_{initial}$ (ppm)
R-5, R-9, R-11Kaolin,Silica	0%, Reservoir Brine	20	25	200

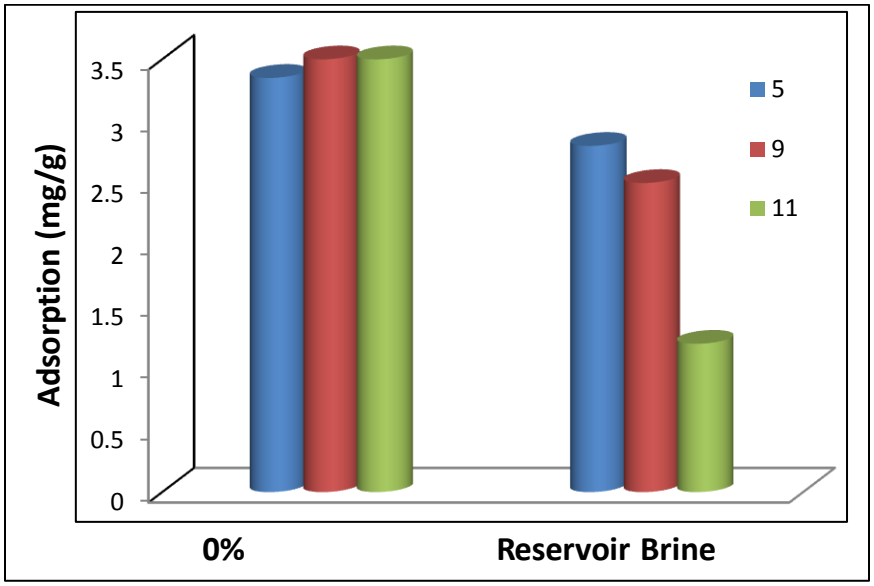

Figure 3-26: Effect of Salinity on Adsorption over Formation Minerals

3.7.5 Effect of Background Ions on Adsorption

a. Effect of $NaHCO_3$ & Na_2CO_3

Rock	Salinity/Brine	Polymer to Rock (mg/g)	Temp(°C)	$C_{initial}$ (ppm)
Calcite	1.54g/l NaHCO3	10,15,20,30,40	25	200
Calcite	3.04g/l NaHCO3	10,15,30,40,50	25	200
Calcite	3.04g/l NaHCO3	10,15,30,40,50	25	200

Apart from the $NaHCO_3$ &Na_2CO_3, the other salts were according to

Salt	g/l
NaCl	134.6
$CaCl_2$	25.6
$MgCl_2$	5.60
KCl	1.4

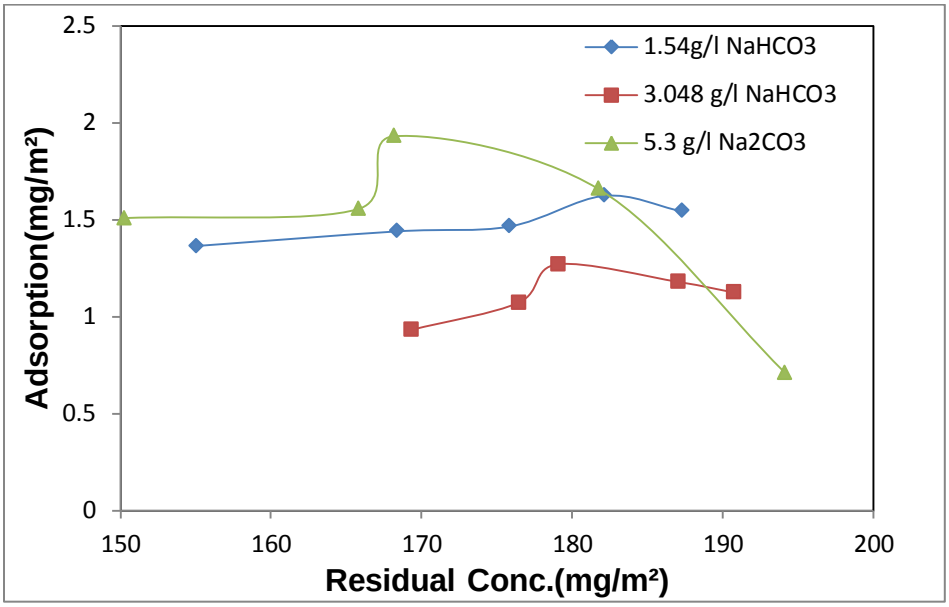

Figure 3-27: Effect of NaHCO3 & Na2CO3 on Adsorption

b. Effect of Urea

Rock	Salinity/Brine	Polymer to Rock (mg/g)	Temp(°C)	$C_{initial}$ (ppm)
Calcite	6g/l Urea	10,15,20,30,40	25	200
Calcite	1.54g/l NaHCO3	10,15,20,30,40	25	200

Apart from urea and NaHCO3, following salts were included in both

Salt	g/l
NaCl	134.6
$CaCl_2$	25.6
$MgCl_2$	5.60
KCl	1.4

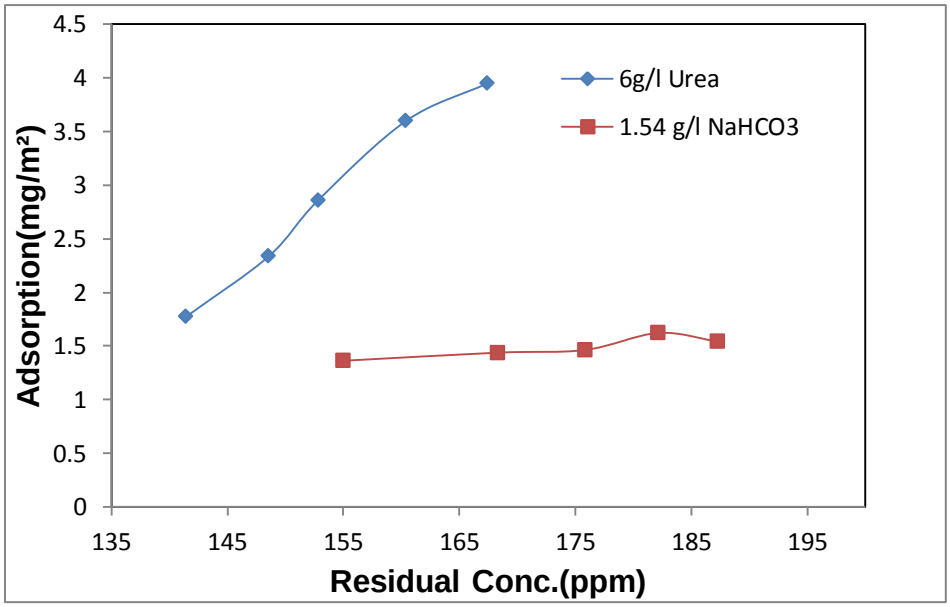

Figure 3-28: Effect of Urea on Adsorption

c. Effect of individual ions

Rock	Salinity/Brine	Polymer to Rock (mg/g)	Temp(°C)	C initial (ppm)
Calcite	As per the graph	10	25	200

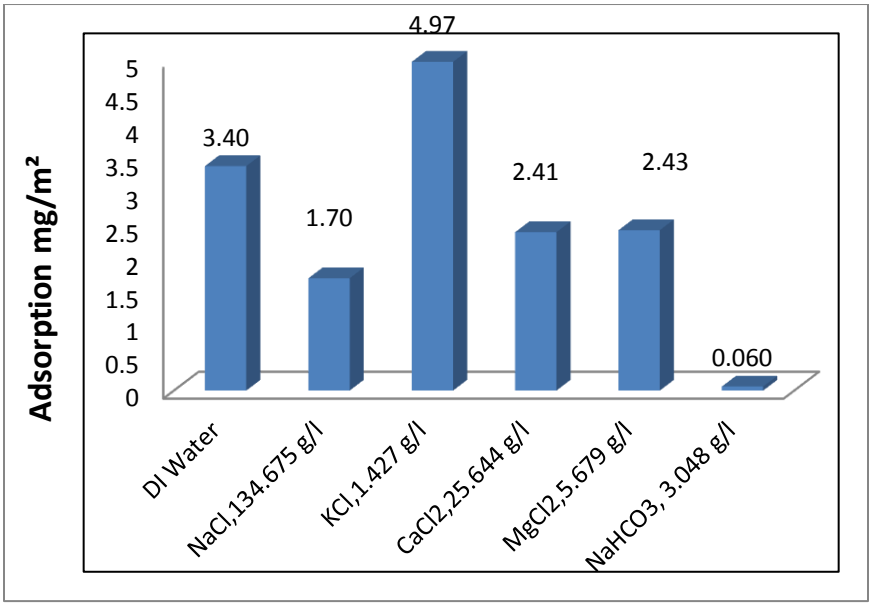

Figure 3-29: Effect of individual salts on Adsorption

c. Effect of conditioning

Rock was conditioned for 36 hours before the polymer was added to make the final concentration 200ppm. This is the point where actual adsorption o polymer started.

Rock	Salinity/Brine	Polymer to Rock (mg/g)	Temp(°C)	C initial (ppm)
Calcite	As given below	10,15,20,30,40	25	200

Salt	g/l
NaCl	**134.6**
CaCl2	**25.6**
MgCl2	**5.60**
KCl	**1.4**
NaHCO3	**1.52**

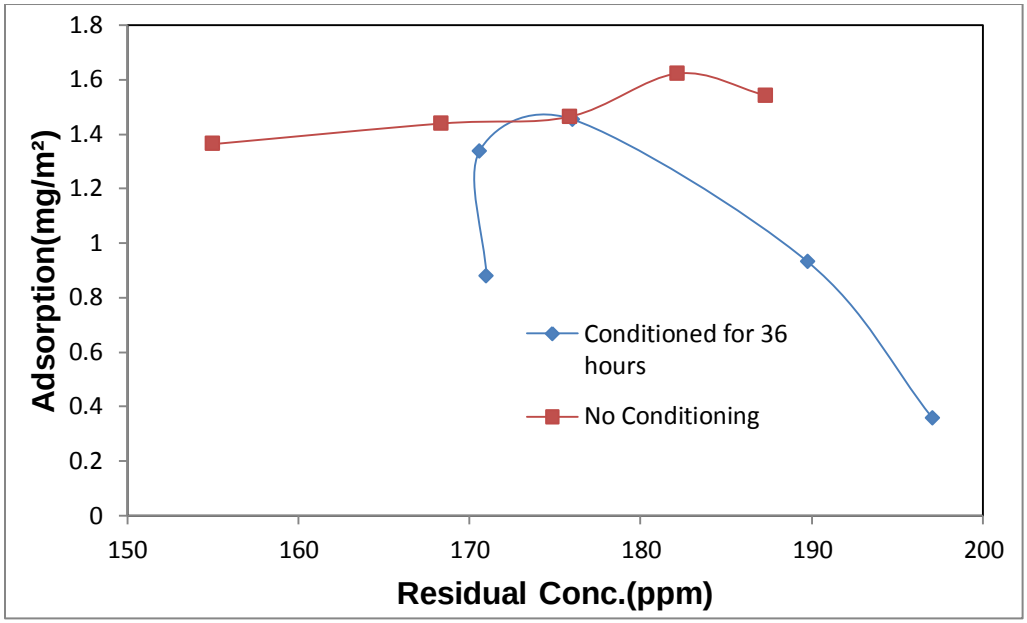

Figure 3-30: Effect of Conditioning on Adsorption

3.7.6 Effect of Temperature

Rock	Salinity/Brine	Polymer to Rock (mg/g)	Temp(°C)	C initial (ppm)
All four	Reservoir Brine	2	25,75	200
All four	50%[1]	30	25,50	200
Calcite	167g/l	3	25,80	200

Where 50% corresponds to the one in section 3.7.4

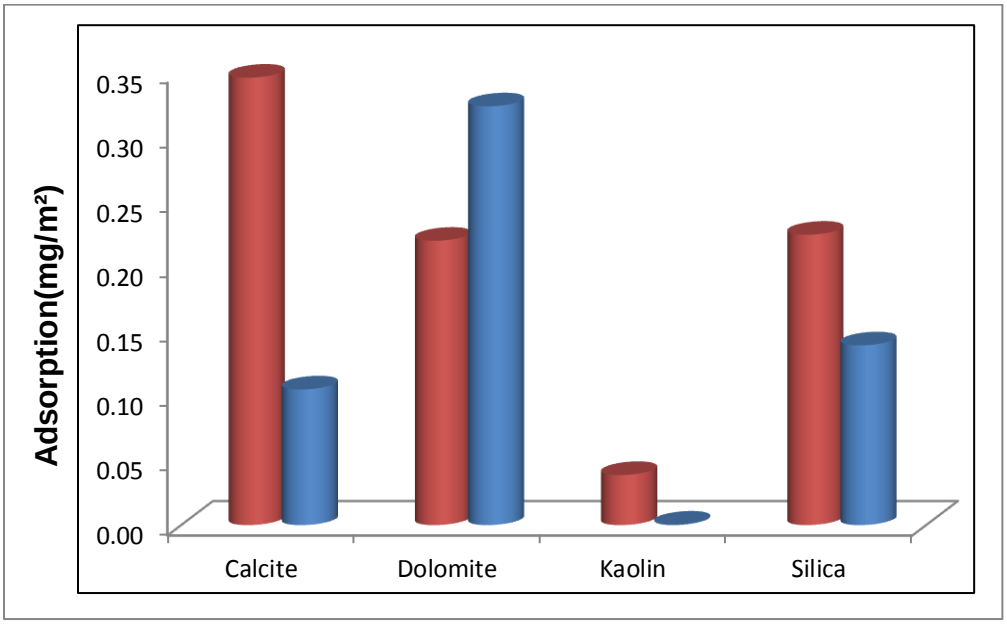

Figure 3-31: Effect of Temperature on Adsorption over Four Minerals in Reservoir Brine

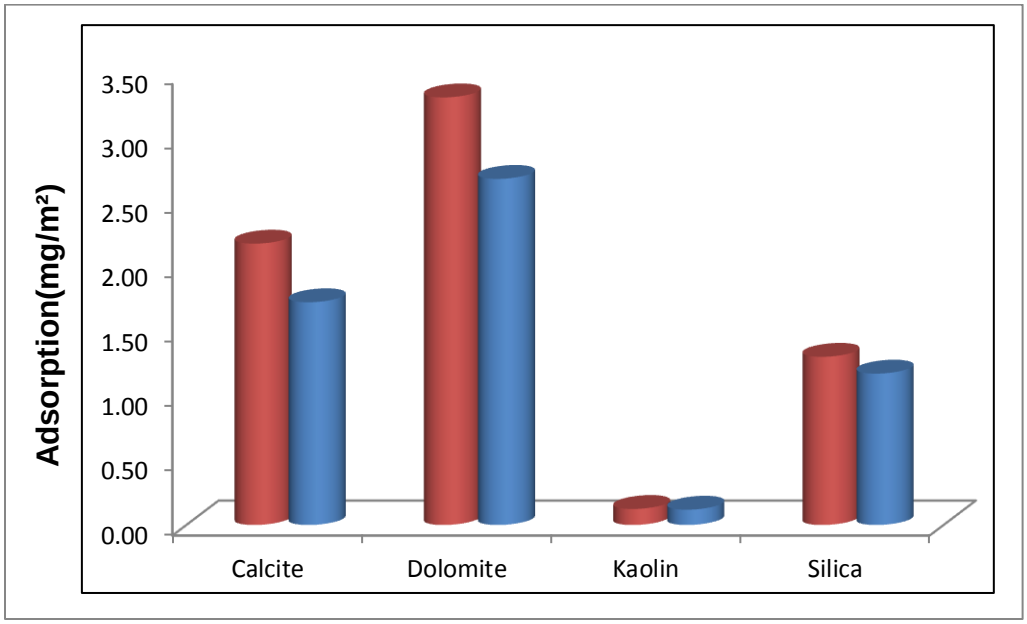

Figure 3-32: Effect of Temperature on Adsorption over Four Minerals at 50% Salinity

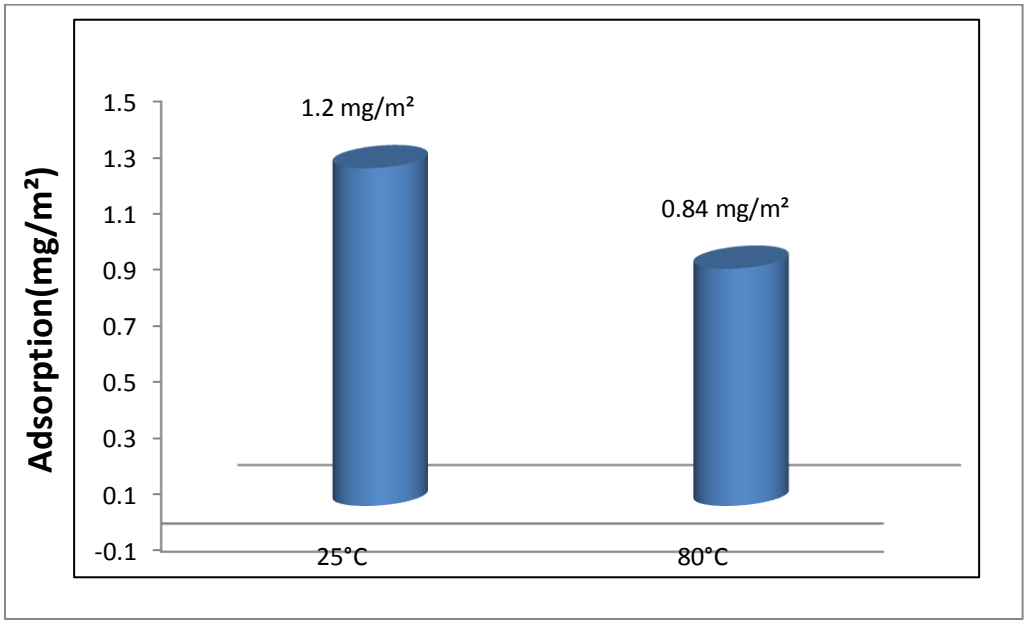

Figure 3-33: Effect of Temperature on Adsorption over Calcite

3.7.7 Discussion of Adsorption Results:

Time required for equilibration: From the Figure 3-19 & 3-20 it is clear that the adsorption reaches equilibrium faster at 75℃ compared to 25℃. The time required to reach equilibrium is different for all the rocks. At 25℃, the adsorption over **Calcite** and Dolomite equilibrate in around 8-10 days. The same amount of time (around 7 days) has also been reported by Tempio et al. [130] for adsorption of Xanthan over Calcite and by El'tekov et al. [131] for the adsorption of Dextran over Sibunit powder. El'tekov et al. [131] further concluded that adsorption of polymers over minerals proceeds quickly during the initial stage of adsorption which is characterized by the adsorption values equal to about 60–70% of the equilibrium, while subsequent stages may last for days.In our case 50-60% of the equilibrium is achieved during the first 36 hours and the rest of the adsorption process which is slow proceeded during the next 8 days. However the rate of adsorption is bumped up with an increase in temperature. The time required to reach 90% of the equilibrium in case of 75 ℃ is around 30 hours which is way less than the time required to reach the same amount of adsorption at 25℃. **Dolomite** also exhibits behavior similar to Calcite.

Silica is the first one which reaches equilibrium or maximum adsorption requiring approximately 150 hours at 25℃ and 12 hours at 75℃. **Kaolin** takes around 240 hours at 25℃ and 24 hours at 75℃. The time required for Kaolin is higher compared to Silica even though the adsorption capacity for Kaolin is low. This be attributed to the high

specific surface area of Kaolin (26.6 m^2/g) used in the experiment even though the capacity on Kaolin is low.

Adsorption on Different Minerals: Adsorption in the reservoir brine is maximum on Dolomite with plateau value of 1.58 mg/m^2. For Silica and Calcite this value is 1.30 and 1 mg/m^2 respectively. While for Kaolin this value is less than 0.05 mg/m^2. The adsorption isotherms on these minerals are represented in Figure 3-21. The adsorption level measured for carbonate minerals (Calcite & Dolomite) is in the same range as reported by Somasundaran [132] for the adsorption of starch over calcite(1.3mg/m^2) . Rinaudo & Noik [133] also reported the adsorption of amylopectin on calcite (13 mg/g). Xia & Marek [115] reported the adsorption of guar gum (a polysaccharide) on quartz surface ,the maximum value of adsorption attained in their case is 0.4 mg/m^2. Xia [134] in another paper reported the adsorption level of starch on quartz to be around 1.5 mg/m^2. The results reported above are at different salinity and some even in DI water. Although the adsorption level obtained in our case is close to those reported in literature it is still difficult to relate these results as those experiments were performed at different condition and with different polymers than ours.

Effect of Salinity on Adsorption: Figure 3-23 & Figure 3-24 show the effect of salinity on adsorption level for all the four minerals with initial concentration of 200ppm and 500ppm respectively. As evident from the figures, adsorption level goes down with an increase in salinity for all the minerals and for the initial concentrations, 200ppm as well as 500ppm. This effect is in contradiction with the normal trend of polymer adsorption

with salinity. For HPAM as well as Xanthan, an increase in salinity results in an increment of adsorption density[25].The difference in the results may be attributed to the nature of the polymer “Schizophyllan” or the salinity level we are using because most of the reported results are at lower salinities compared to ours.

Effect of temperature: Figure 3-31 shows the effect of temperature on adsorption. As expected for a typical adsorption process the adsorption density has gown down from 1.2 mg/m^2 to .84 mg/m^2 with an increase in temperature from 25℃ to 80℃. Same effect has been reported by Sorbie [25]

3.8 GPC Result & Discussion

Figure 3-34 shows the comparison of GPC profiles for a fresh polymer of 200ppm and the same polymer after adsorption taken from the supernatant. The GPC profile shifts in the right hand side suggesting a decrease in MW of the remaining polymer solution. This may be either the high M.W chains are preferentially getting adsorbed over the rock surface or there may be a mechanical degradation of the sample as it was placed over shaker at 250rpm for 10 days. The second case may get an upper hand in analysis as there is a small MW shoulder in the after adsorption GPC profile

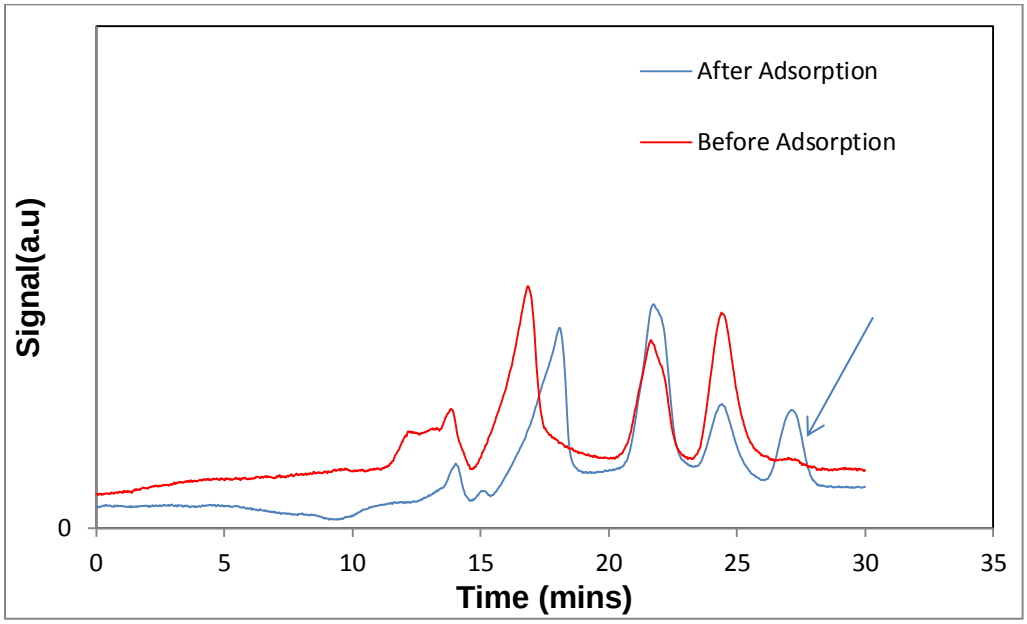

Figure 3-34: GPC of SPG before and after Adsorption

3.9 Microcalorimetry Results & Discussion

a. Calcite

Rock	Salinity/Brine	Polymer & Rock	Temp(°C)	Cinitial (ppm)
Calcite	167g/l	25 ml , 150mg	35	200

Figure 3-34 shows the heat released during the course of adsorption. This is also known as Heat Flow. As illustrated from the figure, there is a major heat flow during the first 3 hours of the adsorption after which there is no or very little heat flow. This heat flow is so negligibly small that the instrument is not able to detect it. This is the reason behind the long time required for the adsorption to reach equilibrium. The heat flow analysis is done as follows:

Heat released during the adsorption=258.37 J

Heat released per gram of the rock = 258.37/0.150 = 1.7KJ/g

Heat released per m^2 of the rock= 1.7/1.67 =1 KJ/m^2

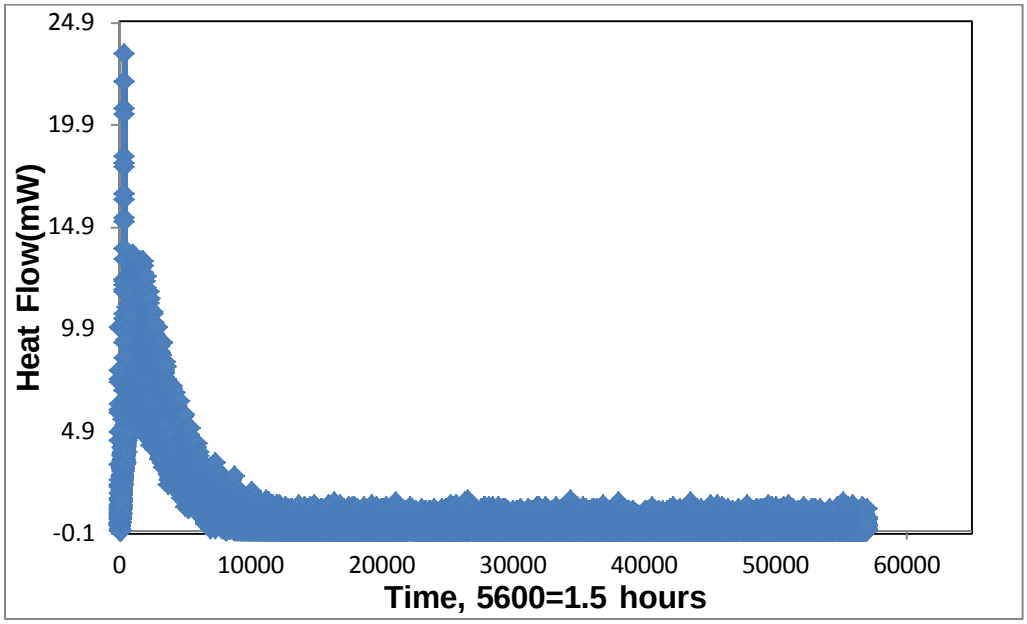

Figure 3-35: Heat Flow with Calcite Rock

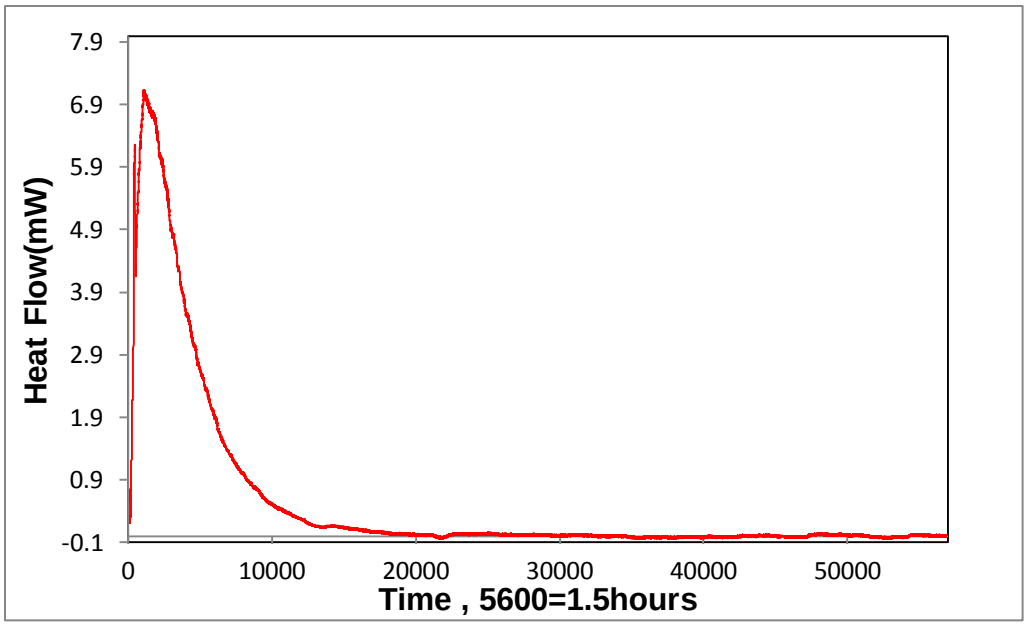

Figure 3-36: 12 point moving average of Heat Flow

Chapter 4: Dynamic Adsorption of Schizophyllan

4.1 Adsorption Experiment (Dynamic)

4.1.1 Available Methods

The measurement of polymer retention in dynamic /core flooding experiments is generating a concentration profile of the effluent samples and then applying the material balance to calculate the retention[60]. There are two approaches illustrated by Willhite and Dominguez[52] to measure the dynamic adsorption. Figure 3-6 shows the two methodologies (method A &B).

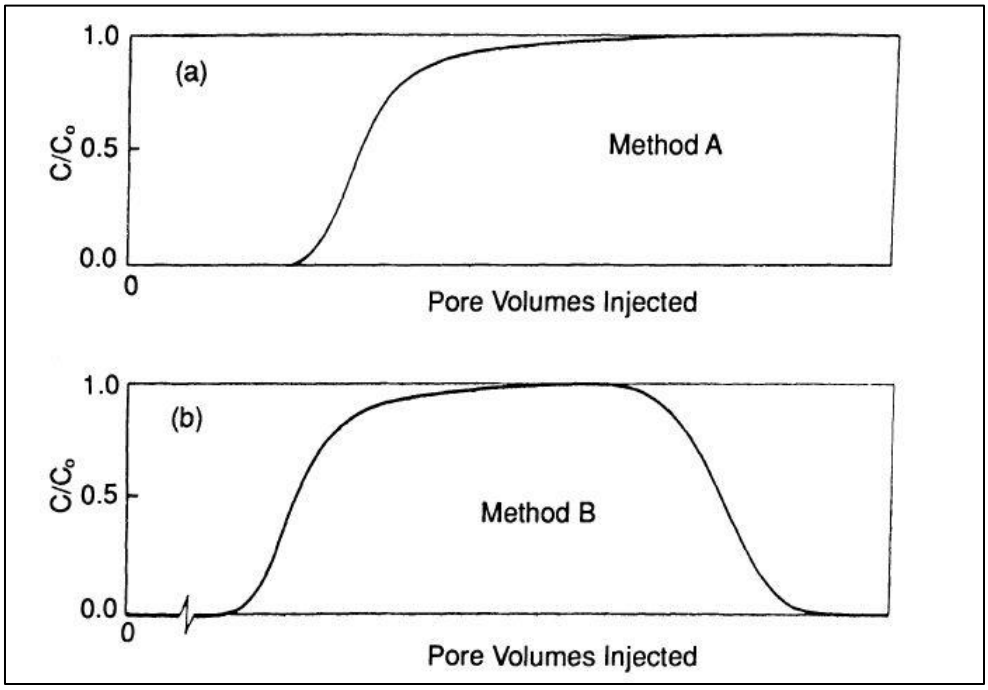

Figure 4-1: Two methods for dynamic adsorption measurement

In Method A, a polymer solution is injected into the core at a constant frontal-advance rate until the effluent concentration reaches the injected polymer concentration. However, there may be some inaccessible pore volume which must be taken into account in order to interpret the results correctly. The adsorption value calculated by this method also involves the reversible adsorption plus if there is a chance of hydrodynamic entrapment that will also be included in the results. So, this method has a great chance to produce false results. On the other hand, Method B includes the first method (Method A) along with a brine post flush which can produce the reversibly adsorbed polymer. Thus, one is inevitably led to Method B in any case where a complete mass balance is possible.

4.1.2 Core Properties & Preparation

The carbonate cores used in the core flow experiments were obtained from Kocurek Industries. The cores were supplied in 1.5" Dia x 12" Length which was later on cut to make them 1.5" Dia x 3" Length. The properties of the cores provided by the supplier are mentioned in Table 4-1.

Table 4-1: Properties of Cores provided by supplier

Core	Gas Permeability(mD)	Brine Permeability(mD	Porosity	Catalogue#
8A	200	70	18%	B101C
2A	15-20	8-10	14%	B101B

The core properties, Gas Permeability and Porosity were determined once again in the lab in order to match the values provide by the supplier.

Core Cleaning: After cutting and trimming the cores to make their surface leveled so as to make them perfect cylinder, cleaning was done using Soxhlet extraction unit to remove any contamination. Then the cores were dried in a drying oven at 90℃ for 24 hours.

Gas Permeability: The gas permeability of the cores was determined using a steady state digital gas permeameter as shown in Figure 3-7. Permeability was determined using the Darcy's law.

Gas Porosity: The gas porosity of the cores was determined using the helium gas expansion method. Digital helium expansion gas porosimeter from Ergotech[119] as shown in Figure 3-8 was used.

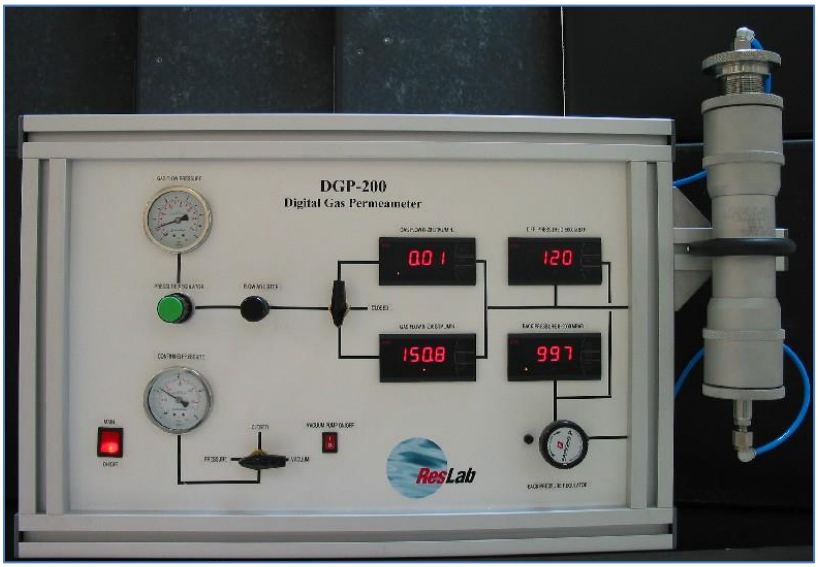

Figure 4-2: Reslab digital gas permeameter

Figure 4-3: Ergotech helium gas expansion digital porosimeter

4.1.3 Core Flow Experiment Scheme

4.1.4 Experiment1:

a. The core used in this experiment was 8-A.

b. The core was first saturated in a brine of composition presented in Table 3-5.

c. Brine was injected into the core at three rates (0.5, 1, 1.5 cm^3/min) to determine the average absolute permeability.

d. A 200 ppm polymer solution was injected at three different rates (2.2, 1.1, 0.22 cm^3/min). Three different rates were used to analyze the hydrodynamic entrapment of the polymer. The polymer solution was made in the same brine composition. The flow rate was changed once the ΔP was constant.

e. After the polymer injection, brine was injected (at 0.22 cm^3/min) until the ΔP was constant.

f. Effluent samples were collected (in 15 ml corning tubes) right after the polymer injection started until the experiment was stopped.

g. Viscosity, MWD and Concentration of the samples was determined using the methods described.

Table 4-2: Brine Composition

Salt	g/l
NaCl	134.675
KCl	1.427
CaCl2	25.644
MgCl2	5.679
NaHCO3	1.524213
TDS	167.425

4.1.5 Experiment2:

a. The objective of this experiment was to see the influence which the oil already presented in the core would make on the adsorption behavior of polymer.

b. The core used in this experiment was 2-A.

c. The core was first saturated in a brine of composition presented in Table 3-5.

d. Brine was injected into the core at three rates (0.5, 1, 1.5 cm^3/min) to determine the average absolute permeability.

e. Crude oil was injected into the core (at 0.2 cm^3/min) until no more water was produced. This brought the core to S_{wi}.

f. After the previous step, brine was injected at 0.2cm^3/min until ΔP was constant. It resulted in oil production which stopped after some time.

g. Polymer injection was started at this point, it also produced oil which is the incremental oil recovered after water flooding. Polymer injection was continued until the ΔP was constant.

h. Brine was again injected to produce the reversibly adsorbed and entrapped polymer. This step was terminated once no more polymer produced.

i. The viscosity and concentration of effluents was calculated using the same procedure as described previously.

j. Residual Resistance Factor (RRF) for both the experiments is calculated using:

$$\boldsymbol{RRF = \frac{\Delta P after\ polymer\ injection}{\Delta P before\ polymer\ injection}}$$

k. The whole experimental scheme can be represented as:

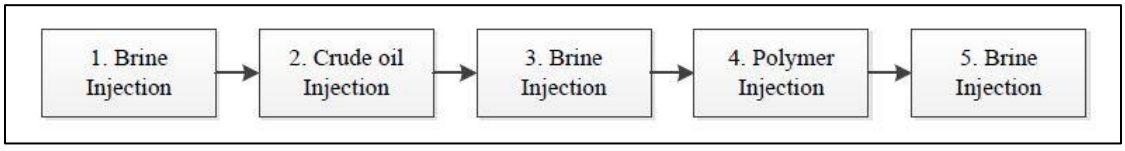

Figure 4-4: Experimental Scheme of Core Flooding 2

4.1.6 Viscosity of Core Flooding Effluents

The viscosity of the core flooding effluents was measured in order to study the effect of degradation of polymer on its viscosity when it flows through the porous media/core. Viscosity was also used as an online criterion to stop the core flow experiment during the brine post flush. The viscosity of the samples was measured using the Discovery Series Rheometer from TA Instruments (Figure3-9,[135]) . The geometry used for measurement was 40 mm with 3° cone angle one peltier plate.

Figure 4-5: DHR3 Rheometer from TA Instruments

4.2 Results

4.2.1 Core Properties

The calculated values of brine permeability and porosity is given in Table 4-2

Table 4-3: Core Properties determined in the Lab

Core	Permeability(mD)	Porosity	Pore Volume(cm^3)
8A	162.5	17.26%	14.28
2A	18	13.05%	10.36

FTIR Spectra of Cores:

Figure 4-6 and Figure 4-7 show the FTIR Spectra of the two cores used in experiments. The presence of the calcite peaks confirms the carbonate nature of the material of cores.

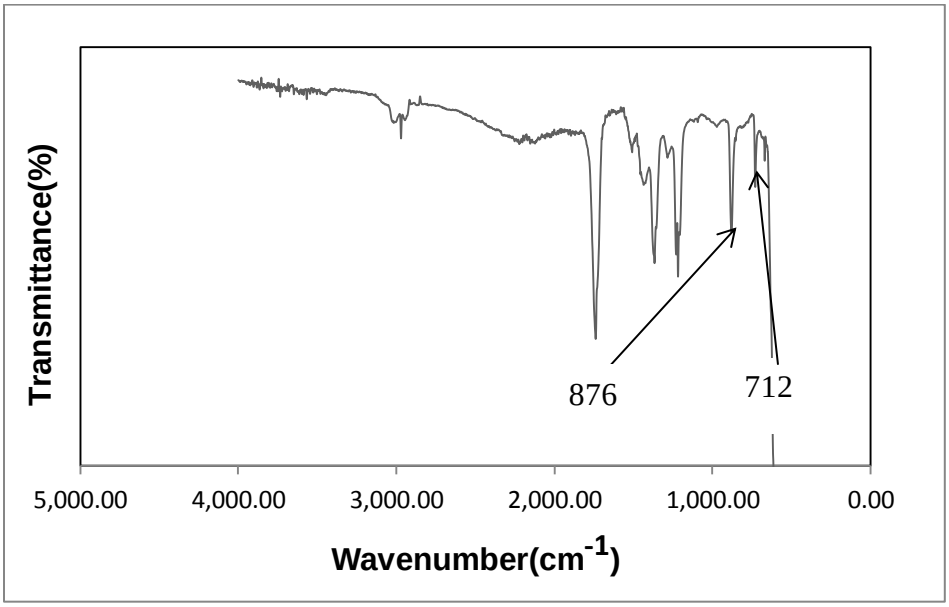

Figure 4-6: FTIR of 8A

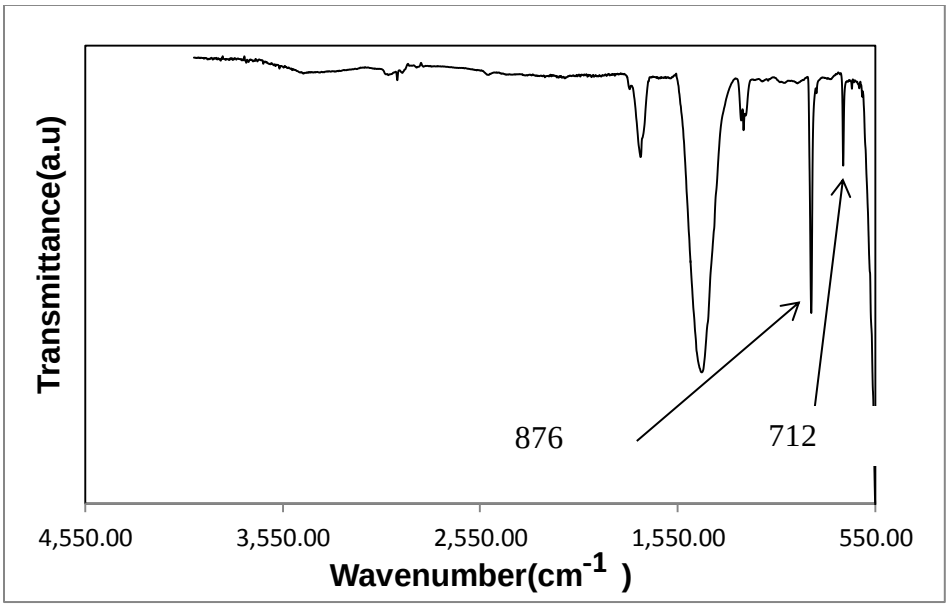

Figure 4-7: FTIR of 2A

4.2.2 Core Flooding Number 1

Figure 4-8 shows the effluent samples normalized concentration on primary y-axis and normalized viscosity on secondary y-axis. The normalized viscosity is at a shear rate of 13.33 s^{-1}. A total of around 20 pore volumes are injected out of which initial 9 are the polymer injection volumes. The PV required to reach the maximum normalized concentration is around 7 at which the normalized concentration reached 0.75. The concentration never reached the injected concentration. There can be numerous reasons behind this, out of which one is the high adsorption inside the core. After 9 PV of polymer injection brine injection was started to produce the reversibly adsorbed polymer. In fact 22% of the total polymer produced during this entire experiment was during the post brine flush which tells the total amount of reversibly adsorbed polymer. The other calculations are as follows:

Total Polymer Injected=25.4 mg

Total Polymer Produced Before Post Brine Flush=14.16 mg------- (A)

Polymer Produced as a result of Post Brine Flush=4.06------- (B)

Total Polymer Produced= A+B=18.22 mg

Polymer Adsorbed (Trapped) = (25.4-18.22) mg =7.18mg

Adsorption (per gram of core rock)=7.18mg/178.88g=40.138μg/g of core weight.

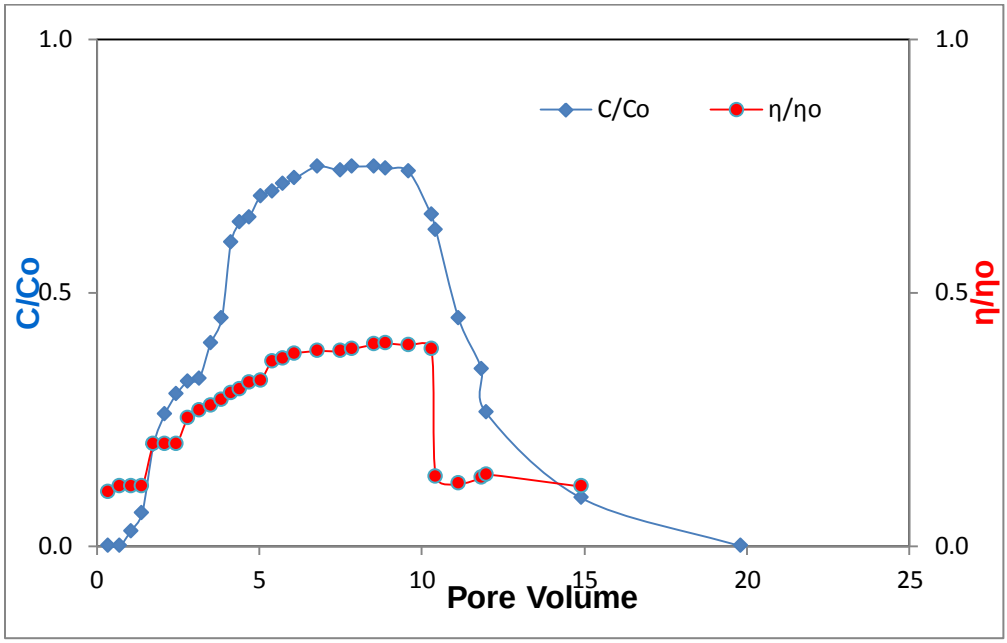

Figure 4-8: Core Flooding 1

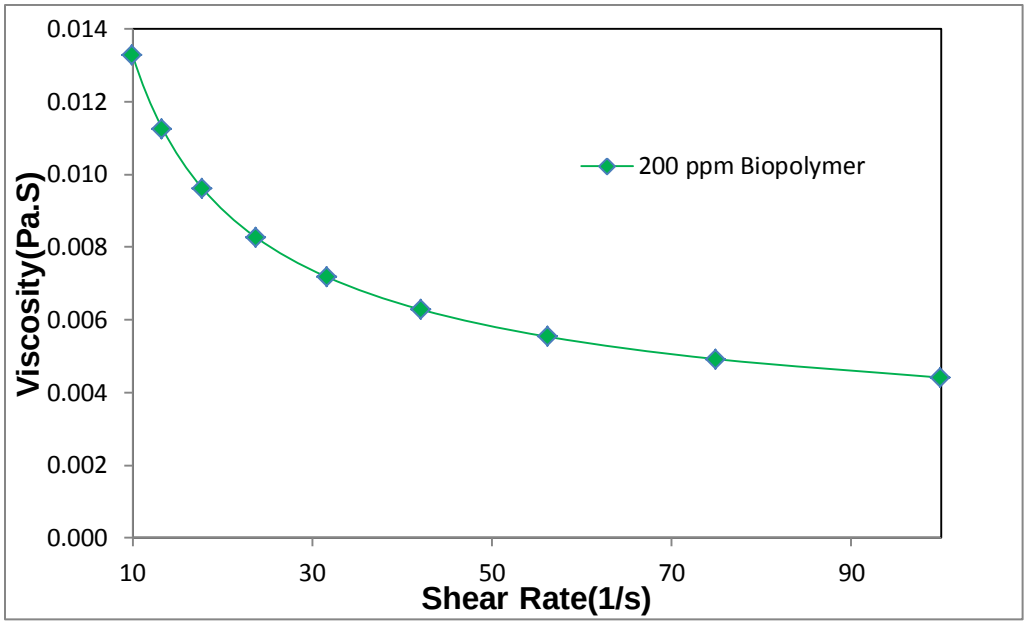

Figure 4-9: Shear Profile of 200ppm Schizophyllan

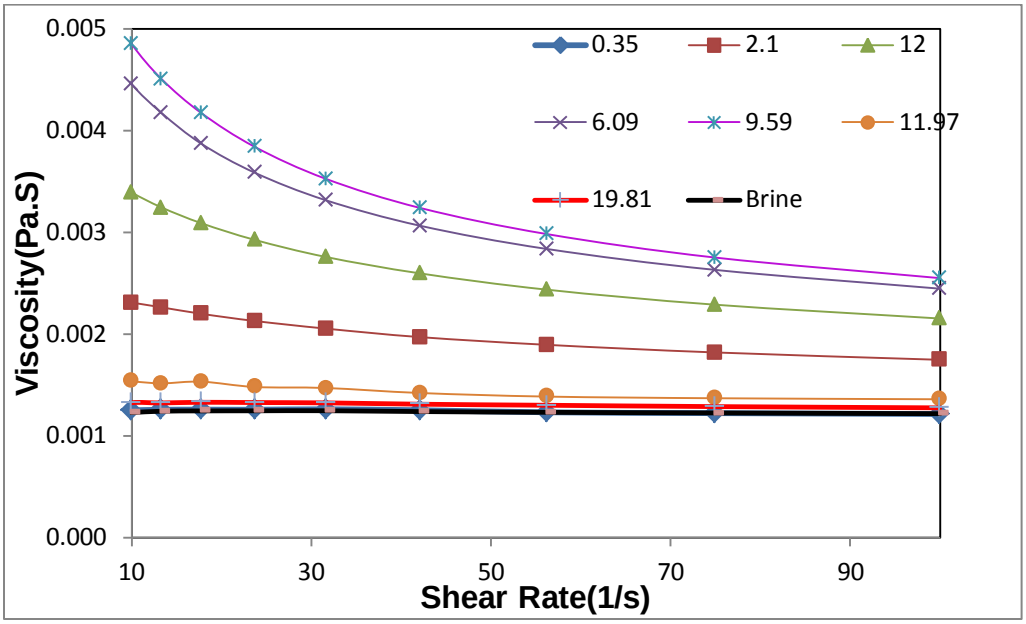

Figure 4-10: Shear Profile of Core Flooding Effluents

4.2.3 Core Flooding Number 2

Figure 4-11 shows the normalized concentration viscosity. After producing the oil using water, polymer was injected till 17 pore volumes which resulted in incremental oil recovery. After 17 pore volumes the injection line was switched to brine which was injected till 23rd PV.

Total Polymer Injected=35.4 mg

Total Polymer Produced Before Post Brine Flush= 30.45 mg------- (A)

Polymer Produced as a result of Post Brine Flush=3.59------- (B)

Total Polymer Produced= A+B=34.04 mg

Polymer Adsorbed (Trapped) = (35.4-34.04) mg =1.35mg

Adsorption (per gram of core rock)=1.35mg/194.55g=7μg/g of core weight.

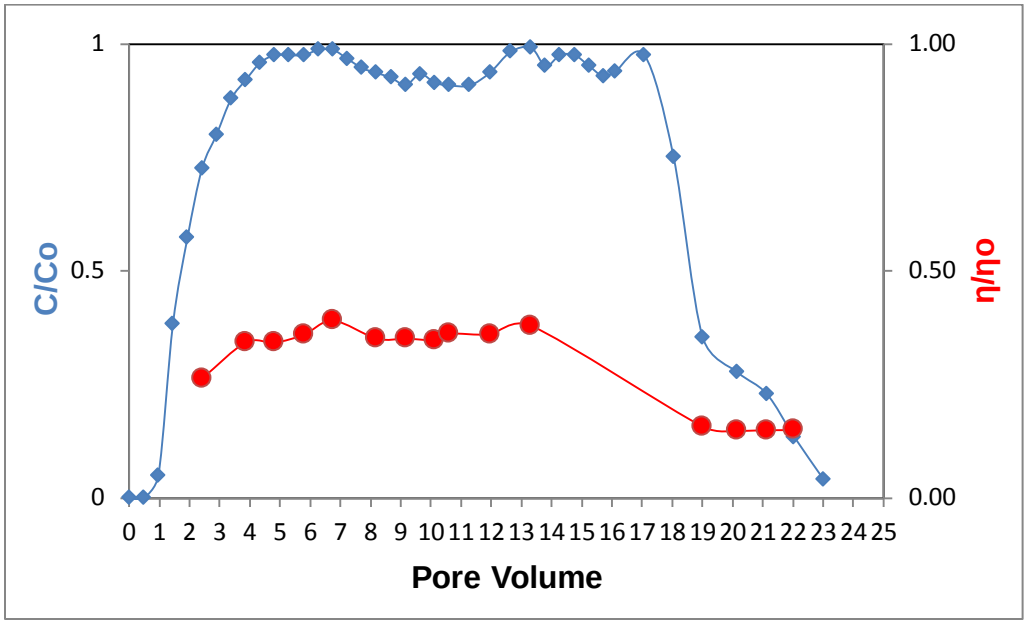

Figure 4-11: Core Flooding 2

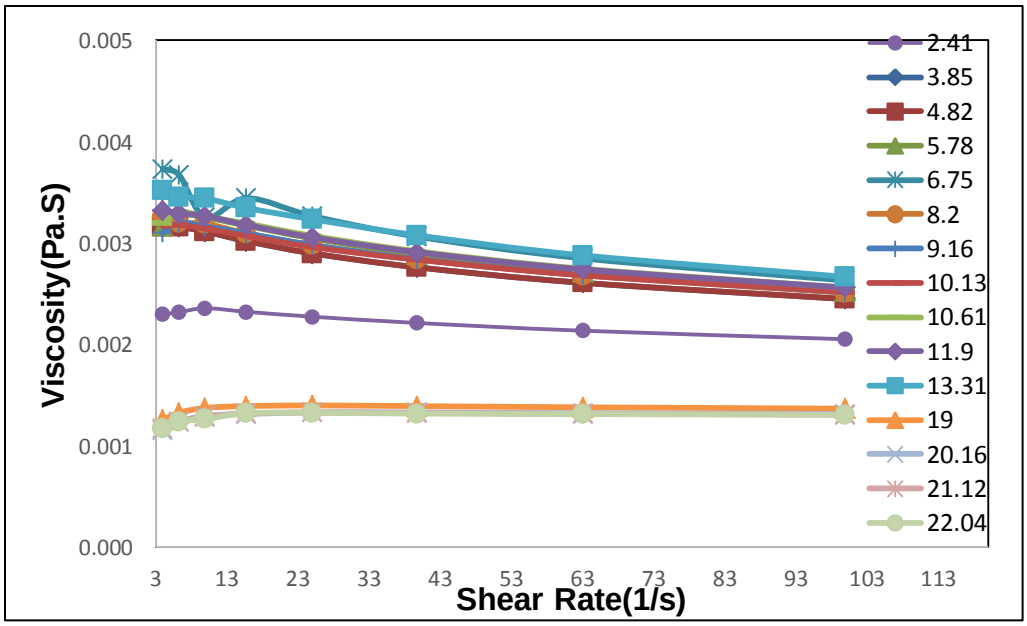

Figure 4-12: Shear Profile of Core Flooding Effluents

4.3 Discussion

Adsorption in second case is when there was initial oil present is less than the adsorption in first case when there was no oil used. This may be linked to the oil wetting property of carbonate rocks. The initial oil present may have occupied all the adsorption sites which left no room for polymer adsorption. The maximum normalized viscosity achieved in first case is only after 10 pore volumes of injection whereas for second case it reaches in 6-7 pore volumes. This also shows the extent of adsorption is less in second core flow experiment. The degradation of polymer during core flow which is characterized by the viscosity effluents can be seen on secondary axes of Figure 4-8 and 4-11. In both the cases the maximum normalized viscosity reached is 0.40 which shows a significant degradation.

Chapter 5: Adsorption of Switchable Surfactant: Materials and Experimental Method

5.1 Material

Minerals: Four minerals Calcite, Dolomite, Kaolin and Silica were from the same batch which was used for Schizophyllan adsorption. A different reservoir rock was received from ADNOC to run the adsorption experiment. The reservoir rock is referred as R-168 in this thesis.

Surfactants & Chemicals

Ethomeen C12: This switchable surfactant was obtained from AKZO NOBEL Co. C-12 is a tertiary amine surfactant which consists of one coco alkyl group (which is a mixture of alkyl chains from C8 to C18) and two EO groups as branches attached to the Nitrogen atom. Figure 5-1 shows its structure. It is a nonionic surfactant molecule at neutral and high pH which does not dissolve in water. It can be switched to cationic surfactant by adjusting the pH towards the acidic end. It will protonate and dissolve at low pH.

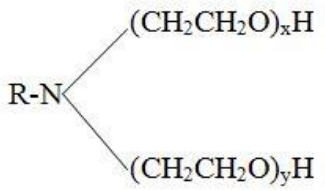

x=y=1; R=Coco group, Mixture of 6 to 18 carbon

Figure 5-1: Structure of C-12

Sodium Dodecyl Sulfate (SDS): SDS was supplied by Sigma-Aldrich**.** Accurate weight of SDS (activity ≥99.0%) was dissolved in DI water to calibrate the cationic surfactant TEGO.

TEGO: 1, 3-Didecyl-2-methylimidazolium chloride (TEGO trant A 100) was supplied by Metrohm. It is a cationic surfactant which was used to calibrate the anionic surfactant SDES.

SDES: STEOL CS-330 is a sodium lauryl ether sulfate ethoxylated to an average of 3 moles. It was obtained from Stepan. It was used for the titration of C-12. It was used in place of SDS because of its greater salt tolerance than SDS.

The complete titration flow can be represented as (Figure 5-2):

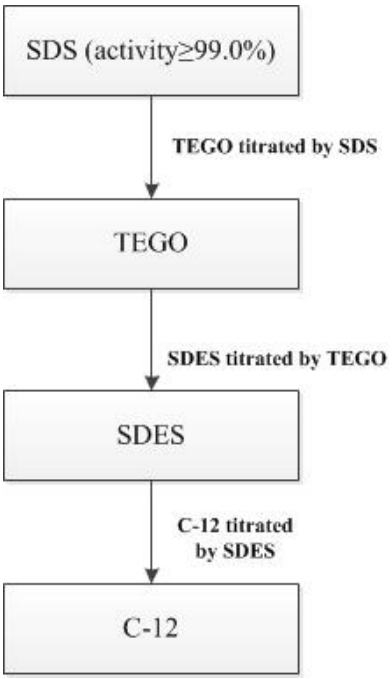

Figure 5-2: Titration Scheme

Methylene Blue (MB): 30 mg of methylene blue hydrate is added to 1 liter of KCl-HCl solution. The composition of this solution is 5.52 g/l KCl and 126mM HCl.

Chloroform: Obtained from Sigma-Aldrich (catalog # 439142)

5.2 Titration

5.2.1 TEGO Standardization using SDS:

TEGO is a cationic surfactant which is used as a standard cationic titrant in place of Hyamine 1622 because of its better response in potentionmetric titrations[136].However, It can absorb water and thus need to be standardized. SDS is used for this purpose because of its high activity (≥99.0%). TEGO has a molecular weight of M =399.7 g/mol while SDS is 288.372g/mol. 1.60 g of TEGO was added to 1 liter DI water to make an approximate solution of 4mM. This was titrated with 10 mg of SDS in 20 ml DI water. The Metrohm 905 Titrando with optrode electrode was used for titration.[137].Figure 5-3 shows the end point of titration. The concentration of TEGO came out to be 3.84 mM which means the activity is 96%.

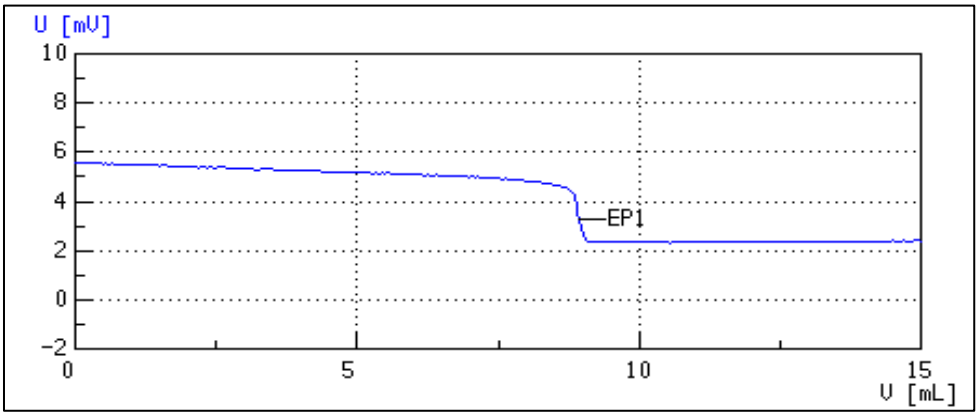

Figure 5-3: Standardization of TEGO

5.2.2 SDES Standardization using TEGO:

SDES standardization was done using the same method which was used for titration of C-12. The concentration used throughout this chapter for SDES after standardization is 0.412 mM. The procedure is described in the next section.

5.2.3 Concentration Determination of C-12:

A number of different methods like acid base titration, chromatographic analysis, infrared spectroscopy and NMR are used for the quantitative analysis of surfactants[138]. But the one which has been used in this thesis for Ethomeen C-12 is known as Epton's calorimetric titration. This methods was first proposed by Epton in 1947[139].

1st step: Add 5 mL Chloroform and 2 mL methylene blue solution in a glass vial.

2nd step: Add a certain amount of C12 sample in the glass vial. All the methylene blue will stay in the upper aqueous phase while the lower chloroform phase is colorless.

3rd step: Start titrating the surfactant sample with SDES. After adding some SDES solution, vigorously shake the vial by hand, in order to partition all the ion-pairs into chloroform phase. If the color of upper aqueous phase just turns from slightly blue to colorless after one drop of SDES, the endpoint is reached. The endpoint can't be judged until two phases are completely separated due to the blue chloroform phase dispersed in aqueous phase. It takes a long time to completely separate two phases by gravity. So, centrifuge can be used to accelerate the phase separation process. The actual end point is reached when the absorbance of the upper layer reaches less than 0.05.

4th step: A blank need to be done to calibrate the titration results. Prepare a sample with 5 mL chloroform and 2 mL methylene blue solution without any C12 solution. Add DI water in the vial to reach the similar final aqueous volume of C12 titration case. Repeat 3rd step. The titrant consumed by blank should be subtracted from the sample titration, as shown in following equation:

$$\boldsymbol{C_{Sample}}\left(\frac{\boldsymbol{mole}}{\boldsymbol{g}}\right) = \frac{(\boldsymbol{Vtitrant - Vblank})(\boldsymbol{ml}) * \boldsymbol{Ctitrant}\left(\frac{\boldsymbol{mol}}{\boldsymbol{ml}}\right)}{\boldsymbol{Msample}(\boldsymbol{g})} \qquad \textbf{Equation 5-1}$$

Each sample should be titrated three times with different amount. The plot: C12 amount vs. SDES volume should be linear. The R_2 of the linear regression should be greater than 0.9. The C12 sample concentration can be calculated from the slope of the linear regression and SDES titrant concentration, as shown in Figure 5-4.

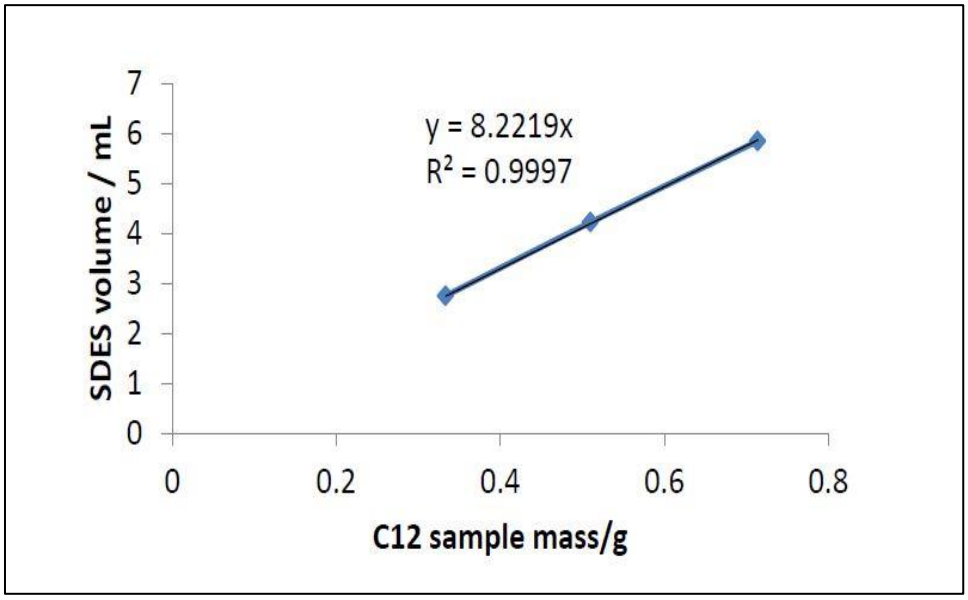

Figure 5-4: Titration of C12 sample mass vs. SDES volume

5.3 Solubility of C-12

C-12 is mostly insoluble at neutral and high pH. At these conditions it is a neutral molecule which can be protonated to change its behavior. As soon as its molecules get proton they combine to form a cationic molecule which makes it water soluble at low pH. The dissolution reaction can be written as:

$RN(EO)_2 + H+ \rightarrow RN^{+}H(EO)_2$ **Equation 5-2**

The cloud point is the temperature above which a surfactant solution becomes turbid or no more soluble. For CO_2 Foam EOR at high temperature, the greater this parameter is the better it is. For C-12 this parameter varies with the pH of system. Figure5-4 Shows the effect of pH on cloud point of C-12[140]. It increases to 140°C at a pH of 4 from almost insoluble at pH of 8 or higher. The pH of the system in our case is lowered by dissolving CO_2 in the brine.

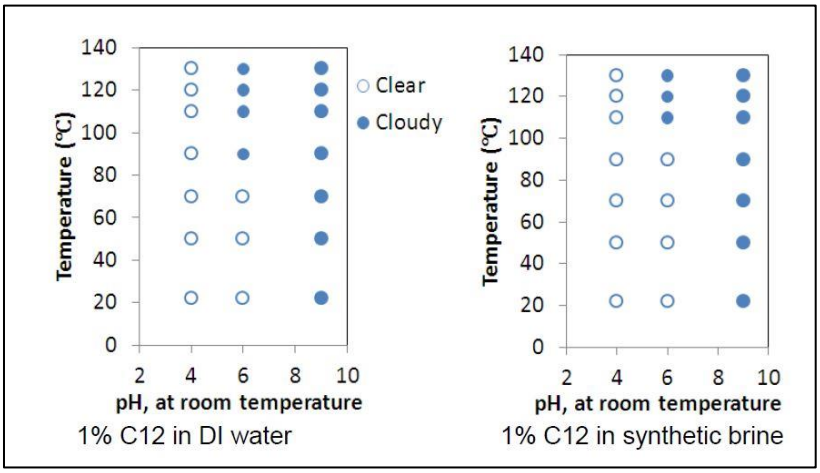

Figure 5-5: Cloud point of C-12 as a function of pH

The pH of the system at different CO2 pressure can be simulated by using PHREEQC software [141]. Figure 5-5 & 5-6 shows the pH as a function of CO2 pressure in DI water & 22% salinity water at 120°C and 25°C. Thus applying CO_2 pressure will make the surfactant dissolve in DI water/brine. Figure 5-7 shows the effect of CO_2 dissolution on C-12 solubility. The first case is when there is no CO_2 pressure applied which gives a cloudy solution referring to insolubility of C-12 at the prevailing pH while the clear solution is obtained after a CO_2 pressure of 2 atm is applied in a Swagelok cylinder(Part No. 304L-HDF4-1000-PD) and the solution is poured back to bottle. The solution thus obtained remains clear or surfactant remains soluble for a long time after removing it from the pressurized cylinder.

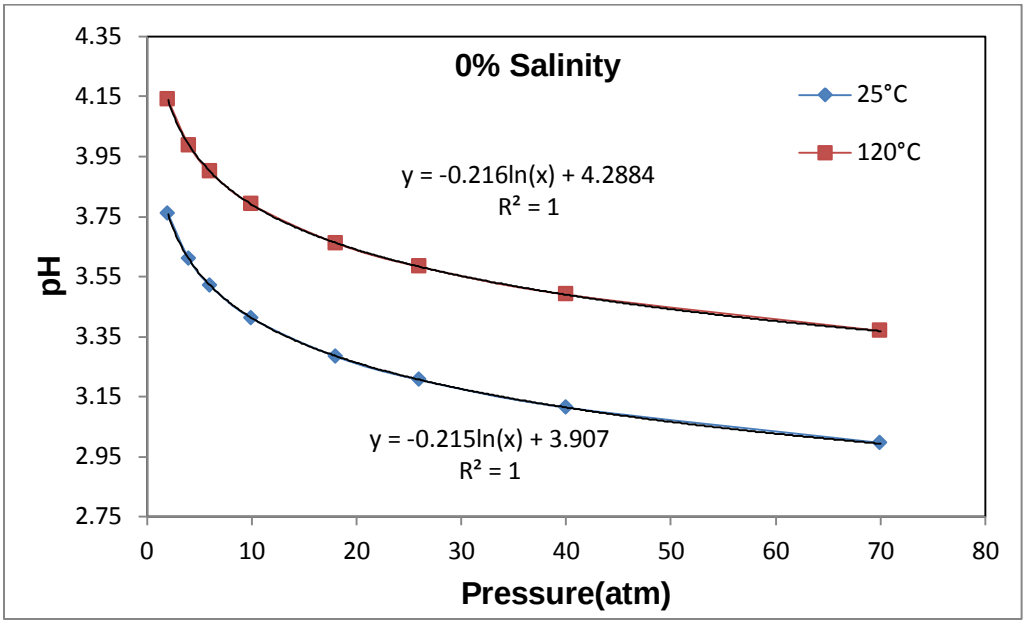

Figure 5-6: pH as a function of CO_2 pressure in DI water

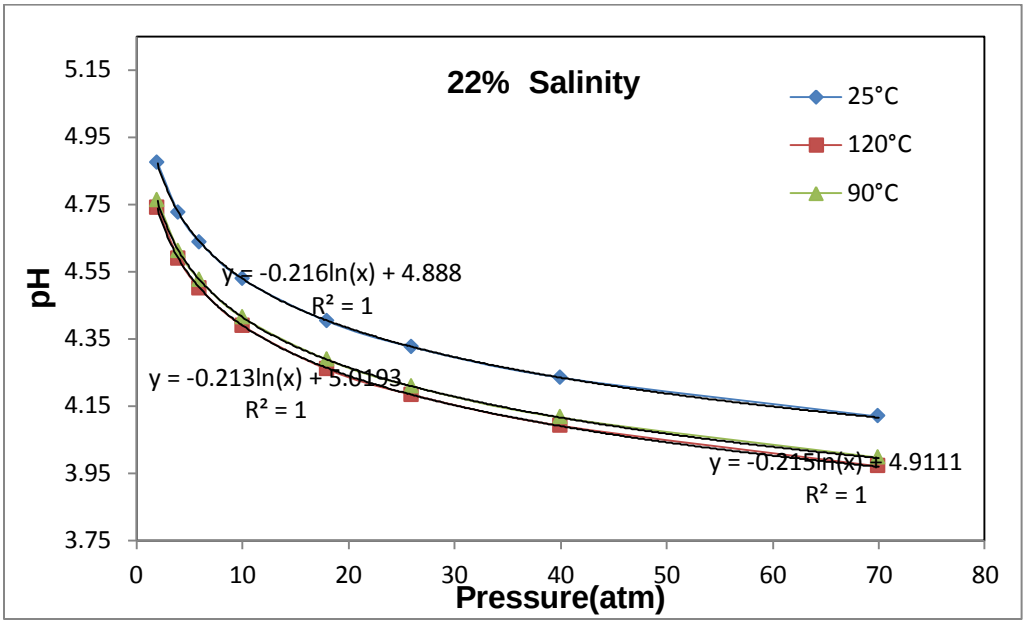

Figure 5-7: pH as a function of CO_2 pressure in 22% salinity brine

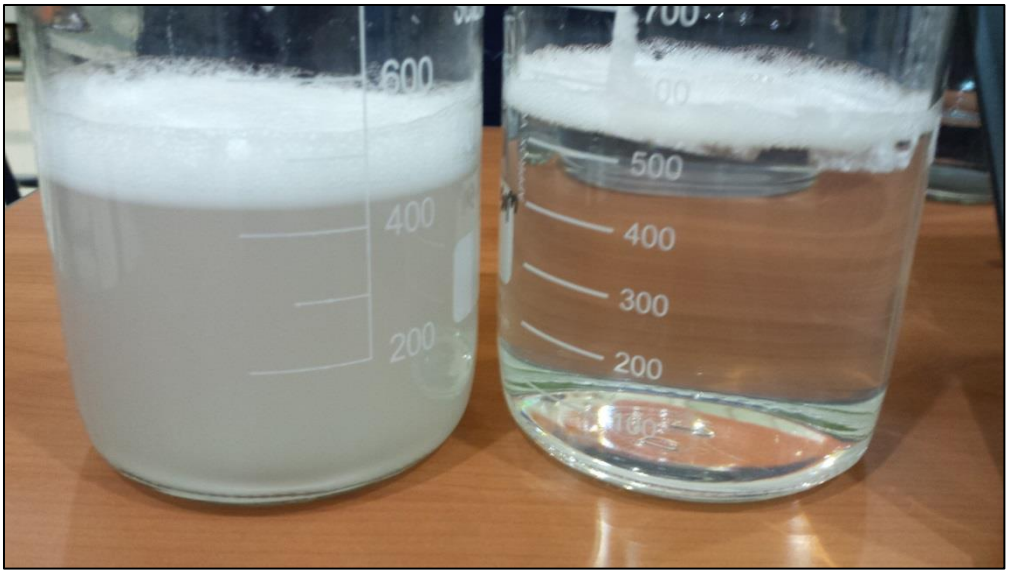

Figure 5-8: C-12 in DI water before and after CO2 pressure of 2atm

5.4 Adsorption Experiment Procedure

Adsorption at 25°C: (1) A stock solution of desired concentration was prepared in 1 Liter glass bottle (Duran, Item #21801545). The resulting cloudy solution was poured into the 1 Liter Swagelok Cylinder (Part#304L-HDF4-1000-PD) and pressurized with 3atm CO_2. After three hours the pressure was released and the clear solution obtained was poured back to the glass bottle. The concentration of this solution was measured using MB two- phase titration.

(2) Different weighed amounts of mineral and C-12 solution was loaded into the 150 ml Swagelok Cylinders (Part #304L-HDF4-150-T-PD). The cylinder was purged several times with CO2 to reduce the fraction of other gases in solution.

(3) The cylinder was finally pressurized with 3 atm CO_2

(4) The cylinder was kept on shaker for 24 hours after which it was kept vertical to settle down all the rocks.

(5) The supernatant of the cylinder was withdrawn and centrifuged for 10 minutes to settle down all the minerals.

(6) The concentration of supernatant obtained in step 5 is determined using the MB two-phase titration method.

Adsorption at 90°C: The adsorption at high temperature needs higher pressure of CO_2 to maintain the required pH. At 90°C the pressure of CO_2 required to prevent the precipitation of C-12 or to achieve a pH of 4.5 is 7atm. This pressure also has to be during the time of taking the supernatant sample otherwise even a slight decrease in

pressure may result in pH reduction which will cause precipitation and hence erroneous adsorption value. This issue was solved by using an outage tube (Swagelok Part# M-DTM4-F4-104) for sampling from the cylinder. After the adsorption at 90°C the cylinder is placed to settle the rock and supernatant sample is drawn from the outage tube while applying a pressure from the other end. Figure 5-8 shows the same setup.

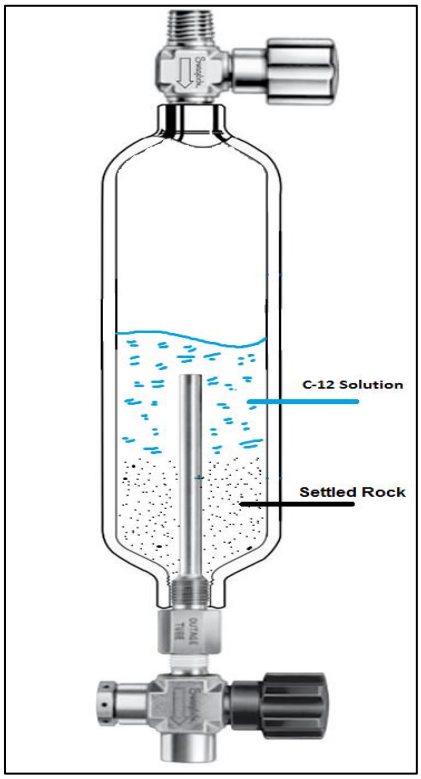

Figure 5-9: High Temperature Adsorption Setup

5.5 Direct Sample Analysis

AxION Direct Sample Analysis (DSA) system integrated with the AxION 2 Time-of-Flight (TOF) mass spectrometer was used for the direct measurement of molecular weight of C-12.The system is collectively known as DSA/TOF system (PerkinElmer, Waltham, MA)[142]. The DSA operates on principles of atmospheric pressure chemical ionization (APCI) and directly ionize the sample at the entrance to the mass spectrometer The AxION is a high-resolution mass spectrometer, meaning it can record ion masses to better than five parts-per-million (ppm) precision relative to their expected masses. The procedure requires no sample preparation, method development and upfront chromatographic separation which allow it to do the complete analysis in less than 20 seconds. Figure 5-9 shows the DSA setup[143].

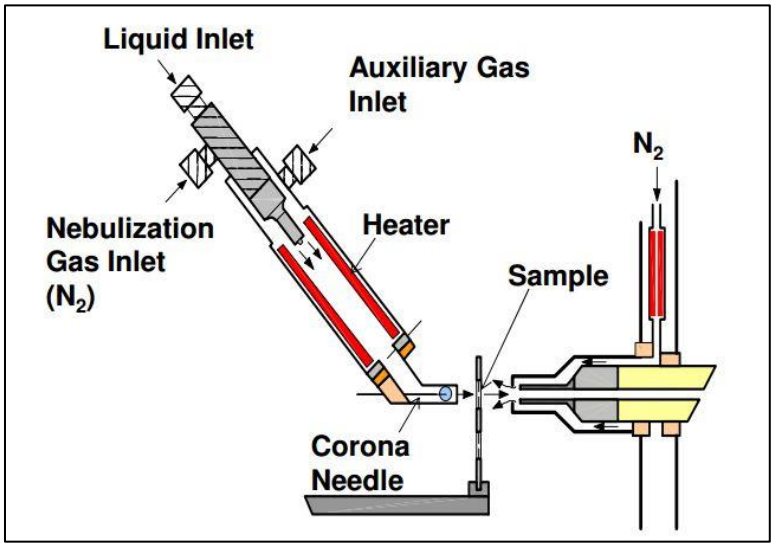

Figure 5-10: DSA Setup

5.6 Results & Discussion

5.6.1 Characterization of Formation Rock Used (R-164)

Figure 5-10 shows the FTIR spectra of the reservoir rock used for adsorption. This spectrum is very similar to the spectra of pure calcite (Figure 3-9). The peaks at 876 and 712 cm^{-1} confirm the nature of the rock to be calcite. Appendix B shows the X-RD of the same rock. Table 5-1 shows the EDX of reservoir rock and Figure 5-12 shows its SEM image. The average particle size is around 6 μm.

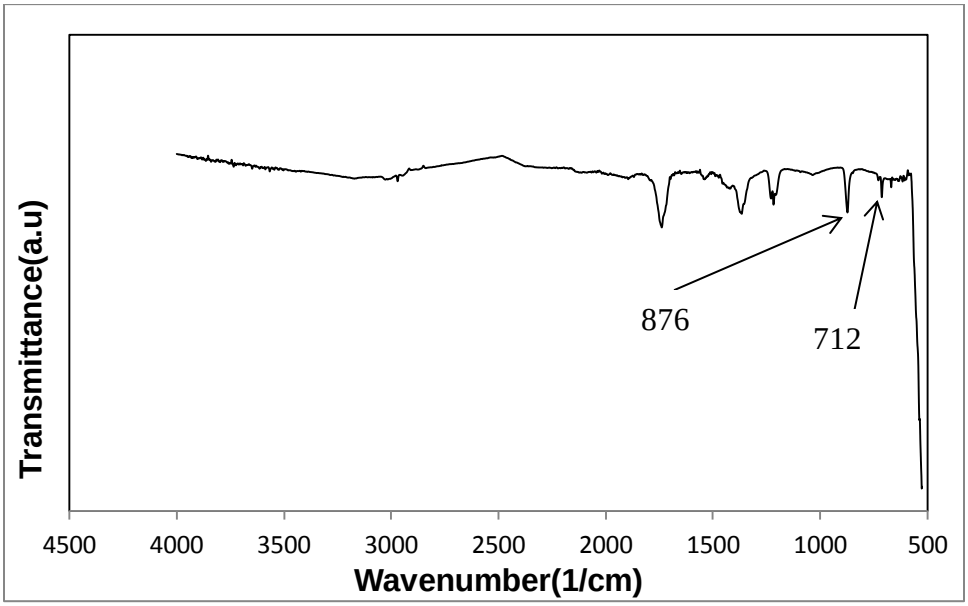

Figure 5-11: FTIR of R-164

Table 5-1: EDX of R-164

Element	Wt. %	At %
C	50.79	64.05
O	29.16	27.61
Ca	16.78	6.34
Mg	2.99	1.86
K	0.27	0.13

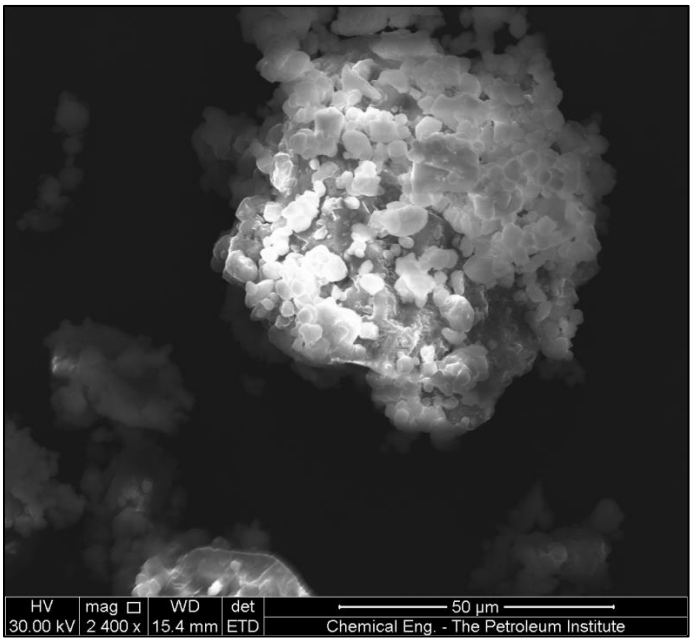

5-12: SEM of R-164

5.6.2 M. W of Ethomeen C-12:

The M.W of C-12 is 288g/mol as reported by AkzoNobel Co. Leyu Cui[140] reported the activity of C-12 to be around 91-94% which is less than the activity reported by the company (97-100%). The difference arises from the fact that company assumes the surfactant's coco alkyl group has chains of C6 to C18 carbon. However, our Leyu's analysis revealed that the C12 surfactant contains negligible amount of C6 to C10 components. In our Direct Sample Analysis (DSA) C-12 is found to have coco alkyl group chains from C8-C12 molecules with no C6 chains detected. Figure 5-4 shows the fraction of different molecular weight molecules in the system. It clearly shows the chains of as high as 355 g/mol MW and as low as 217 g/mol MW which corresponds to C8 & C18 respectively. The major fraction (around 55-60%) is of the molecules with coco alkyl group chain length of 12. Table 5-1 presents the chain length with their percentage.

Table 5-2: Fraction of Chain Lengths in C-12

Chain Length	%
C8	5.724194
C10	11.77582
C12	55.54892
C14	12.13205
C16	10.30165
C18	4.51737

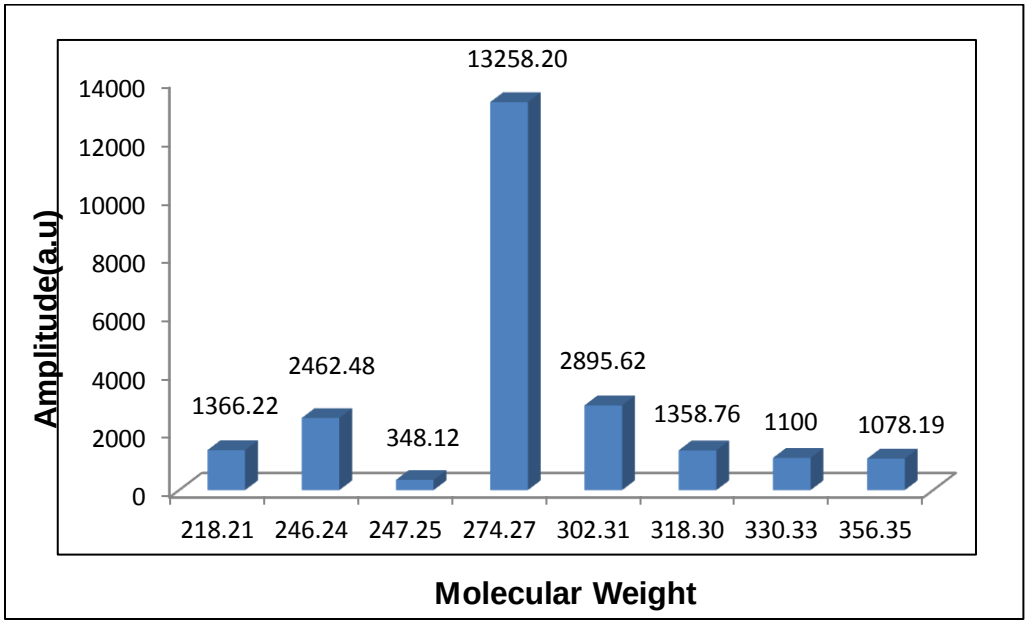

Figure 5-13: MWD of C-12

5.6.3 Adsorption

a. **Adsorption without CO2 Pressure**:

The first adsorption experiment was run by first preparing a clear solution of C-12 in a Swagelok cylinder (Part No. 304L-HDF4-1000-PD) using CO_2 pressure of 3atm. After the clear C-12 solution was obtained the adsorption was run in 50 ml Corning tubes (Part No: 430291). Since the tube does not have two open ends so, no CO_2 pressure was used. This will result in CO_2 stripping from the solution during the shaking as a result of which the C-12 will precipitate and would adsorb in more quantity than the normal capacity. The aim of this experiment was to see the effect of C-12 precipitation on adsorption. The experiment was run at 25°C and in 0% Salinity. The initial concentration of surfactant used was 1%. Figure 5-5 to 5-8 shows the adsorption isotherm on different minerals. The maximum adsorption is obtained for Silica 6.64 mg/m² and minimum for calcite which is 1.30 mg/m².

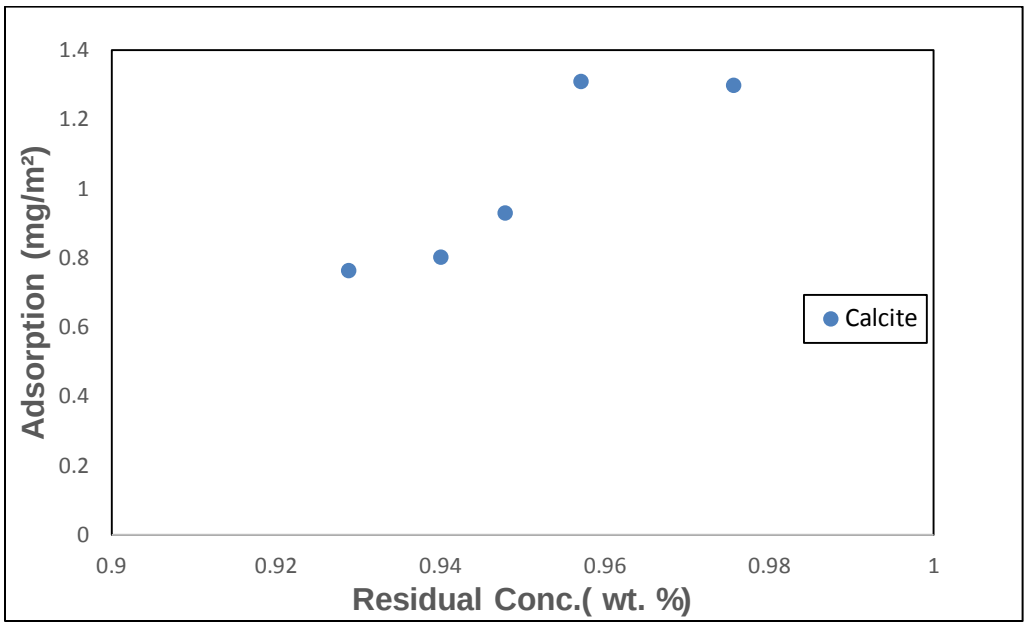

Figure 5-14: Adsorption over Calcite without CO2 Pressure

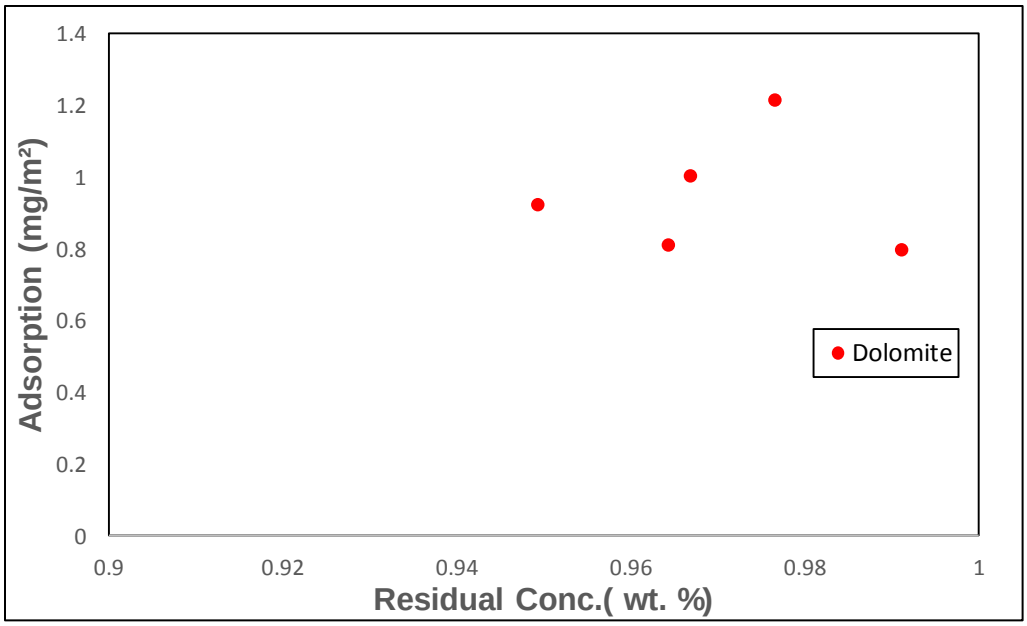

Figure 5-15: Adsorption over Dolomite without CO2 Pressure

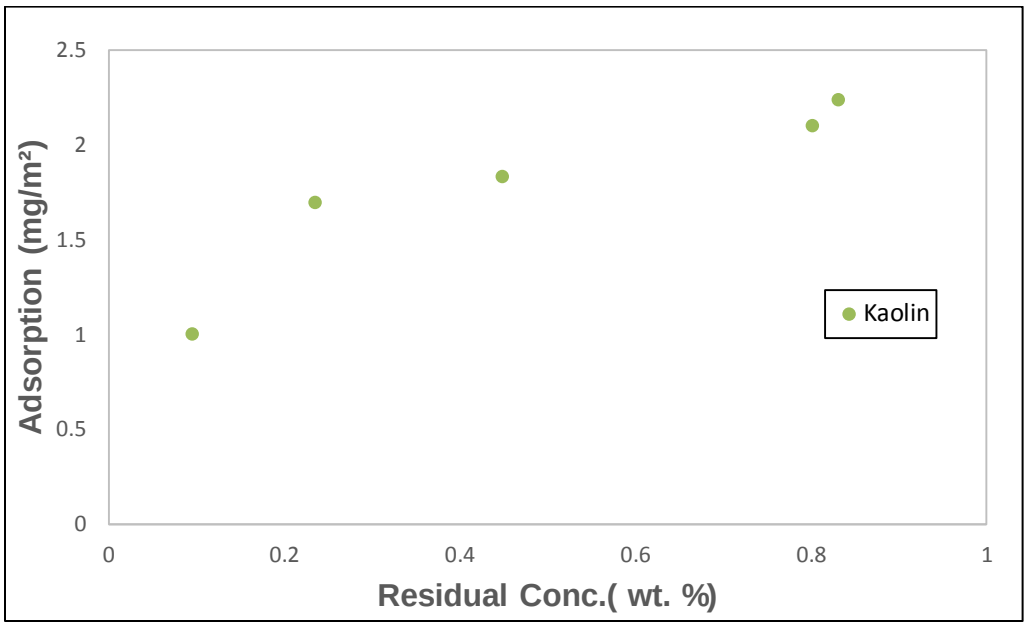

Figure 5-16: Adsorption over Kaolin without CO2 Pressure

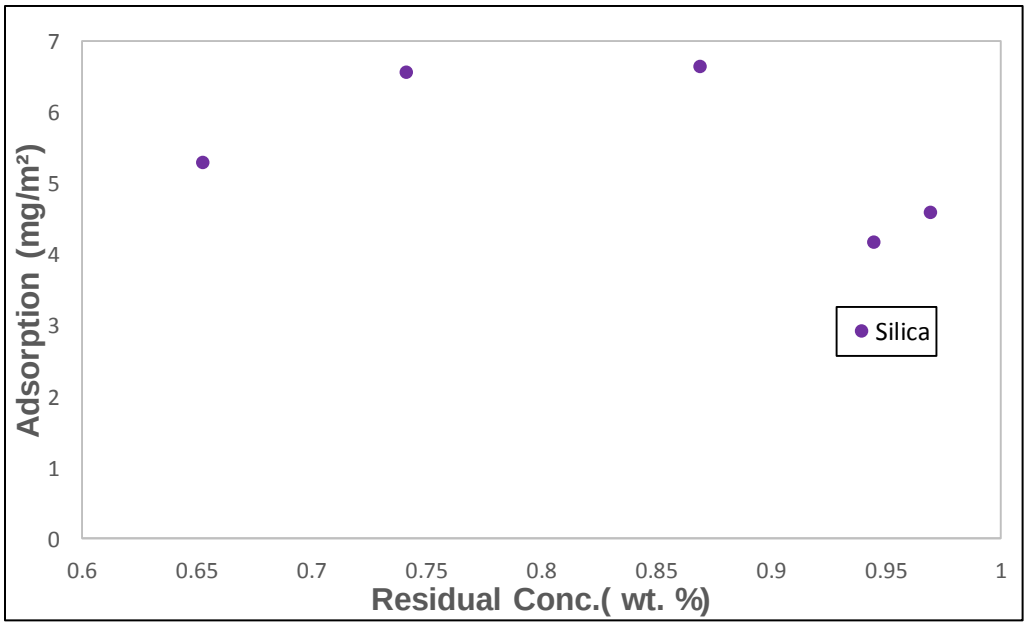

Figure 5-17: Adsorption over Silica without CO2 Pressure

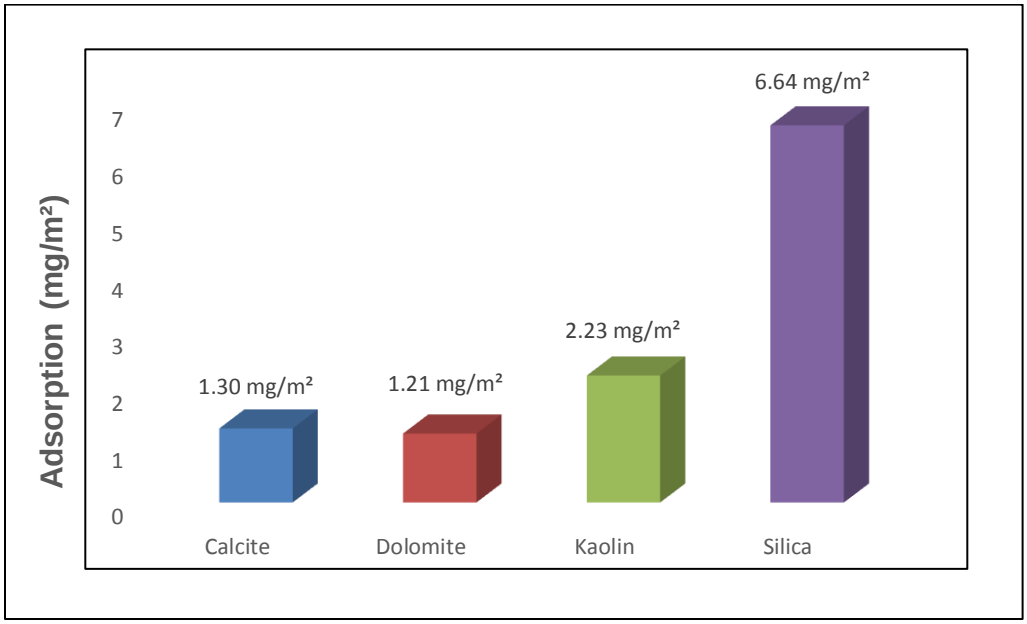

Figure 5-18: Adsorption Plateau over four minerals without CO_2 Pressure

b. Adsorption on Calcite with CO2 Pressure

This experiment was run with a CO2 pressure of 3atm. The adsorption procedure with CO_2 has already been explained in previous section (5.4). Cylinder with pressurized CO_2 will have a pH sufficiently low to dissolve the C-12. In this case no precipitation of C-12 will expectedly result in less adsorption compared to previous case. Two experiments were run one with different initial concentration of Surfactant (0.5% and 1% by wt.). The adsorption plateau from both the experiments is 0.23 mg/m².

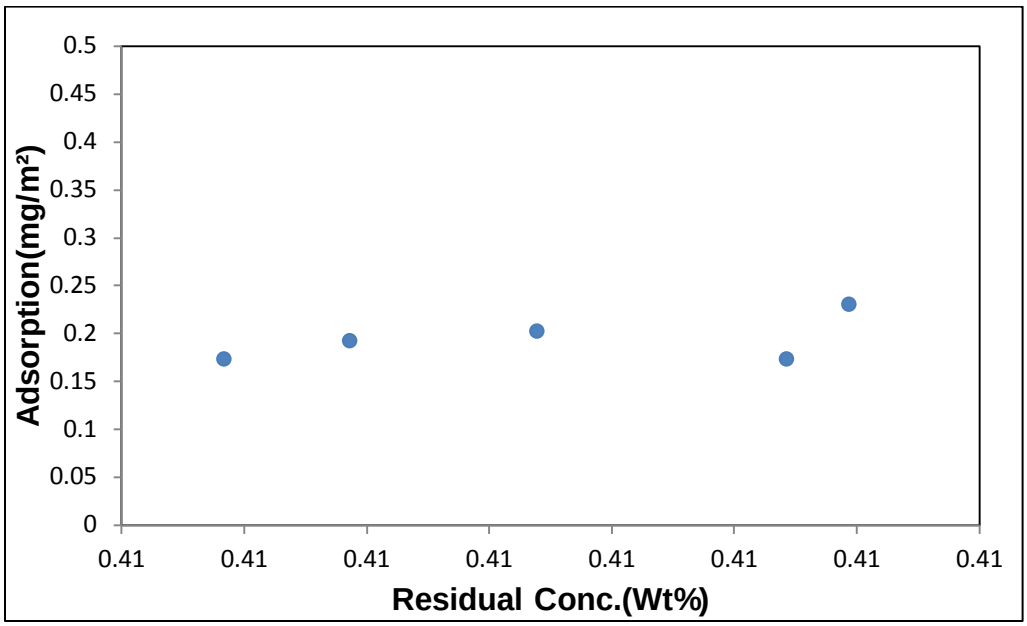

Figure 5-19: Adsorption 1 over Calcite with CO_2 Pressure

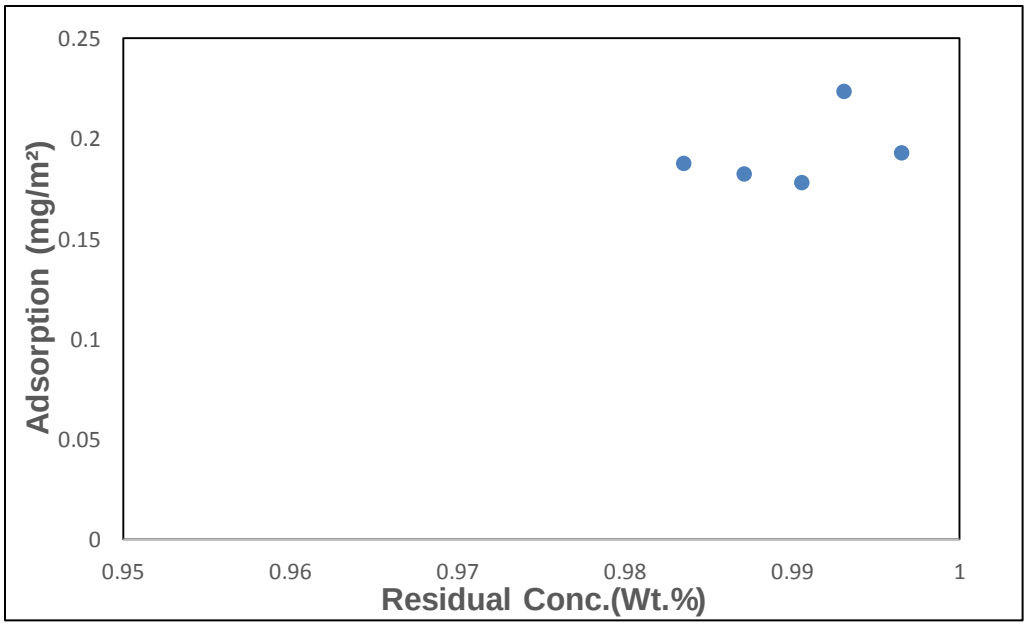

Figure 5-20: Adsorption 2 over Calcite with CO_2 Pressure

c. Adsorption on Pure Silica: Effect of Salinity and Temperature

This experiment was performed to study the effect of salinity and temperature on adsorption of C-12 on Silica. Figure 5-12 shows the decreasing trend of adsorption as salinity is raised from 0% to 22%. The adsorption also goes down significantly with an increase in temperature. The adsorption plateau has decreased from 6.05mg/m² to 2.3 mg mg/m².

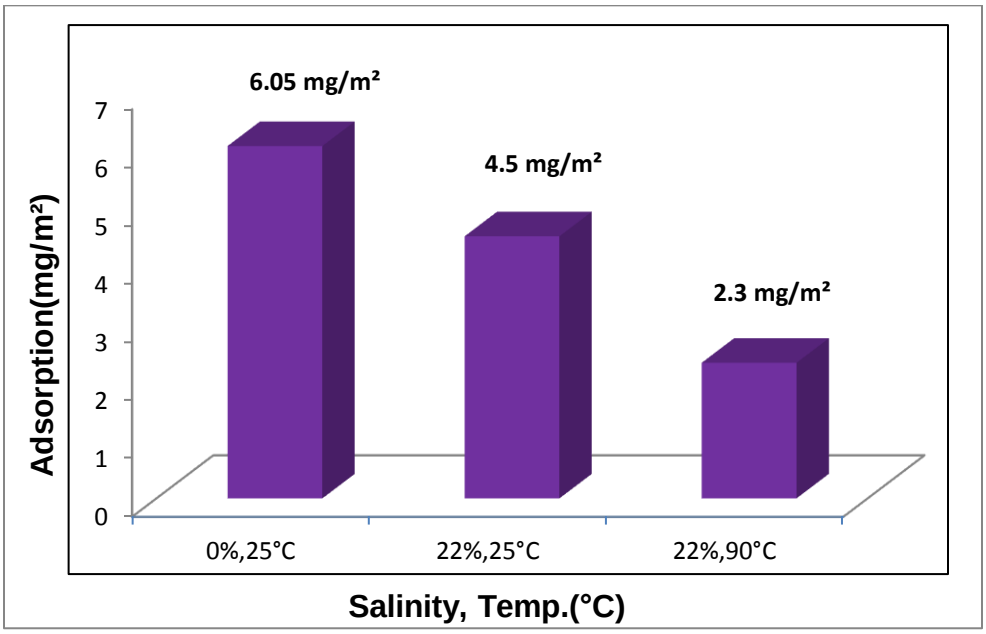

Figure 5-21: Effect of Salinity and Temperature on Adsorption over Silica

d. Adsorption on Formation Rock: Effect of Temperature

This experiment shows the adsorption of C-12 on formation mineral which is mainly calcite. The adsorption as expected is low. Figure 5-13 shows the comparison of two adsorption level with same condition except the temperature. The effect of Temperature is quite promising for adsorption on formation minerals as it has gone down to almost zero

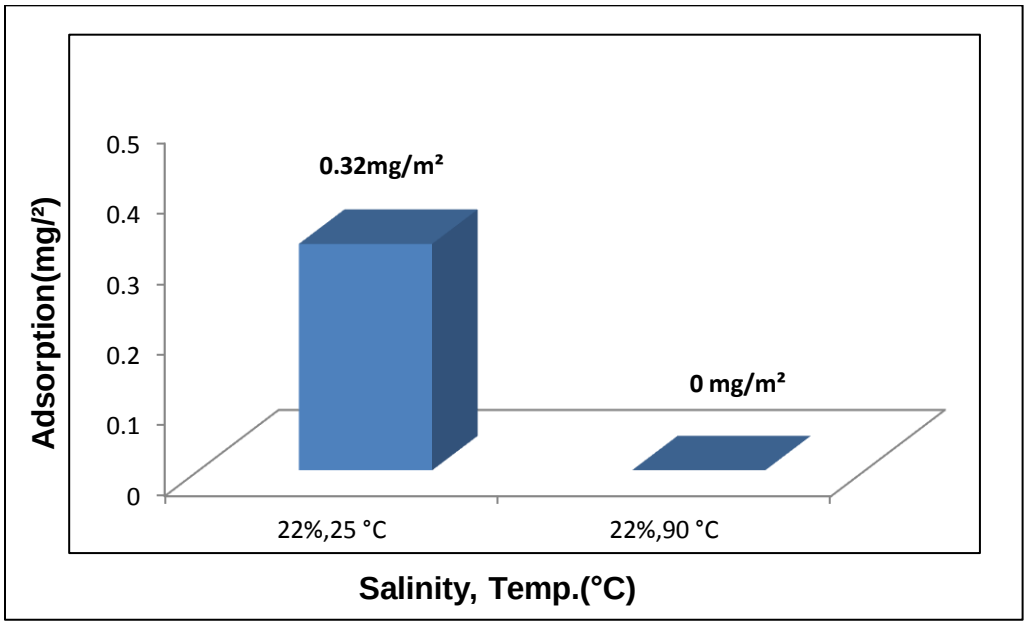

Figure 5-22: Effect of Temperature on Adsorption over Formation Rock-164

5.6.4 Discussion of Adsorption Results

Figure 5-17 shows the adsorption plateaus without CO_2 pressure on all the four minerals. The maximum adsorption is obtained for Silica which is because of the negative charge present over silica surface. C-12 being a cationic surfactant has a greater tendency to adsorb strongly over silica. The next level of adsorption density is on kaolin. Kaolin also has a negative charge over its surface. For Calcite and Dolomite the adsorption is low and equal this is because of the positive surface charge over both of these carbonate rocks.

Adsorption on calcite rock reduces to 0.23 mg/m² from 1.30 mg/m² when run under CO_2 pressure. CO_2 pressure maintained the enough pH so as to make the C-12 always soluble in the solution or it prevented C-12 from precipitating.

Effect of salinity and temperature on adsorption density on silica is shown in Figure5-20. The salinity and temperature both have the same effect of decreasing the adsorption as both of these are increased. The effect of salinity on adsorption has already been explained by Leyu et al. [117] where they explained the adsorption site neutralization(sites with negative charge) by the positive charge ions present in the solution. For temperature, the adsorption is a physical process which decreases with temperature. So we are also getting the same results.

Adsorption on reservoir rock was expected to be low because of the pure carbonate nature of the rock. It also decreases with temperature and almost no adsorption occurs at 90°C. This is a promising result for the use of this surfactant in the carbonate reservoirs at high temperature.

Chapter 6: Conclusions & Future Work

6.1 Conclusion

The static adsorption results over different minerals shows Schizophyllan to be adsorption maximum over carbonate minerals compared to siliceous minerals. However due to the presence of siliceous impurities in reservoir rocks the adsorption is low compared to pure calcite. The adsorption level also goes down with salinity, temperature and background ions like Na^{+}, Ca^{+2} and Mg^{+2}. The results are promising for the fields with higher salinity. The GPC result shows the preferential adsorption of bigger chain molecules compared to smaller chains. This is expected behavior for polymers adsorbing over surfaces.

Dynamic adsorption of Schizophyllan is low compared to static adsorption value. This is attributed to the large time of equilibration required by the Schizophyllan to adsorb over the carbonate surface. Adsorption in the presence of oil is 7μg/g compared to 40μg/g when there is no original oil in place. This is because lot of adsorption sites were already taken or occupied by the crude oil resulting in low adsorption. This is again a very promising aspect of Schizophyllan injection into fields. There is a significant reduction in viscosity of the Schizophyllan while flowing through core. The maximum viscosity reached by any effluent in both the cases is around 40% to the injected viscosity.

Adsorption of C-12 without any CO_2 pressure is high which is attributed to its precipitation during the adsorption test as a result of CO_2 stripping from the solution. Adsorption on calcite goes down to 0.23 mg/m² with CO_2 pressure from 1.30 mg/m² with no CO2 pressure. Adsorption over silica is high in DI water (6 mg/m²) and decreases with salinity (4.5 mg/m²) and temperature (2.3 mg/m² at 90°). Adsorption over reservoir rock is relatively high (0.32mg/m²) compared to pure calcite (0.23 mg/m²) which is because of the siliceous impurities present in the rock. Adsorption on reservoir rock goes down to almost zero at 90°C compared to 0.32 mg/m².

6.2 Future Work

- Static as well as Dynamic Adsorption of Schizophyllan at 120°C and in formation brine is proposed.
- Dynamic Adsorption in the presence of tracer is also proposed so as to evaluate the IPV and better understand the injectability of polymer.
- Adsorption of C-12 should be studied at higher temperatures equal to field of application
- Thermal degradation characteristics of the C-12 should also be examined before finalizing it for field application.

Appendix A

X-RD of minerals used for Polymer Adsorption

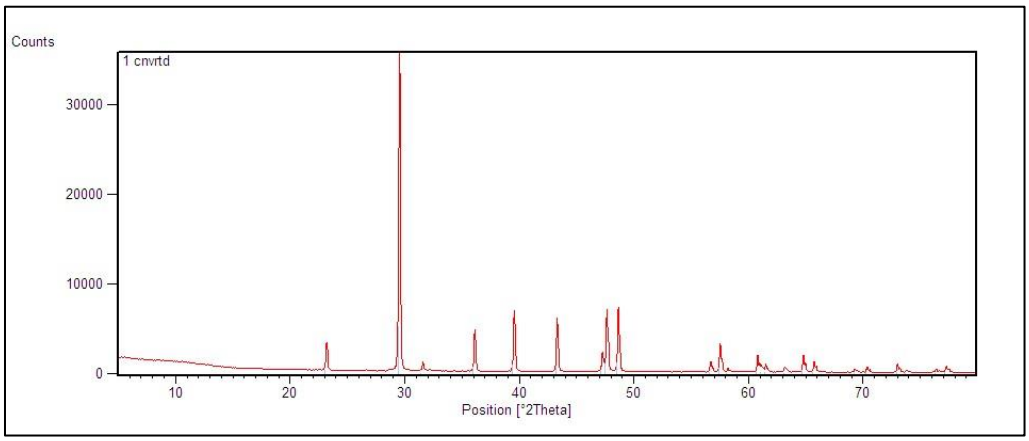

Figure A- 1:X-RD of Calcite

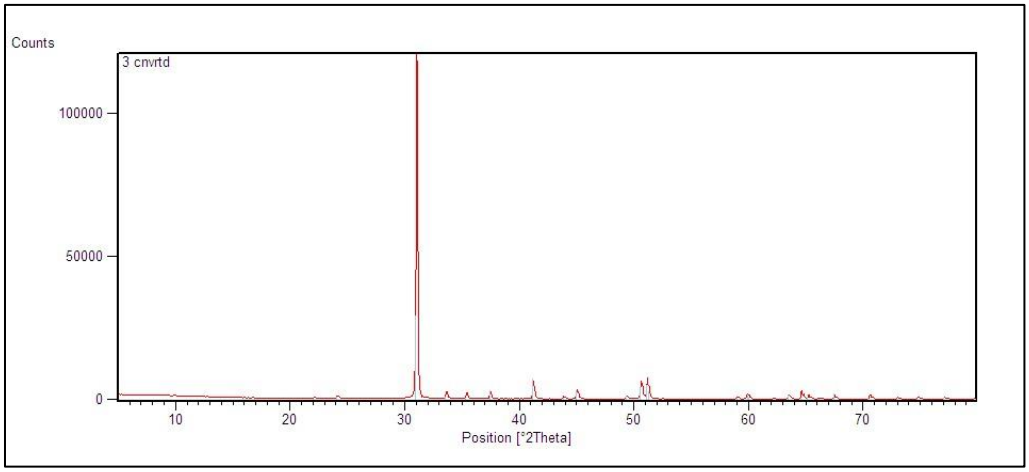

Figure A- 2:X-RD of Dolomite

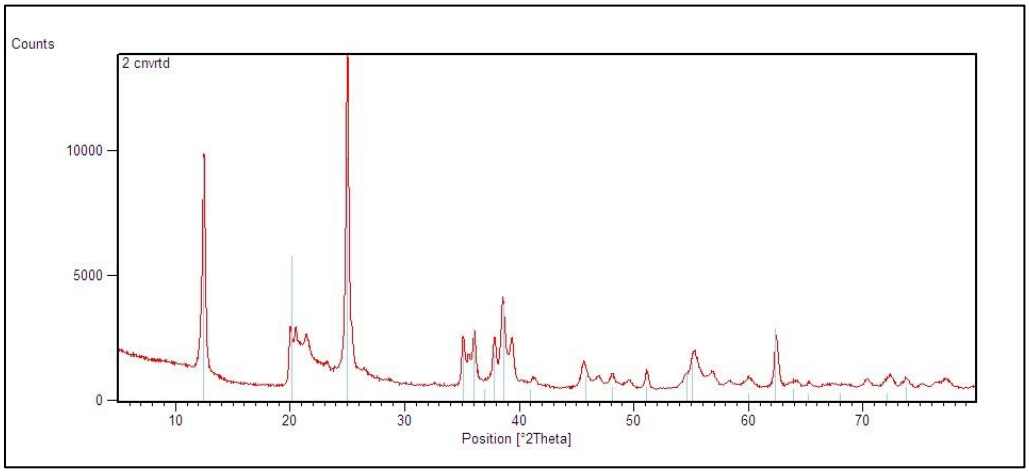

Figure A- 3: X-RD of Kaolin

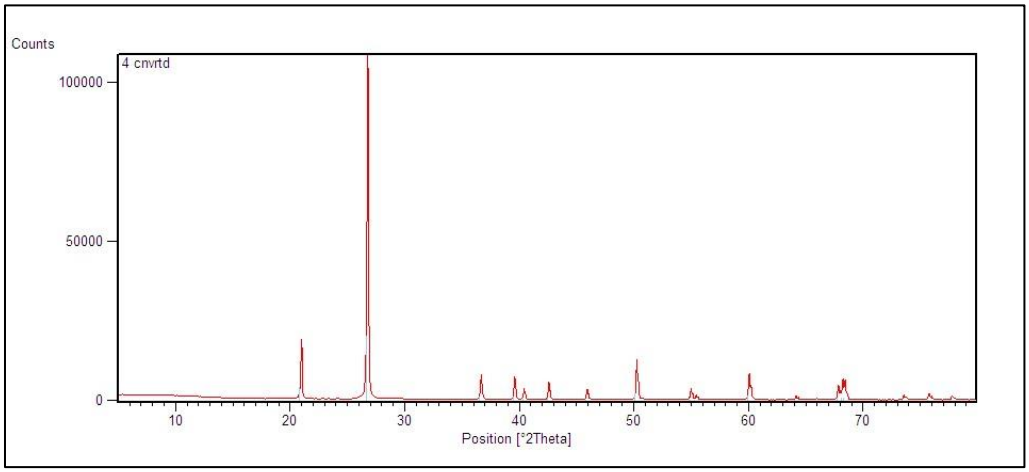

Figure A- 4: X-RD of Silica

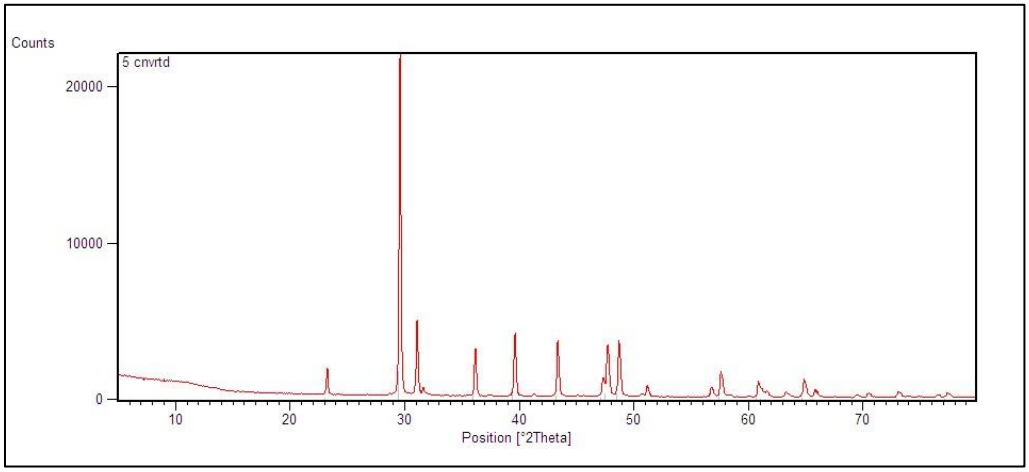

Figure A- 5: X-RD of R-5

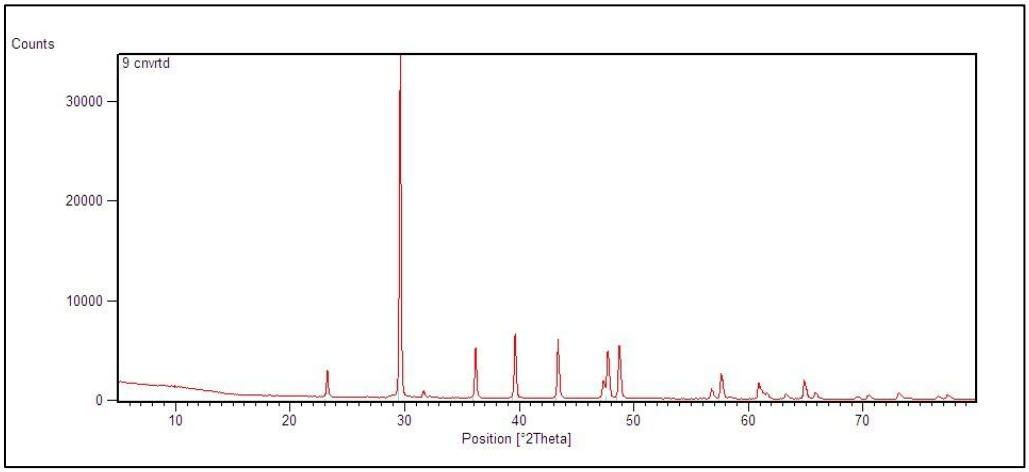

Figure A- 6: X-RD of R-9

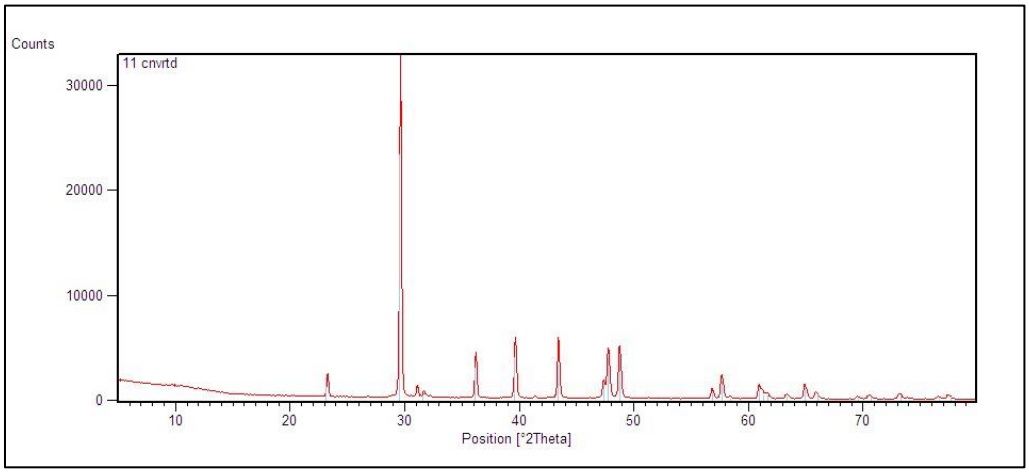

Figure A- 7: X-RD of R-11

Appendix B

X-RD of Reservoir Rock used for C-12 Adsorption

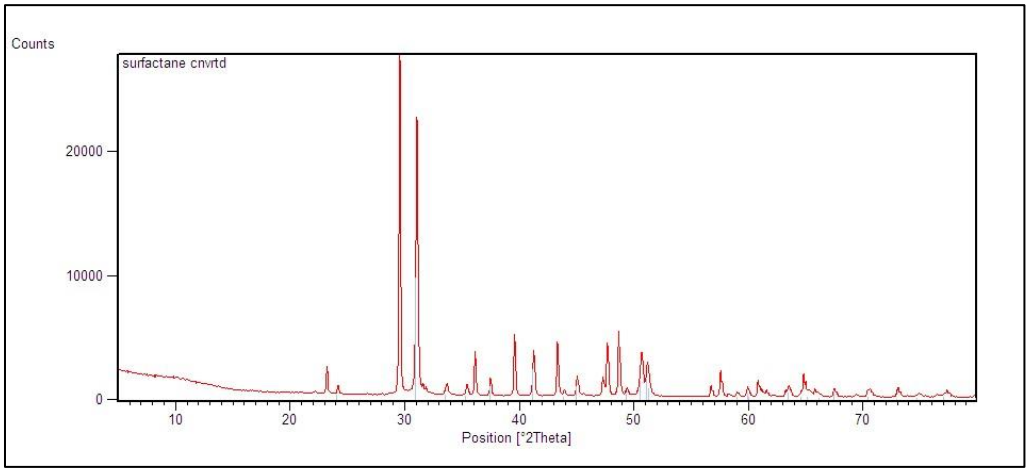

Figure B- 1: X-RD of R-164

References

1. Fletcher, A.J.P., et al., *The Successful Implementation of a Novel Polymer EOR Pilot in the Low Permeability Windalia Field*, Society of Petroleum Engineers.
2. Amro, M.M., El-Sayed, A.-A.H. Al-Homahdi, E.S., Al-Saddique, M.A., Al-Awad, M.N., *Investigation of Polymer Adsorption on Rock Surface of High Saline Reservoirs*. Chemical Engineering and Technology, 2002. **25**(10): p. 1005-1013.
3. (ERCB), E.R.C.B. *Potential Of EOR in Alberta oil pools phase 1 report for Energy* 2011.
4. Omar, A.E., *Effect of Polymer Adsorption on Mobility Ratio*, Society of Petroleum Engineers.
5. Bondor, P.L., G.J. Hirasaki, and M.J. Tham, *Mathematical Simulation of Polymer Flooding in Complex Reservoirs.*
6. *OPEC World Oil Outlook 2013.*
7. Alvarado, V.M., Eduardo, *Enhanced Oil Recovery: An Update Review.* Energies, 2010. **3**(9): p. 1529-1575.
8. *IEA World Energy Outlook 2013.*
9. Shell.com, *Enhanced Oil Recovery*, 2012.
10. Doghaish, N.M., *Analysis of Enhanced Oil Recovery processes---a literature review*, 2009, Dalhousie University (Canada): Ann Arbor. p. 114.

11. Al-Hashmi, A.-A.R., *Polymer Retention During Flow of Polymer Solutions Through Porous Media*, in *Department of Chemical Engineering and Chemical Technology* 2008, Imperial College London, London.

12. Glossary, S.O.

13. Lake, L.W., *Enhanced oil recovery*1989: Prentice Hall.

14. Taber, J.J., F.D. Martin, and R.S. Seright, *EOR Screening Criteria Revisited - Part 1: Introduction to Screening Criteria and Enhanced Recovery Field Projects.*

15. Taber, J.J., F.D. Martin, and R.S. Seright, *EOR Screening Criteria Revisited—Part 2: Applications and Impact of Oil Prices.*

16. Schlumberger. *http://www.slb.com/services/technical_challenges/carbonates.aspx*.

17. Mazzullo, S.J., *Overview of Porosity Evolution in Carbonate Reservoirs**. Search and Discovery Article, 2004.

18. Moritis, G., *Report on Enhanced Oil Recovery*. Oil & Gas Journal, 2002.

19. Leonard, J., *Production/Enhanced Oil Recovery Report.* Oil & Gas Journal, 1986.

20. Manning R. K., P.G.A., Lake L. W.,Paul G. W., Wesson T. C, *A Technical Survey of Polymer Flooding Projects*, September 1983, Department of Energy.

21. D.;, T.N.B.D.G.G.C.M.J.G.E.H.H.C.R.H.M.H.H.S., *Integrated characterization of Permian Basin Reservoirs, University Lands, West Texas: Targeting the*

Remaining Resource for Advanced Oil Recovery, 1991, Texas Bureau Econ. Geol.,.

22. Manrique, E.J., et al., *EOR: Current Status and Opportunities*, Society of Petroleum Engineers.
23. Wilkinson, J.R., G.F. Teletzke, and K.C. King, *Opportunities and Challenges for Enhanced Recovery in the Middle East*, Society of Petroleum Engineers.
24. Liu, S., *Alkaline Surfactant Polymer enhanced oil recovery process*, in *Chemical Engineering*2008, Rice University: Houston.
25. Finch, C.A., *Polymer-improved oil recovery. K. S. Sorbie Blackie & Son, Glasgow, 1991. pp. xii + 359, price £59.00. ISBN 0–216–92693–9.* Polymer International, 1992. **28**(3): p. 256-256.
26. Raney, K. *Moving Chemical Enhanced Oil Recovery Offshore*. in *Graduate Seminar Presentations*. 2011. Petroleum Engineering TAMU: Shell International Exploration and Production.
27. Gao, H.W., *Mobility control in oil recovery by chemical flooding state of the art review*, 1987, U.S Department of Energy.
28. Dr. Larry W. Lake , D.M.P.W., *Enhanced Oil Recovery (EOR) field data literature search*, 2008, Danish North Sea Partner ,Danish Energy Agency ,Mærsk Olie og Gas AS: Austin, TX
29. Pope, G.A., *Chemical Flooding Overview*, 2007.

30. Seright, R.S., *Improved Techniques for Fluid Diversion in Oil Recovery*, 1994, DOE.

31. Pope, G.A., *Recent Developments and Remaining Challenges of Enhanced Oil Recovery*, JULY 2011, University of Texas at Austin.

32. Davison, P. and E. Mentzer, *Polymer Flooding in North Sea Reservoirs.*

33. Vermolen, E.C.M., et al., *Pushing the envelope for polymer flooding towards high-temperature and high-salinity reservoirs with polyacrylamide based ter-polymers*, Society of Petroleum Engineers.

34. Al-Bahar, M.A., et al., *Evaluation of IOR Potential within Kuwait*, Society of Petroleum Engineers.

35. Alkafeef, S.F. and A.M. Zaid, *Review of and Outlook for Enhanced Oil Recovery Techniques in Kuwait Oil Reservoirs*, International Petroleum Technology Conference.

36. Abbas, S., J.C. Donovan, and A. Sanders, *Applicability of Hydroxyethylcellulose Polymers for Chemical EOR*, Society of Petroleum Engineers.

37. Zaitoun, A. and B. Potie, *Limiting Conditions for the Use of Hydrolyzed Polyacrylamides in Brines Containing Divalent Ions*, Society of Petroleum Engineers.

38. Wu, Y., et al., *Development of New Polymers with Better Performance under Conditions of High Temperature and High Salinity*, Society of Petroleum Engineers.

39. García-Ochoa, F., et al., *Xanthan gum: production, recovery, and properties.* Biotechnology Advances, 2000. **18**(7): p. 549-579.

40. Becker, A., et al., *Xanthan gum biosynthesis and application: a biochemical/genetic perspective.* Applied Microbiology and Biotechnology, 1998. **50**(2): p. 145-152.

41. Kierulf, C. and I.W. Sutherland, *Thermal stability of xanthan preparations.* Carbohydrate Polymers, 1988. **9**(3): p. 185-194.

42. Seright, R.S. and B.J. Henrici, *Xanthan Stability at Elevated Temperatures.*

43. Al-Kaabi, S.K.A.A., *Enhanced oil recovery: challenges & opportunities* World Petroleum Council.

44. Rau, U.H., Andreas Wagner, Fritz, *Eignung von Schizophyllan-Lösungen zum Polymerfluten von Erdöl-Lagerstätten mit hoher Temperatur und Salinität.* Chemie Ingenieur Technik, 1992. **64**(6): p. 576-577.

45. B. Leonhardt*, F.V., E. Lessner, B. Wenzke and J. Schmidt *From Flask to Field – The Long Road to Development of a New Polymer*, in *IOR 2011* 2011, EAGE

46. Yanaki, T., K. Tabata, and T. Kojima, *Melting behaviour of a triple helical polysaccharide schizophyllan in aqueous solution.* Carbohydrate Polymers, 1985. **5**(4): p. 275-283.

47. Norisuye, T., *Triple-stranded helical structure of schizophyllan and its antitumor activity in aqueous solution.* Die Makromolekulare Chemie, 1985. **14**(S19851): p. 105-118.

48. Kony, D.B., et al., *Explicit-Solvent Molecular Dynamics Simulations of the Polysaccharide Schizophyllan in Water.* Biophysical Journal. **93**(2): p. 442-455.

49. Akstinat, M.H., *Polymers For Enhanced Oil Recovery In Reservoirs Of Extremely High Salinities And High Temperatures*, Society of Petroleum Engineers.

50. Delamaide, E., R. Tabary, and D. Rousseau, *Chemical EOR in Low Permeability Reservoirs*, Society of Petroleum Engineers.

51. Marker, J.M., *Dependence of Polymer Retention on Flow Rate.*

52. Dominguez, J.G.W., G. P., *Retention and Flow Characteristics of Polymer Solutions in Porous Media.*

53. Chauveteau, G. and N. Kohler, *Polymer Flooding: The Essential Elements for Laboratory Evaluation*, Society of Petroleum Engineers.

54. Green, D.W. and G.P. Willhite, *Enhanced Oil Recovery*1998: Henry L. Doherty Memorial Fund of AIME, Society of Petroleum Engineers.

55. Zaitoun, A. and N. Kohler, *The Role of Adsorption in Polymer Propagation Through Reservoir Rocks*, Society of Petroleum Engineers.

56. Sorbie, K.S., et al., *Non-equilibrium effects in the adsorption of polyacrylamide onto sandstone; Experimental and modelling study.* Journal Name: In Situ; (USA); Journal Volume: 13:3, 1989: p. Medium: X; Size: Pages: 121-164.

57. Lecourtier, G.C.a.J., *PROPAGATION OF POLYMER SLUGS THROUGH ADSORBENT POROUS MEDIA*

in *Water-Soluble Polymers for Petroleum Recovery*, D.N.S. G.A. Stahl, Editor 1988.

58. DENYS, K.F.J., *Flow of Polymer Solutions Through Porous Media*, 2003, TU Delft.

59. Sheng, J., *Modern Chemical Enhanced Oil Recovery: Theory and Practice*2010: Gulf Professional Pub.

60. SORBIE, K.S., *Polymer-Improved Oil Recovery*1991: Springer Science+Business Media New York.

61. Huh, C., E.A. Lange, and W.J. Cannella, *Polymer Retention in Porous Media*, Society of Petroleum Engineers.

62. Gogarty, W.B., *Mobility Control With Polymer Solutions.*

63. Szabo, M.T., *Laboratory Investigations of Factors Influencing Polymer Flood Performance.*

64. Szabo, M.T., *Some Aspects of Polymer Retention in Porous Media Using a C14-Tagged Hydrolyzed Polyacrylamide.*

65. Vela, S., D.W. Peaceman, and E.I. Sandvik, *Evaluation of Polymer Flooding in a Layered Reservoir With Crossflow, Retention, and Degradation.*

66. Smith, F.W., *The Behavior of Partially Hydrolyzed Polyacrylamide Solutions in Porous Media.*

67. G. Paul Willhite , J.G.D., *Mechanisms of Polymer Retention in Porous Media* in *Improved Oil Recovery by Surfactant and Polymer Flooding*, R.S.S.R. D.O . Shah Editor, Academic Press Inc.: New York.

68. Herzig, J.P., Leclerc, D. M. and Le Goff, P, *Flow Through Porous Media*1970: American Chemical Society.

69. Herzig, J.P., D.M. Leclerc, and P.L. Goff, *Flow of Suspensions through Porous Media—Application to Deep Filtration.* Industrial & Engineering Chemistry, 1970. **62**(5): p. 8-35.

70. Dawson, R.L., Ronald B., *Inaccessible Pore Volume in Polymer Flooding.*

71. Trushenski, S.P., D.L. Dauben, and D.R. Parrish, *Micellar Flooding - Fluid Propagation, Interaction, and Mobility.*

72. Vavylonis, B.O.S.a.D., *Non-equilibrium in adsorbed polymer layers.* J. Phys.: Condens. Matter 2005.

73. Pashley, R. and M. Karaman, *Applied Colloid and Surface Chemistry*2005: Wiley.

74. Fleer, G.J.L., J. In, *Adsorption From Solution at the Solid/Liquid Interface*

1983, New York: Academic Press.

75. Källrot, N. and P. Linse, *Dynamic Study of Single-Chain Adsorption and Desorption.* Macromolecules, 2007. **40**(13): p. 4669-4679.

76. Fleer, G., *Polymers at Interfaces*1993: Springer.

77. Takahashi, A., et al., *Adsorption of Polystyrene at the θ Temperature.* Macromolecules, 1980. **13**(4): p. 884-889.

78. Lecourtier, J., L.T. Lee, and G. Chauveteau, *Adsorption of polyacrylamides on siliceous minerals.* Colloids and Surfaces, 1990. **47**(0): p. 219-231.

79. Lee, L.T., et al., *Adsorption of polyacrylamides on the different faces of kaolinites.* Journal of Colloid and Interface Science, 1991. **147**(2): p. 351-357.

80. Pefferkorn, E., et al., *Adsorption of hydrolyzed polyacrylamides onto amphoteric surfaces.* Journal of Colloid and Interface Science, 1990. **137**(1): p. 66-74.

81. Ahmed, H., J.E. Glass, and G.J. McCarthy, *Adsorption of Water-Soluble Polymers on High Surface Area Clays*, Society of Petroleum Engineers.

82. Kwaguchi, M., C. Suzuki, and A. Takahashi, *Hydrodynamic thicknesses of polyethylene oxides adsorbed in porous media under poor solvent conditions.* Journal of Colloid and Interface Science, 1988. **121**(2): p. 585-589.

83. Pefferkorn, E., A. Carroy, and R. Varoqui, *Dynamic behavior of flexible polymers at a solid/liquid interface.* Journal of Polymer Science: Polymer Physics Edition, 1985. **23**(10): p. 1997-2008.

84. de Gennes, P.G., *Scaling Concepts in Polymer Physics*1979: Cornell University Press.

85. Mungan, N., *Rheology and Adsorption of Aqueous Polymer Solutions.*

86. Deng, Y., J.B. Dixon, and G.N. White, *Adsorption of Polyacrylamide on Smectite, Illite, and Kaolinite.* Soil Sci. Soc. Am. J., 2006. **70**(1): p. 297-304.

87. Hollander, A.F., P. Somasundaran, and C.C. Gryte, *Adsorption characteristics of polyacrylamide and sulfonate-containing polyacrylamide copolymers on sodium kaolinite.* Journal of Applied Polymer Science, 1981. **26**(7): p. 2123-2138.

88. Dang, C.T.Q., et al., *Development of Isotherm Polymer/Surfactant Adsorption Models in Chemical Flooding*, Society of Petroleum Engineers.

89. Cardoso, C.B., R.C.A. Silva, and A.P. Pires, *The Role of Adsorption Isotherms on Chemical-Flooding Oil Recovery*, Society of Petroleum Engineers.

90. Shah, S., S.A. Heinle, and J.E. Glass, *Water-Soluble Polymer Adsorption From Saline Solutions*, Society of Petroleum Engineers.

91. Satter, A., et al., *Chemical Transport in Porous Media With Dispersion and Rate-Controlled Adsorption.*

92. Vossoughi, S., et al., *A New Method To Simulate the Effects of Viscous Fingering on Miscible Displacement Processes in Porous Media.*

93. Yuan, C., M. Delshad, and M.F. Wheeler, *Parallel Simulations of Commercial-Scale Polymer Floods*, Society of Petroleum Engineers.

94. Shah, B.N., et al., *The Effect Of Inaccessible Pore Volume On The Flow Of Polymer And Solvent Through Porous Media*, Society of Petroleum Engineers.

95. Zheng, C.G., et al., *Effects of Polymer Adsorption and Flow Behavior on Two-Phase Flow in Porous*, Society of Petroleum Engineers.

96. Zhang, G. and R. Seright, *Effect of Concentration on HPAM Retention in Porous Media.*

97. Peterson, C.K., T. K., *THE KINETICS OF POLYMER ADSORPTION ONTO SOLID SURFACES.* The Journal of Physical Chemistry, 1961. **65**(8): p. 1330-1333.

98. Grisel, M. and G. Muller, *The salt effect over the physical interactions occurring for schizophyllan in the presence of borate ions.* Macromolecular Symposia, 1997. **114**(1): p. 127-132.

99. Koumoto, K., et al., *Chemical modification of schizophyllan by introduction of a cationic charge into the side chain which enhances the thermal stability of schizophyllan-poly(C) complexes.* Chemical Communications, 2001(19): p. 1962-1963.

100. Norisuye, T., T. Yanaki, and H. Fujita, *Triple helix of a schizophyllum commune polysaccharide in aqueous solution.* Journal of Polymer Science: Polymer Physics Edition, 1980. **18**(3): p. 547-558.

101. Lange, L.H., *Concentrating Phosphate-Bearing Material such as that with a Quartz Gang*, U. Patent, Editor 1931: USA.

102. Ma, X., *Lyotropic Ion Effects in Guar Gum Adsorption on Various Minerals* in *Chemical Enineering* 2007, University of British Columbia Vancouver.

103. Steenberg, E. and P.U.v.C.H. Onderwys, *The Depression of the Natural Floatability of Talc: The Mechanism Involved in the Adsorption of Organic Reagents of High Molecular Mass*1982.

104. Liu, Q., *The role of mineral surface composition and hydrophobicity in polysaccharide/mineral interactions*, in *Chemical Engineering*1988, University of British Columbia: Vancouver.

105. B.A. Jucker, H.H., S.J. Hug, A.J.B. Zehnder, *Adsorption of bacterial surface polysaccharides on mineral oxides is mediated by hydrogen bonds.* Colloids and Surfaces B: Biointerfaces. **9**(6): p. 331-343.

106. J. Wang, P.S., D.R. Nagaraj, *Adsorption mechanism of guar gum at solid–liquid interfaces.* Minerals Engineering,

2005. **18**(1): p. 77-81.

107. Liu, Q.Z., Yahui;Laskowski, J.S., *The adsorption of polysaccharides onto mineral surfaces: an acid/base interaction*

International Journal of Mineral Processing, 2000/12//.

108. Nakatani, J., S. Ozawa, and Y. Ogino, *Adsorptive interactions of glucose and carbon dioxide with basic sites over alumina.* Journal of the Chemical Society, Faraday Transactions, 1990. **86**(10): p. 1885-1888.

109. J.Ofori Amankonah, P.S., *Effects of dissolved mineral species on the electrokinetic behavior of calcite and apatite.* Colloids and Surfaces, 1985. **Volume 15**: p. 335–353.

110. Parks, G.A., *The Isoelectric Points of Solid Oxides, Solid Hydroxides, and Aqueous Hydroxo Complex Systems.* Chemical Reviews, 1965. **65**(2): p. 177-198.

111. G.A. Nyamekye, J.S.L., *Adsorption and electrokinetic studies on the dextrin–sulphide mineral interactions.* Journal of Colloid and Interface Science, 1993. **157**: p. 160–167.

112. Qi Liu, J.S.L., *The interactions between dextrin and metal hydroxides in aqueous solutions.* Journal of Colloid and Interface Science, June 1989. **Volume 130**(1): p. 101-111.

113. Qi Liu, J.S.L., *The role of metal hydroxides at mineral surfaces in dextrin adsorption, I. Studies on modified quartz samples.* International Journal of Mineral Processing, July 1989. **26**(3-4): p. 297-316.

114. Qi Liu, J.S.L., *The role of metal hydroxides at mineral surfaces in dextrin adsorption, II. Chalcopyrite-galena separations in the presence of dextrin.* International Journal of Mineral Processing, September 1989. **27**(1-2): p. 147-155.

115. Xiaodong Ma, M.P., *Effect of alkali metal cations on adsorption of guar gum onto quartz.* Journal of Colloid and Interface Science, 2005. **289**(1): p. 48–55.

116. Ma, K., et al., *Adsorption of cationic and anionic surfactants on natural and synthetic carbonate materials.* Journal of Colloid and Interface Science, 2013. **408**(0): p. 164-172.

117. Cui, L., et al., *Adsorption of a Switchable Cationic Surfactant on Natural Carbonate Minerals*, Society of Petroleum Engineers.

118. *C. E. P. M. (2014, May 27). PANalytical X'Pert Pro MPD X-ray Diffractometer (XRD).*Available from: http://swes.cals.arizona.edu/CEPM/cepm_instrumentation.html.

119. ;Available from: http://www.minisitehq.com/ergotech/site/page/DigitalPorosimeterHeliumExpansionVolumeMeters/1525.

120. Taylor, K.C. and H.A. Nasr-El-Din, *Xanthan biopolymers: A review of methods for the determination of concentration and for the measurement of acetate and pyruvate content.* Journal of Petroleum Science and Engineering, 1993. **9**(4): p. 273-279.

121. DuBois, M., et al., *Colorimetric Method for Determination of Sugars and Related Substances.* Analytical Chemistry, 1956. **28**(3): p. 350-356.

122. GPC,A.;Available from: http://www.chem.agilent.com/library/usermanuals/public/g1362-90011_rid-a_usr_en.pdf.

123. E Killman, R.E., Makromol. Chem., 1971.

124. III,T.;Available from: http://www.tainstruments.com/main.aspx?id=215&n=1&siteid=11.

125. Abdel-Mohsen, A.M., et al., *Preparation, characterization and cytotoxicity of schizophyllan/silver nanoparticle composite.* Carbohydrate Polymers, 2014. **102**(0): p. 238-245.

126. Wang, J., et al., *Structural Characterization, Chain Conformation, and Morphology of a β-(1→3)-d-Glucan Isolated from the Fruiting Body of*

Dictyophora indusiata. Journal of Agricultural and Food Chemistry, 2009. **57**(13): p. 5918-5924.

127. Ji, J., et al., *Rapid identification of dolomite using a Fourier Transform Infrared Spectrophotometer (FTIR): A fast method for identifying Heinrich events in IODP Site U1308*. Marine Geology, 2009. **258**(1–4): p. 60-68.

128. Lenka VACULÍKOVÁ, E.P., Silvie VALLOVÁ and Ivan KOUTNÍK, *Characterization and Differentiation of Kaolinites from Selected Czech Deposits Using Infrared Spectroscopy and Differential Thermal Analysis* Acta Geodyn. Geomater.

129. Saikia, B., G. Parthasarathy, and N.C. Sarmah, *Fourier transform infrared spectroscopic estimation of crystallinity in SiO2 based rocks.* Bulletin of Materials Science, 2008. **31**(5): p. 775-779.

130. Tempio, J.S. and J.L. Zatz, *Interaction of xanthan gum with suspended solids.* Journal of Pharmaceutical Sciences, 1981. **70**(5): p. 554-558.

131. El'tekov, A.Y., N.A. El'tekova, and V.I. Roldughin, *Kinetic coefficients of the adsorption of polysaccharides from aqueous solutions by Sibunit.* Colloid Journal, 2007. **69**(2): p. 248-251.

132. Somasundaran, P., *Adsorption of starch and oleate and interaction between them on calcite in aqueous solutions.* Journal of Colloid and Interface Science, 1969. **31**(4): p. 557-565.

133. Rinaudo, M. and C. Noik, *Adsorption of polysaccharides on a calcite using spin labelled polymers*. Polymer Bulletin, 1983. **9**(10-11): p. 543-547.

134. Ma, X., *Role of solvation energy in starch adsorption on oxide surfaces*. Colloids and Surfaces A: Physicochemical and Engineering Aspects, 2008. **320**(1–3): p. 36-42.

135. Instrument,T.;Available from: http://www.tainstruments.com/main.aspx?id=136&n=1&siteid=11.

136. Bian, Y., *Manual for Surfactant Titration* 2010, RICE UNIVERSITY.

137. Titrator,M.;Available from: http://www.metrohmusa.com/Products/Titration/Potentiometric/Titrando/905-Titrando/.

138. Cullum, D.C., *Introduction to Surfactant Analysis*1994: Springer Netherlands.

139. EPTON, S.R., *A rapid method of analysis for certain surface-active agents*. Vol. 160. 1947: Nature. 795.

140. Cui, L., *Application of Foam for Mobility Control in Enhanced Oil Recovery (EOR) Process*, 2014, Rice University

141. Vilela, A. and I. Fjelde, *Modeling of Interaction Between CO2 and Rock in Core Flooding Experiments*, Society of Petroleum Engineers.

142. DSA/TOF,Available from: http://www.perkinelmer.com/CMSResources/Images/44-152512APP_01_Illicit_Drugs.pdf.

143. Perkin, D.; Available from: http://www.raci.org.au/document/item/1286.